Durham University

Durham E-Theses

Nanoscale fillers. Fillers for high oxygen permeability polymer films

Jonathan D. B. Fay

How to cite:

Fay, Jonathan D. B. (2007) Nanoscale fillers. Fillers for high oxygen permeability polymer films. Doctoral thesis, Durham University.

Use policy

The full-text may be used and/or reproduced, and given to third parties in any format or medium, without prior permission or charge, for personal research or study, educational, or not-for-profit purposes provided that:

- a full bibliographic reference is made to the original source
- a https://etheses.durham.ac.uk/id/eprint/2333/ is made to the metadata record in Durham E-Theses
- the full-text is not changed in any way

The full-text must not be sold in any format or medium without the formal permission of the copyright holders.

Please consult the full Durham E-Theses policy for further details.

Academic Support Office, The Palatine Centre, Durham University, Stockton Road, Durham, DH1 3LE
e-mail: e-theses.admin@durham.ac.uk Tel: +44 0191 334 6107
https://etheses.durham.ac.uk

Nanoscale Fillers

Fillers for High Oxygen Permeability Polymer Films

A thesis presented for the degree of

Doctor of Philosophy

by

Jonathan D. B. Fay

The copyright of this thesis rests with the author or the university to which it was submitted. No quotation from it, or information derived from it may be published without the prior written consent of the author or university, and any information derived from it should be acknowledged.

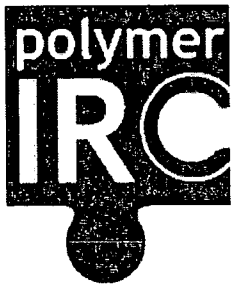

Department of Chemistry

October 2004 – December 2007

Published 2008

- 6 JUN 2008

Abstract

A wide range of polymer film products are available with varying degrees of permeability to a variety of gases, from oxygen to water to aromatic species. The barrier properties are determined primarily by the choice of the matrix polymer, and fine tailoring can be introduced through the addition of filler materials such as inorganic platelets and polymer blend materials. It was identified that hollow and porous particles would be potentially interesting classes of filler particles. The effect of the addition of such particles appears little studied.

Gel particles were prepared by free radical emulsion polymerisation of styrene and DVB in presence of hydrophobic solvents. Porous particles were prepared by the surfactant free emulsion copolymerisation of VBC and DVB, followed by Friedel-Crafts alkylation to yield hypercrosslinked microporous nanoparticles. Porous and gel particles were added to polymer films and the oxygen permeability and mechanical properties of these films determined. It was found that the addition of hypercrosslinked microporous nanoparticles increased the oxygen permeability of the films up to ~50 % when added at 40 wt% loading. Further to these studies, hollow nanoparticles were prepared by the emulsion phase ATRP of DVB when initiated by mPEG-*b*-PS inisurf in the presence of a hydrophobic solvent.

Acknowledgements

The author acknowledges the following people for their assistance in this work:
Neil Cameron for supervision throughout the project and Andrew Matthews (Cryovac) and Sharon Cooper for supervision during the earlier stages of the Ph.D. Thanks also to Nate Miranda, Mini Brebion, and Darrell Austin for hosting and assisting with my visit to the plant at Duncan, SC.; also my gratitude to those others that welcomed me so warmly, the organisers and the entertainers. Kind thanks are offered to the technical and analytical staff in Durham without who's cooperation this work would not have been possible. I also thank those helpful folk from outside of Durham, Steven Ensley at Cryovac for making and measuring the Amalloy films, the E.M. unit at Newcastle for imaging the films at short notice, and Hongjun Niu at Liverpool for running the pycnometry experiments. Finally, I acknowledge the financial contributions of both Cryovac Ltd., and EPSRC.
My personal thanks are extended to past and present members of the NRC group that I have had the pleasure to work alongside over the three years, particularly Paco Fernández Trillo and Matt Gibson for help with the chemistry, and Géraldine Rohman for much needed personal discussions and support (perhaps even The Johnson is worthy of a mention here). And of course, thanks to Scott Watson for his continuing friendship.
My most grateful thanks are extended to Daniella for her patience and understanding through the tough times and the good. I couldn't have done it without you!

Declaration

I declare that no material in this thesis has been previously submitted for a degree at this or any other university.

Copyright

The copyright of this thesis rests with the author. No quotation from it should be published without their prior written consent and information derived from it should be acknowledged.

Contents

List of Figures

List of Tables

List of Abbreviations

A ..... Area

AFM ..... Atomic force microscopy

AGET ATRP ..... Activators generated by electron transfer ATRP

AIBN ..... Azobisisobutyronitrile

a.m.u. ..... Atomic mass units

atm ..... Atmospheres

ATRP ..... Atom Transfer Radical Polymerisation

BET ..... Brunauer-Emmett-Teller

BJH ..... Barret-Joyner-Halenda

CSC ..... Core-shell-corona

CST ..... Core-shell templating

DCE 1,2-dichloroethane

DCM ..... Dichloromethane

DDAB ..... Didodecyldimethylammonium bromide

DLS ..... Dynamic light scattering

DNA ..... Deoxyribonucleic Acid

dnNBipy ..... 4,4'-dinonyl-2,2'-bipyridyl

DTAB ..... Dodecyltrimethylammonium bromide

DMA ..... Dynamic mechanical analysis

DMF ..... Dimethylformamide

DP ..... Degree of polymerisation

DVB ..... Divinyl benzene

E ..... Young's modulus

γ ..... Surface tension

G ..... Gibb's free energy

IUPAC ..... International union of pure and applied chemistry

k_p ..... Propagation rate constant

KPS ..... Potassium persulfate

LLDPE ..... Linear low density polyethylene

MALDI-ToF ..... Matrix assisted laser desorption ionisation - time of flight

MCM-41 ..... Mobile crystalline material-41

MMA ..... Methyl methacrylate

M_n ..... Number average molecular weight

$[M_p]$ ..... Monomer concentration in growing particle

mPEG ..... Poly(ethylene glycol) methyl ether

mPEG-*b*-PS ..... Poly(ethylene glycol) methyl ether *block* polystyrene

MSD ..... Multimodal size distribution

M_w ..... Weight average molecular weight

$\overline{n}$ ..... Number of free radicals per particle

NMP ..... Nitroxide mediated polymerisation

NMR ..... Nuclear magnetic resonance

N_p ..... Particle density

NTU ..... Nephelometric turbidity units

ODA ..... Octadecylamine

OTR ..... Oxygen transmission rate

o/w ..... Oil-in-water

PAA ..... Polyacrylic acid

PDI ..... Polydispersity index

PEG ..... Poly(ethylene glycol)

PEO ..... Poly(ethylene oxide)

PI ..... Polyisoprene

PIT ..... Phase inversion temperature

PMAA ..... Polymethacrylic acid

PMMA ..... Poly(methyl methacrylate)

PolyHIPE ..... Poly(High Internal Phase Emulsion)

PPy ..... Polypyrrole

PS ..... Polystyrene

PTFE ..... Poly(tetrafluoroethylene)

pVBC ..... Poly(vinylbenzyl chloride)

RAFT ..... Reversible addition-fragmentation chain transfer

R_p ..... Rate of polymerisation

S ..... Surfactant to internal phase ratio

SDS ..... Sodium dodecyl sulfate

SEC ..... Size exclusion chromatography

SEM ..... Scanning electron microscopy

TEM ..... Transmission electron microscopy

TEOS ..... Tetraethoxysilane

T_g ..... Glass transition temperature

THF ..... Tetrahydrofuran

V-50 ..... 2,2-azobis(2-amidinopropane) dihydrochloride

VBC ..... Vinylbenzyl chloride

WAXS ..... Wide angle X-ray scattering

w/o ..... Water-in-oil

Chapter 1

Introduction

1.1 Motivation

The aim of the work described in this thesis is to synthesise particles of <50 nm diameter that are either hollow or porous, and to incorporate these into polymer films to increase the oxygen permeability.

1.2 Thesis Outline

This thesis is divided into parts, each of which discusses a significant step in the journey towards meeting the end objective. Due to the different fields covered by each part, each comprises a literature review chapter that addresses the main points to be covered, before an experimental chapter to detail the approach and techniques used and a chapter of results and discussion to present the data analysis and interpretation.

The thesis begins with polymerisation in emulsions to yield gel nanoparticles, then moves to the synthesis of hypercrosslinked porous particles, including the development of the synthesis from the gel particle synthesis. The preparation of hollow particles by interfacially restricted controlled radical polymerisation (ATRP) follows this, before ending with a study of the inclusion of hypercrosslinked porous particles in films.

Part I

Polymer Latex Nanoparticles

All truths are easy to understand once they are discovered; the point is to discover them.

Galileo Galilei

Chapter 2

Literature Review

The aim of this chapter is to present a summary of the literature published on the subject of polymer latex particle synthesis and characterisation, paying particular attention to the preparation of nanoparticles by emulsion polymerisation approaches.

2.1 Introduction

Once contentious, the concept of polymerisation is now well known and accepted. It has been recognised in nature in the formation of such structures as DNA, in polysaccharides and in proteins. The synthetic polymer industry today is a major contributor to the global economy: Western Europe's per capita consumption of plastics is in the region of 90 kg per annum.[1] The majority of polymers are organic, being that they are composed of carbon based monomers, however inorganic polymers are also known[2] and indeed produced on large scales, for example polysiloxanes (silicones).

Polymerisation reactions can be categorised as either step growth or chain growth. Frequently, step growth polymerisation involves the loss of a small molecule during

the reaction, for example in the polymerisation of glucose the step growth formation of a saccharide bond results in the loss of a water molecule, however this is not always the case, for example the polymerisation of urethanes. In the latter polymerisation reaction type there is no loss, simply the addition of another monomer unit to the growing polymer, for example the chain growth free radical polymerisation of styrene.

There are other means by which polymers may be broadly classified, with terms such as thermosets and thermoplastics (relating to the ability to melt), elastomers and plastics (relating to the ability to deform elastically), linear, branched, homo- and co-polymers, of which there are statistical, alternating, block and graft varieties (each relating to architecture). These classifications are discussed in introductory textbooks.[3]

Furthermore, the chain growth polymerisation of vinyl containing monomers may be initiated by inter alia ionic (anionic and cationic) or free radical initiators. Ionic polymerisation requires the monomer to be electronically activated by appropriate groups residual to the vinyl bond. Explicitly, cationic initiator species (acids and Lewis acids) require the bond to be electron rich, and so electron donating groups are required to activate the π-bond to attack. Conversely, anionic initiator species (metal alkyls) require the vinyl bond to be electron deficient, and so electron withdrawing groups are required. The nature of counter ions also affects the polymerisation, and so these systems may be considered complex. In favour of ionic polymerisation is that high molecular weight polymers can be generated rapidly at low temperatures.

Free radical polymerisation of vinyl monomers is practically simpler (although arguably as mechanistically complex), requiring only that the resultant radical species formed during the polymerisation is sufficiently stable to allow propagation (i.e. chain growth) before termination.

2.2 Free radical polymerisation

The key steps in free radical polymerisation (as all polymerisations) are initiation, propagation and termination (figure 2.1). Initiation is the means by which the polymerisation reaction is begun, requiring the generation of a radical and capture of that radical by a monomer molecule. Initiators may be activated by thermal decomposition (peroxides, AIBN, KPS), photolysis (KI) or redox reactions (H_2O_2 & Fe^{2+}). Ionising radiation may also be used to generate radicals and thus initiate free radical polymerisation. Propagation is the addition of monomer units on to the growing polymer chain, and continues for as long as there is monomer to be consumed, and the radical species is stable to termination. Termination is the process by which the radicals are removed from the system, which may occur by combination, disproportionation, combination with new initiator radicals or with other impurities. Chain transfer is an additional mechanism by which the propagation of a polymer chain may be terminated, however this is not termed a 'termination' reaction as the radical is still present in the system. Again, these points are discussed in introductory texts.[3]

Polymerisation reactions can be carried out in bulk, solution, or emulsion systems. In the case of bulk polymerisation the reaction is carried out with initiator in pure monomer, and as a result the purity of the products of bulk phase polymerisations is generally high. Because the reaction is exothermic there is often a lack of control arising from auto-acceleration (due to inefficient heat dispersion). The gel effect can also be observed at high conversions as viscosity rises and steady state kinetics are lost. Low conversions are targeted to overcome these problems. An alternative means to overcome the problems of inefficient heat dispersion is to polymerise the monomer in solution. In this case, the polymerisation is carried out in a solvent for the polymer which aids to disperse heat and lower viscosity, however the solvent itself introduces a mechanism by which control is lost, in the form of chain transfer

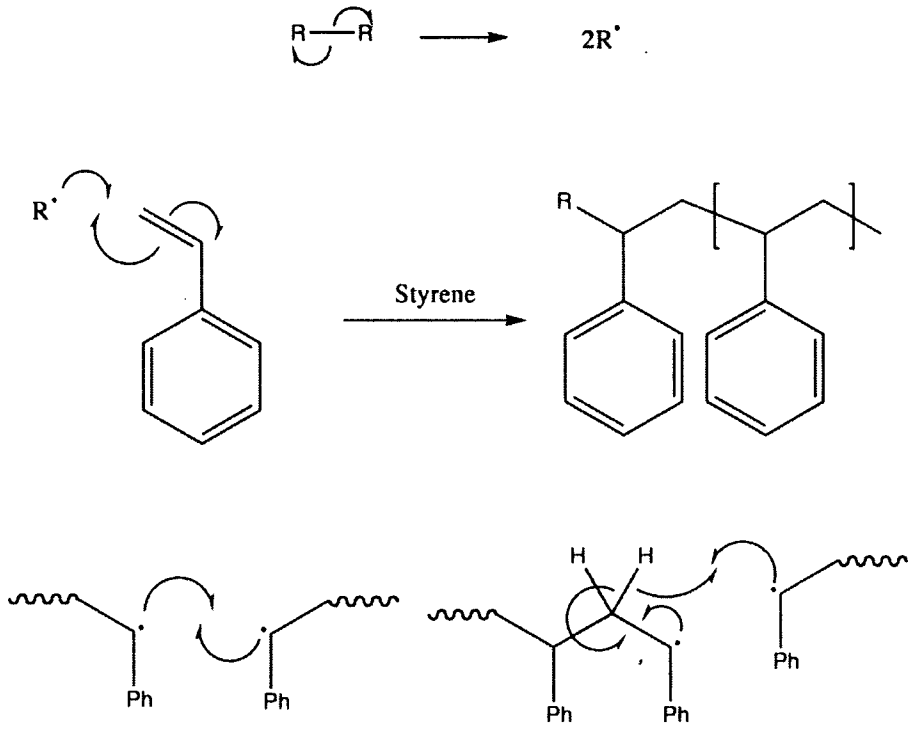

Figure 2.1: Mechanism of free radical polymerisation of styrene. Top: Radical generation. Middle: Initiation & propagation. Bottom: Termination by combination (left) and disproportionation (right).

(in which a radical is transferred to the chain transfer agent, in this case the solvent, typically by extraction of a hydrogen atom). Suspension polymerisation is most similar to emulsion polymerisation in that an oil soluble monomer is dispersed in an aqueous bulk phase. In the case of suspension polymerisation, this occurs without the aid of a surfactant and droplets are typically large (up to 500 μm in diameter). Emulsion polymerisation differs in that the surfactant used to stabilise the dispersion provides for the formation of much smaller droplets and micelles. The large volume of water present in these systems very effectively extracts the heat of polymerisation, however solids content is low and purification steps are necessary where surfactants are employed.

These general free radical polymerisation methods can be used to prepare polymers of high molecular weight, with relatively large polydispersities (PDI, calculated as the ratio of the weight to number average molecular weights: M_w/M_n). The influ-

Figure 2.2: Photographic images of w/o emulsion systems comprising SDS, isopentanol, water and decane, with decreasing surfactant : water ratio from left to right: (macro)emulsion, nanoemulsion and microemulsion.

ence of termination must be minimised for a controlled free radical polymerisation reaction, and this is achieved through kinetic control (see Part III).

2.3 Emulsions

An emulsion is a dispersion of an internal phase, α_1, within a continuous phase, α_2, with which α_1 is immiscible, facilitated by the presence of a surfactant. If α_1 is an oil, for example toluene, and α_2 is water, the dispersion is an oil-in-water emulsion, abbreviated to o/w. If α_1 were an oil miscible monomer such as styrene, then it is conceivable that the droplets could be polymerised to form polymeric particles. If the two phases are reversed then a water-in-oil (w/o) emulsion is formed, and again it is conceivable that the oil could be polymerised. Should the volume of the internal phase exceed ~74%, then porous scaffold structures (polyHIPEs) can be synthesised.[4,5]

Different emulsion systems are classified by their droplet dimensions and stability to phase separation. Of these, macro-, nano- and microemulsions can differ from each other in composition by only the relative amounts of each of the phases: Miniemulsions are different in that they require high shear mixing and, typically, additional hydrophobic species. Photographic examples of the first three emulsion types are depicted in figure 2.2.

2.3.1 (Macro)emulsions

These dispersions are polydisperse with respect to droplet size, ranging from micelles and swollen micelles of nanometer dimensions through to micron sized droplets. The large droplets scatter all wavelengths of light and consequently give the emulsions their opaque white appearance. The large surface areas of such droplets gives rise to the thermodynamic instability of emulsions. It is known that the creation of surface or interface requires energy, G, related to the interfacial tension, γ and the surface area, A:

$$\delta G = \gamma \delta A \tag{2.1}$$

Surfactant residing at the oil-water interface reduces γ, making the formation of the interface more favourable. However, δG is in this case still positive and so energy is required to create the surface in dispersing the droplets, typically supplied by stirring or shaking. The stability of the emulsion is then kinetic, provided by the electrostatic barrier of the surfactant, with sedimentation and creaming, coagulation and flocculation being the main mechanisms[6] by which droplets may revert to the thermodynamically stable two (or three) phase system (separate oil and water (and surfactant) phases). (Macro)emulsions are therefore thermodynamically unstable.

2.3.2 Nanoemulsions

Appearing a translucent blue colour due to the preferential scattering of blue light,[7] nanoemulsions have droplets of the order of 50–200 nm, although this definition is not fast, with one author even offering two typical ranges of droplet diameter.[8,9] Nanoemulsions are monodispersed with respect to droplet size distribution but again, these systems are thermodynamically unstable. Nanoemulsion droplet size distribution is affected by the mechanism employed to disperse the droplets. For example, homogenisation can be achieved through stirring or vortex mixing, sonication, or so

called low energy methods of controlled component addition. In the last of these examples it has been observed that the order in which the components of the emulsion are mixed together influences droplet formation.[8,10] For example, the addition of water to a surfactant in oil solution gives more monodispersed o/w droplets than the reverse case, attributed to a lower interfacial energy as the system is forced to undergo a phase inversion.[8,11] Similarly, forcing emulsions through a thermally induced phase inversion (i.e. through the PIT) is a favoured route to nanoemulsion formation.[12,13] The main mechanism by which nanoemulsions undergo phase separation is Ostwald ripening.[14]

2.3.3 Microemulsions

Microemulsions comprise dispersed droplets of the order of 10 nm in diameter, and hence do not scatter light, appearing optically transparent. Microemulsions are thermodynamically stable dispersions due to the large increase in entropy from dispersing the small droplets offsetting the enthalpy required to produce the large total surface area. Microemulsions form spontaneously, requiring no agitation (although in practice often a small amount of mixing is required), but of all of the emulsion systems, they require the greatest quantity of surfactant to stabilise the greatest relative surface area. Microemulsion cubic and lamellar phases can exist in addition to the simpler o/w and w/o phases.

2.3.4 Miniemulsions

As mentioned previously, miniemulsions differ from the three previous types of emulsion in that a constant input of energy through agitation is required to maintain droplet stability, without which phase separation would occur rapidly. Hydrophobic species such as hexadecane[15] are commonly used to assist in stabilising these dis-

persions. Being solubilised in the centre of the oil droplet, the hydrophobe reduces droplet coalescence via Ostwald ripening by preventing the diffusion of oil out of the droplet by establishing an increasing concentration gradient in the event of oil loss. Droplets typically range between 50–500 nm in diameter.

2.4 Emulsion polymerisation

Emulsion polymerisation is the polymerisation of a monomer in the biphasic medium of an emulsion. The monomer is dispersed as emulsion droplets (sometimes with a solvent) stabilised by a surfactant (sometimes also a cosurfactant) in an immiscible continuous phase. As described previously, emulsion systems are polydispersed with respect to droplet size distribution, however the products of emulsion polymerisation are typically more monodispersed than the parent emulsion. Emulsion polymerisation and latex particle synthesis[16–18] is now a multiply reviewed subject, and so that which follows is only a brief discussion.

Based on the work of Smith and Ewart,[19] the kinetics of emulsion polymerisation are divisible into three intervals, I, II and III as depicted in figure 2.3. In this treatment of emulsion polymerisation, interval I is the particle nucleation stage, interval II is particle growth under steady-state conditions, and interval III is termination of growth under starved conditions. These kinetics are described by equation 2.2, in which R_p is the rate of polymerisation, k_p is the propagation rate constant, N_p is the particle density, $[M]_p$ is the monomer concentration in the growing particle and $\overline{n}$ is the number of free radicals per particle.

$$R_p \propto k_p N_p [M]_p \overline{n} \tag{2.2}$$

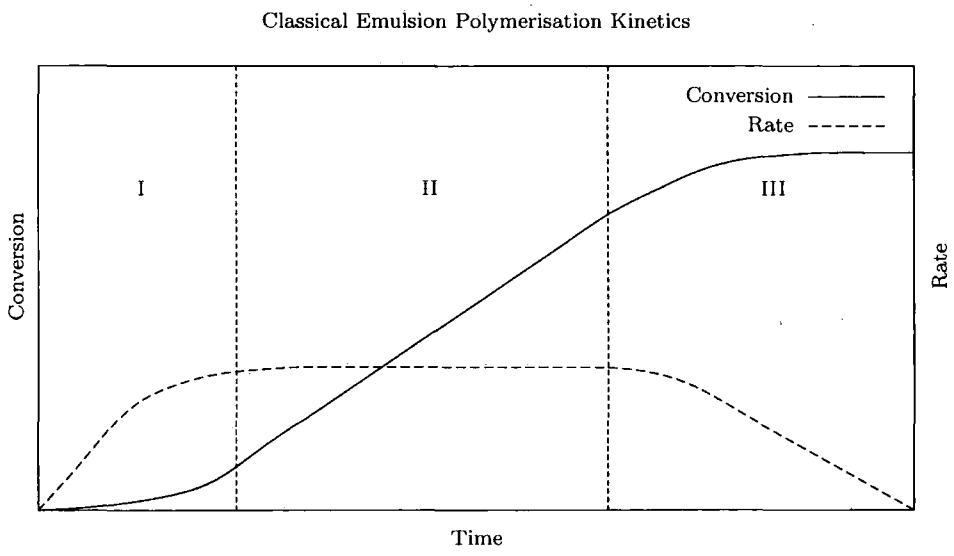

Figure 2.3: Classical emulsion polymerisation kinetics, indicating intervals I, II and III. Adapted from Herrera-Ordóñez et al.[20]

2.4.1 Interval I: Nucleation of particles

From the mechanisms outlined below it is apparent that nucleation can occur only when micelles (and to a limited extent, droplets) are present in the system, therefore once the micelles are consumed (typically $< 10\%$ conversion) nucleation rate becomes essentially zero (as the contribution from droplet nucleation is negligible), and the number of particles remains approximately constant.

Homogeneous nucleation

The monomers used in o/w emulsion polymerisation are necessarily hydrophobic in order that an emulsion is formed, however an amount of monomer, up to that allowed by the solubility limit, is freely dissolved in the continuous phase. Aqueous phase radicals can initiate the oligomerisation of aqueous phase monomer, with propagation proceeding until a critical degree of polymerisation is reached, at which point the polymer must be solubilised by free surfactant or by entering a micelle. These primary particles then enter interval II; particle growth.

Micellar nucleation

The relative number of micelles and swollen micelles is much greater than the number of large monomer droplets in emulsion systems, typically 10^{18} and 10^{10}, respectively,[17] and therefore the total surface area presented by the former is very much greater. The probability of the capture of radicals is therefore greater in the case of micelles and swollen micelles in comparison to the emulsion droplets due to the larger surface area, and so micelles and swollen micelles act as a locus for particle nucleation because of their higher rate of radical capture.

Droplet nucleation

The rate of particle nucleation by droplet radical capture is low due to the relatively low surface area of emulsion droplets. When oil soluble initiators are used, particle nucleation by direct polymerisation of the droplet is again low, in this case because the rate of termination by the recombination of radicals is so high. When droplets approach the same length scale as micelles, as is the case in miniemulsions, droplet nucleation does become a dominant mechanism by which particles may be formed.

2.4.2 Interval II: Particle growth

Harkins[21,22] demonstrated a linear decrease in droplet diameter with time, and found that the large monomer droplets of a polymerised emulsion contained significantly less polymer than expected. Therefore the contribution by droplet nucleation was identified as limited, while the micelles contained significantly more polymer than expected and their contribution identified as significant. From these observations it was determined that monomer diffuses from the large emulsion droplets to the micelles during the growth phase of the polymerisation. In this way, the emulsion

droplets act as reservoirs that feed the growing particles with monomer and surfactant during the reaction. The rate of polymerisation decreases as the droplets become depleted and finally consumed. The end of interval II is marked as the onset of this process, illustrated by the decrease in rate from steady state kinetics.

2.4.3 Interval III: Particle termination

By definition, no monomer droplets remain during interval III, and so the increase in conversion necessarily corresponds to the polymerisation of monomer present within the latex particles. This can occur by capture of radicals, which are generated throughout the polymerisation, by the latex particle. The dominant mechanism by which termination occurs is chain transfer to the polymer.

2.4.4 Controversial aspects

Most controversy surrounding this proposed mechanistic model pertains to its failures in its under-estimations of particle numbers, that nucleation is often observed to occur outside of interval I, that observed polymerisation rates often deviate from the model and that the model fails for hydrophilic monomers.[16,20]

Controversy also surrounds the mechanism of emulsion polymerisation initiated by oil soluble initiators. Oil soluble initiators are considered to require the desorption of a radical for initiation to be successful, else the compartmentalised nature of the droplet would lead to rapid recombination of propagating radicals and thus termination, otherwise radicals terminate immediately via the cage effect. However, an alternative school of thought suggests that a significant source of initiating radicals comes from the aqueous phase, even with initiators of very low aqueous solubility, due to observations correlating the kinetics of oil soluble initiator emulsion poly-

merisation with those of water soluble initiators. Experimental data to support this theory comes from the emulsion polymerisation of butyl acrylate in the presence of an aqueous phase radical-scavenging monomer.[15]

2.5 Microemulsion polymerisation

2.5.1 Features

The first reported microemulsion polymerisation was Atik and Thomas' communication[23] in 1981. Since then, very many reports have been published on the subject, including numerous reviews.[17,24,25]

Microemulsion polymerisation can, for certain systems, give fine control over latex particle size through tailoring the surfactant to monomer ratio.[26] However, the large quantity of surfactant required is the significant disadvantage of microemulsion polymerisation, making the process relatively costly due to the need to add and subsequently remove this surfactant. If microemulsion polymerisation is ever to be a large commercial process, it must be developed to yield a process with increased solid polymer content. Greater solids content (up to 30 wt%[27]) has been achieved for a range of acrylate monomers[28] and styrene[29] by dropwise addition feeding of monomer during the microemulsion polymerisation process.

The number of polymer chains per particle is low[17] due to the small droplet size and the possibility for droplet nucleation, and it is often observed that the final latex particle size is larger than the parent microemulsion, indicative of a complex mechanism.

2.5.2 Kinetics

The kinetics of microemulsion polymerisation differ from emulsion polymerisation kinetics as droplet nucleation can be the dominant nucleation mechanism. Typically, micelles are present throughout the polymerisation of microemulsion systems,[30] and so nucleation by this means can occur even at high conversions.

Extended interval I has been observed in the polymerisation of styrene in microemulsions,[31] only progressing to interval II at 20–35% conversion (because of initiator depletion) *cf* 2–15% for emulsion polymerisation (in which it is the consumption of micelles that limits nucleation rate and dictates the switch to interval II). Particle nucleation has also been observed to occur throughout the entire microemulsion polymerisation of styrene through observing the number of particles as a function of conversion, together with the broadening of the particle size distribution.[16,32] Droplet nucleation can also occur throughout the polymerisation process in the case of methacrylate monomer,[30] as long as initiator fragments can still be generated, and until all droplets are consumed through nucleation or through acting as monomer reservoirs. This causes increasing particle size polydispersity with conversion as nucleation events compete with growth throughout interval II. Similar observations were made during the microemulsion polymerisation of methyl methacrylate,[30] although in this case a further deviation from classic emulsion polymerisation kinetics was observed, with a slow homogeneous nucleation initiation period followed by a rapid increase in polymerisation rate attributed to a switch to a dominant droplet nucleation mechanism. A contradictory result is reported by Suzuki et al.,[33] in which no variation in particle size distribution is observed with increasing conversion. Differences in opinion exist as to the reasons behind the relative rates of oil and water soluble initiators and the consequences with respect to the mechanism of microemulsion polymerisation.[25,33,34]

To further complicate and hinder the elucidation of a general mechanism, many of the systems studied differ in monomer and surfactant, often requiring the presence of different cosurfactants (typically alcohols). This has lead to a whole body of work studying the effects of cosurfactants on microemulsion polymerisation, again with contradictory findings; some stating trends with alcohol variation,[35] others stating no correlation.[36,37] No general scheme for microemulsion polymerisation can yet be inferred.

Consensus exists regarding the major termination mechanism in microemulsion polymerisation being chain transfer to monomer,[32,38] not chain transfer to polymer as is the case in emulsion polymerisation. Furthermore, the rate of termination is suppressed in microemulsion polymerisation in comparison to emulsion polymerisation.[39]

2.6 Miniemulsion polymerisation

Because of the inherent instability of miniemulsions, the choice of surfactant,[40] stabiliser and costabiliser,[41] and even reactor dynamics[16] all affect the particle diameters of latexes prepared by miniemulsion polymerisation. Although the nature of the initiator has little influence over the rate of micellar nucleation, its influence over droplet nucleation is more pronounced[15] and so, since droplet nucleation is significant when droplets are small (as is the case in miniemulsion polymerisation), the choice of initiator can also affect latex particle size.[42] Regardless, the lengthscales of latex particles are typically of the same order as the miniemulsion droplets from which they are formed.[42,43]

Chapter 3

Experimental

The aim of this chapter is to explain the experimental procedures used in the synthesis of poly(styrene-co-divinylbenzene) nanoparticles, and to introduce the analytical techniques used in their characterisation.

3.1 Introduction

As indicated in the preceding review, there are many examples of polymer latex particle synthesis reported in the literature. Attempts were made to reproduce a number of polystyrene nanoparticle syntheses from emulsions stabilised by SDS, and DTAB and DDAB. The aim of this work was two-fold; to learn emulsion polymerisation techniques and analyses, and through the inclusion of inert solvents, to see if porous nanoparticles could be synthesised.

3.2 Synthesis

3.2.1 Materials

Styrene (99%, Sigma) and DVB (divinylbenzene, technical grade, 80%, Aldrich) were washed over basic alumina (Activated Basic, Brockmann type II, Aldrich) to remove inhibitor prior to use. AIBN (2,2-azobis(2-methyl propionitrile), 98%, Acros) was recrystallised according to a published method,[44] KPS (potassium persulfate, Aldrich), SDS (sodium dodecyl sulfate, 99%, Sigma), DTAB (dodecyltrimethylammonium bromide, 99%, Sigma), DDAB (didodecyldimethylammonium bromide, 98%, Aldrich), pentan-1-ol and cyclohexanol (both 99+%, Sigma), toluene, hexane, and THF (tetrahydrofuran, all laboratory reagent grade, Fischer Chemicals) were used as supplied.

3.2.2 Emulsion polymerisation

SDS microemulsions

Microemulsions were prepared according to published literature procedures,[31,32] with variation by partial substitution of crosslinking monomer. A mixture of styrene (4.85 wt% (also substituted in part with DVB to provide crosslinking)) and pentan-1-ol (3.85 wt%) were added to deoxygenated aqueous solutions of SDS (9.05 wt% SDS, 82.25 wt% water) and stirred by magnetic stirrer bar. KPS was added for aqueous initiated polymerisations, alternatively the oil soluble initiator AIBN was used, dissolved in the oil phase prior to emulsification. The resulting dispersions were heated to 70 °C for three hours. Aliquots were diluted with water and deposited directly onto formvar/copper TEM grids for analysis.

DTAB / DDAB emulsions

Emulsions were prepared by first deoxygenating distilled water (90 g in a 250 ml round bottomed flask fitted with a Suba seal and stirred by magnetic stirrer bar) by bubbling with N_2 for fifteen minutes. Surfactant (3.75 g DTAB, 1.25 g DDAB) was added under a flow of nitrogen, the vessel resealed and N_2 permitted to flow through the air space above the aqueous volume for a further two minutes before facilitating dissolution of the surfactant by magnetic stirring. AIBN (10 mg g^{-1} monomer) was dissolved into a mixture of monomer (styrene and/or DVB) and solvent (toluene or heptane) as required (total internal phase of 5 g), added to the surfactant solution and stirred at room temperature (1 hour, 500 rpm). Single aliquots were drawn at this point for droplet size distribution analysis. The polymerisation was then initiated thermally by immersion of the reaction vessel into a preheated oil bath (60 $\pm$ 2 °C). Removal of the vessel from the oil bath after eighteen hours' reaction time allowed the cessation of the production of radicals from any remaining AIBN, and the polymeric product was then recovered by precipitation into methanol (500 ml) prior to isolation by centrifugation (2 mins, 8000 rpm), and washing with methanol by soxhlet (one week). The resulting paste was crudely dispersed by shaking in water, and then freeze dried to yield a free flowing, white powder. A similar procedure was used in the formation of latexes from emulsions initiated by KPS. In this case, 85 g of water was used initially, and following dispersion of the monomer, KPS (10 mg g^{-1} monomer) dissolved in 5 ml of water was added by syringe before initiation as before.

3.3 Analysis

3.3.1 DTAB / DDAB emulsions

Emulsion droplet size distribution was determined by dynamic light scattering (DLS) using a Beckman-Coulter LS 13 320 Laser Diffraction Particle Sizer, with a detection range of 40 nm to 2000 μm. In all cases the refractive index of the droplets was set at that of styrene (the contributions of DVB, solvent and surfactant ignored). Samples were analysed at 20 °C.

Monomer conversion was measured using Raman spectroscopy. When employed in this application, Raman spectroscopy requires an internal calibration, selected for this is the breathing mode of the styrene ring[45,46] at 1000 cm^{-1} (ν_1). The signal from the vinyl bond at ~1640 cm^{-1} (ν_2) is seen to decrease relative to the aromatic during the polymerisation and the normalised ratio used to calculate % conversion according to equation 3.1, in which M_o and M_t are the values of the ratiosat time 0 and t, respectively.

$$\%\text{Conv} = 100 \cdot \frac{M_o - M_t}{M_o} \tag{3.1}$$

Particle size distribution was determined by DLS using a Brookhaven Instruments Zetasizer, with a quoted detection range of 2 nm to 3 μm. Samples were prepared for analysis by sonication in THF prior to passing through 450 nm PTFE syringe filters (for dust removal) into clean glass cuvettes. The refractive index of the particles was set to that of bulk polystyrene for the analysis. Data was acquired over ten runs each of one minute, at 20 °C, thermostatically controlled by the in-built solid state heating stage. Any data of baseline index[a] less than 8.5 were rejected, and each

[a]Baseline index is an internal measure of data quality ranging from 0 (poor) to 10 (good).

analysis comprised a minimum of seven minutes' total acquisition time. Data were then presented as relative number intensity calculated using the in-built multimodal size distribution (MSD) model. Particle size data was checked qualitatively against TEM images.

TEM (transmission electron microscopy) was used to determine particle morphology in addition to checking particle size information from DLS. A drop of nanoparticles dispersed in THF was deposited onto carbon coated copper grids, rested for approximately fifteen seconds before the excess solvent removed with torn filter paper. The unstained grids were then imaged with an Hitachi 7600 TEM at 100 kV accelerating voltage.

Surface area and pore size distribution data were acquired using a Micromeritics TriStar 3000 gas adsorption analyser. Samples were dried to constant weight at 50 °C under a flow of N_2 using Micromeritics' FlowPrep 060 apparatus. Isotherms were obtained by N_2 sorption. Surface area was calculated by BET method, and pore size and volume by BJH N_2 desorption analysis.

Chapter 4

Results and Discussion

The aim of this chapter is to present and rationalise the observations made when synthesising nanoscale latex particles.

4.1 SDS microemulsion systems

The replicated formation of microemulsions from a literature procedure[31,32] (and variations thereof) was confirmed by the optical clarity of the dispersions. After three hours at 70 °C, a blue-tinted, more opaque dispersion was observed, similar to the findings of Guo et al.[31] It is assumed that the conversion reached was high as the reported conversion for both aqueous and oil soluble initiator systems was approximately 90% in ~60 minutes,[31] although it was not measured for the syntheses reported here.

The latex particles are shown in the TEM images, figure 4.1. The use of oil soluble initiator (AIBN) was shown to produce particles of the region of 50 nm in diameter, whereas the use of aqueous soluble initiator (KPS) in an equivalent dispersion yielded much larger (2 μm) particles.

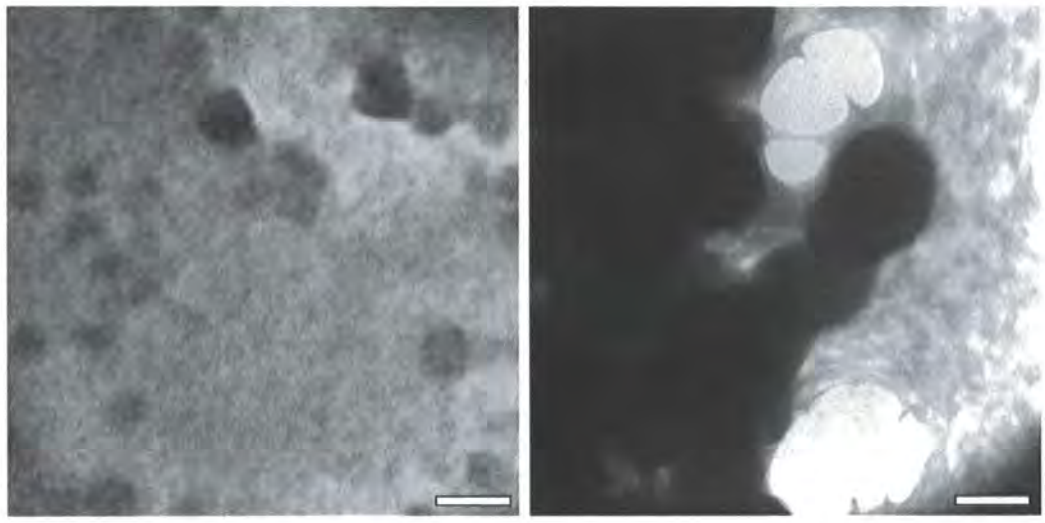

(a) AIBN (b) KPS

Figure 4.1: TEM images of latex particles produced from SDS microemulsions initiated by oil (left) and aqueous (right) phase radical generating species. Scale bars = 50 nm and 2000 nm respectively.

Partial substitution of potentially porogenic solvents in place of monomer (50 wt%) was attempted with toluene and cyclohexanol. Toluene caused no apparent change to either microemulsion nor latex particle size, however inclusion of cyclohexanol broke the emulsion, which we attribute to the co-surfactant effect of the alcohol in competition with pentan-1-ol.

The requirement of high surfactant and co-surfactant content in addition to poor microemulsion stability in the presence of potential porogen solvents lead to the cessation of work with SDS stabilised dispersions.

4.2 DTAB microemulsion systems

Microemulsions of styrene and DVB in water, stabilised by DTAB, have been reported to form latex particles of ~24 nm diameter[26] when initiated by AIBN (at 60–70 °C), where equivalent emulsions produced particles of ~30 nm diameter.[26] The difference between the microemulsion and emulsion systems was the surfactant

to internal phase weight ratio, S, being 2 and 1 respectively. Our own repetition of these syntheses yielded very different results (see figure 4.2). Latex particles from the microemulsion system ($S = 2$) were of approximately 30 nm diameter (similar to the quoted literature value[26]) rising to approximately 100 nm when polymerised in the presence of toluene. Polymerisation of the emulsion system produced a wide range of particle sizes, from microns (4.2(c)) to tens of nanometers (4.2(d)). The polydispersity observed of particles produced from the emulsion system demonstrates a lack of control which is obviously undesirable. It is postulated that larger particles may have been missed in the light scattering analysis by Antonietti et al.[26] as it is common practice to filter samples through $\leq$450 nm filter membranes to remove dust before analysis; this action could also have removed the larger particles from the author's TEM analysis.

4.3 DTAB / DDAB emulsion systems

4.3.1 MMA microemulsions

The formation and polymerisation of MMA microemulsions from a DTAB / DDAB surfactant mixture was reported in 1994 by Bléger et al.[30] Particle diameters of approximately 30 nm were observed. Repeating this method yielded a polydispersed product, shown by TEM in figure 4.3. Although the polydispersity of the latex particles was expected to increase with conversion due to continuous particle nucleation throughout the polymerisation,[30] it seems unlikely that the polydispersity in this case, with particles up to $\sim$200 nm diameter, arises from the same phenomenon of particle growth competing with nucleation. For such a range of particle diameters it is possible that the microemulsion is unstable to significant droplet coalescence during the polymerisation.

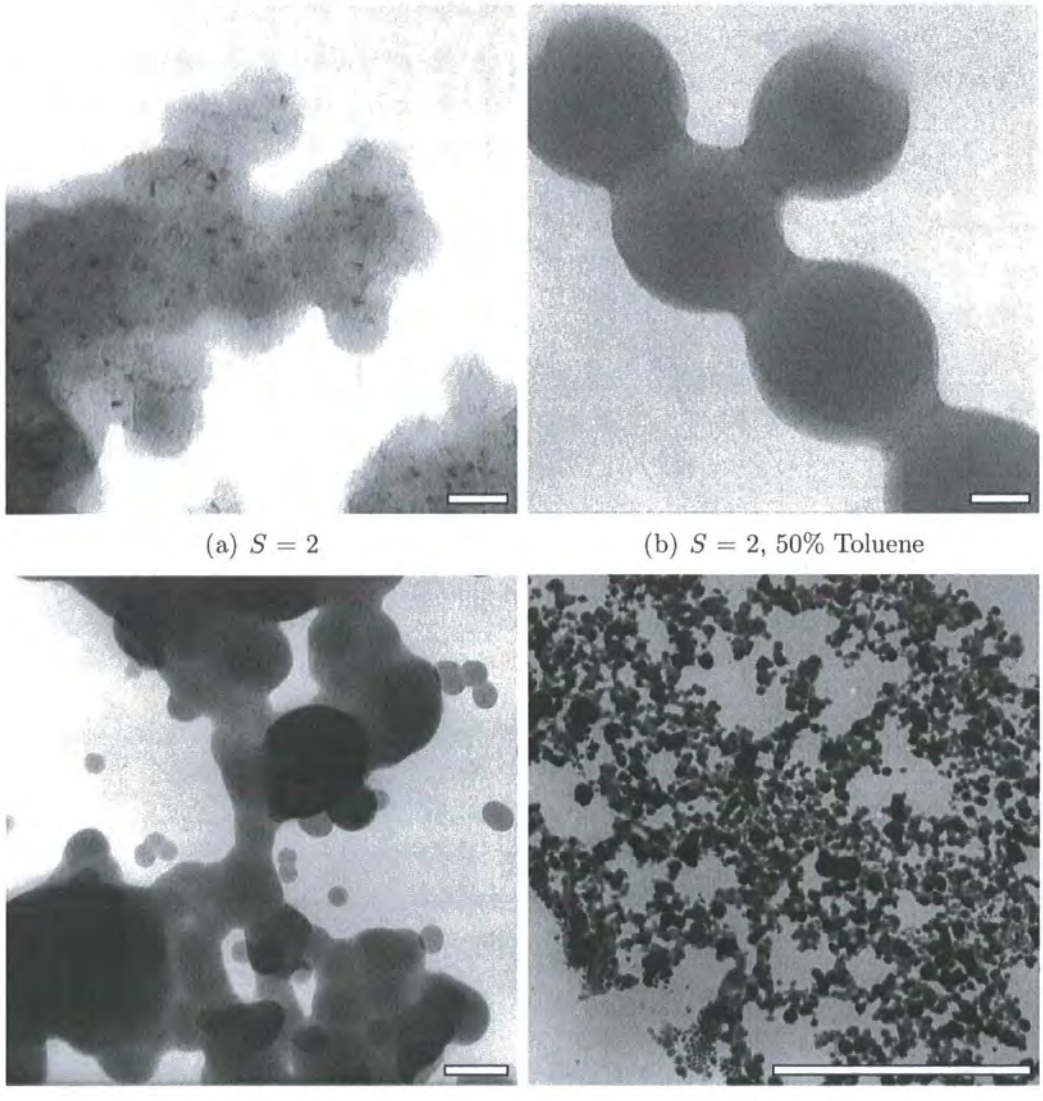

(a) $S = 2$ (b) $S = 2$, 50% Toluene

(c) $S = 1$ (d) $S = 1$

Figure 4.2: TEM images of DTAB microemulsion latex particles with varying S ratio. Scale bars = 50 nm (4.2(a), 4.2(b)) and 1000 nm (4.2(c), 4.2(d)).

Figure 4.3: TEM image of PMMA nanoparticles prepared by microemulsion polymerisation. Scale bar = 100 nm.

4.3.2 Styrene emulsion characterisation

Substitution of the monomer styrene for MMA in the previous procedure yielded cloudy emulsions which creamed in approximately fifteen minutes to give a monomer rich layer above a microemulsion. What follows is data collected on the homogenised systems.

The data presented in figure 4.4 show the relative populations of droplet sizes weighted by volume fraction, and as such the observed maxima are shifted to larger droplet diameters *cf* an equivalent number weighting. In displaying the information in this manner the reader is provided a fuller picture than would be the case with a number weighted population, which would show very little (if any) of the larger droplet population.

All of the emulsion dispersions are observed to be polydispersed, with droplet diameters ranging from ~50 nm to ~100 μm. There appear to be few trends evident across this series of compositions, excepting that in each case the emulsion system comprising the greatest fraction of styrene contains the greatest population of smallest droplets. Addition of other species, be it difunctional monomer (DVB) or solvent,

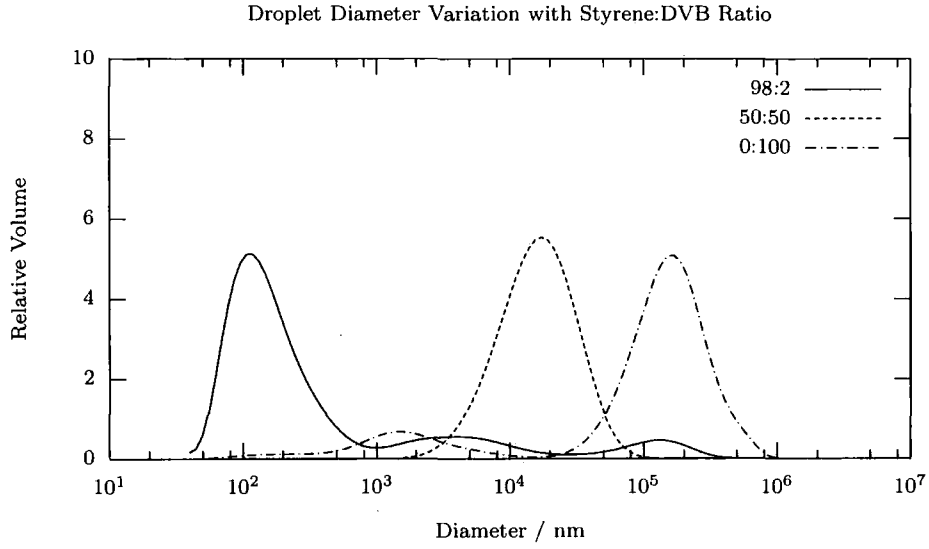

(a) 100 % monomer

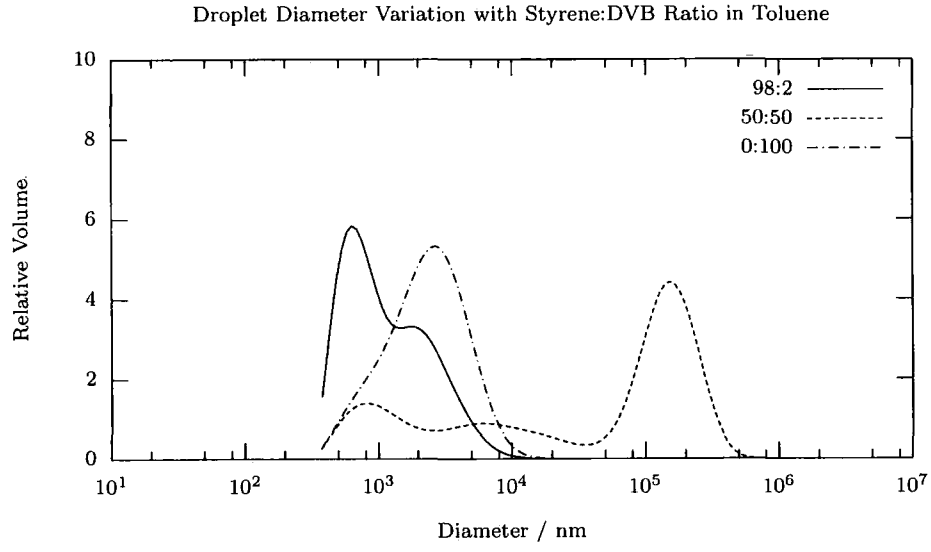

(b) 50% monomer, 50 % toluene

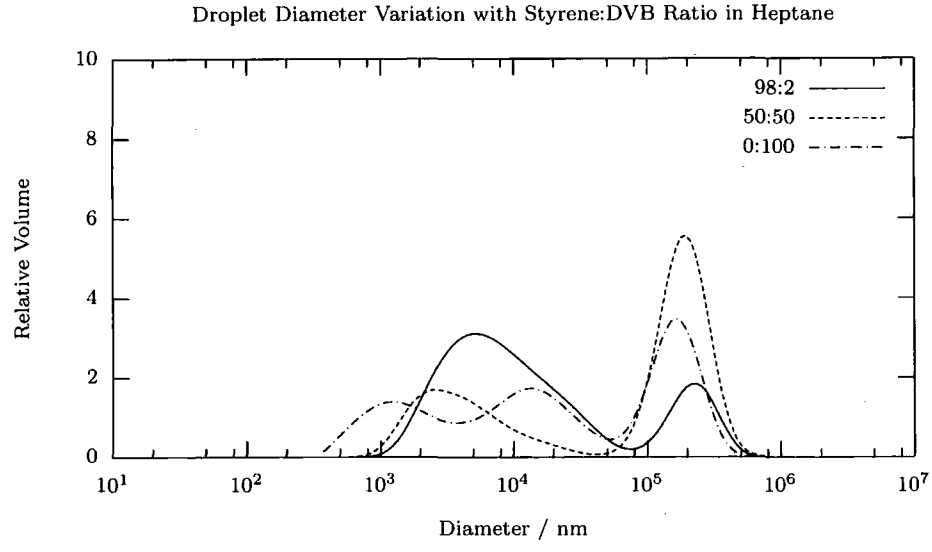

(c) 50% monomer, 50 % heptane

Figure 4.4: DLS data showing emulsion droplet size variation with varying styrene:DVB content (weight ratio) in the presence of solvent (50 wt% monomer, 50 wt% solvent).

Table 4.1: Table of Solvent Solubility Parameters and Mean Emulsion Droplet Diameter.

	δ^a MPa$^{1/2}$	Mean Droplet Diameter^b / μm
DVB[47]	19.0	
Styrene[48]	19.0	0.1^c
Toluene[48]	18.2	1^d
Heptane[48]	15.1	10^d

^{a}Data from referenced sources. ^{b}Data acquired by DLS. Emulsions comprising (by weight) 98:2 styrene:divinyl benzene; ^{c}monomer only, also ^{d}at 50:50 mixture with the corresponding solvent.

yields a shift to larger droplets than is the case for styrene alone, which may be due to alteration of the dispersed phase polarity. This is most clearly demonstrated in the case of 98 % styrene samples, in which the addition of solvent with increasingly lower solubility parameters (table 4.1) than styrene causes a shift to greater droplet diameter. Furthermore, it is likely that the presence of the additional heptane has a greater influence over droplet size distribution than the relative DVB and styrene content as these trends (in figure 4.4(a)) are completely masked and a more uniform set of data presented (figure 4.4(c)).

4.3.3 Kinetic measurements

The rate of consumption of monomer over the course of the polymerisation is shown in figure 4.5. The plot is consistent in form with published studies on the kinetics of emulsion polymerisation,[20] and consequently it is stated that the mechanism of polymerisation here is likely to be that of a classic emulsion polymerisation. Further supporting evidence for this reaction mechanism comes from the evolution of particle size with time, shown in figure 4.6, where growth is apparently uniform and polydispersity essentially constant throughout. These TEM images suggest that intervals I and II are completed rapidly, since this corresponds with micelle consumption and the cessation of new particle nucleation (thus an approximately constant polydispersity is observed even with increasing conversion).

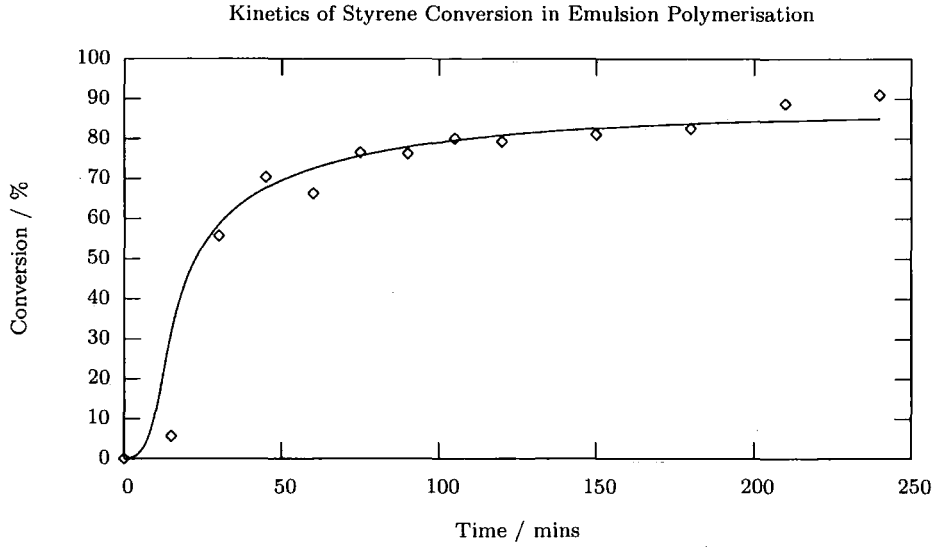

Figure 4.5: Kinetics of polystyrene latex particle formation by emulsion polymerisation. Emulsion composed of water:DTAB:DDAB:styrene:DVB 90:3.75:1.25:4.9:0.1 by weight. Data obtained by Raman spectroscopy.

4.3.4 Polystyrene particle characterisation

Particles were recovered at unoptimised yields of ~80 %. Losses were made at each stage of recovery and purification, most notable being the soxhlet wash in which an appreciable amount of particle slurry was left in the soxhlet 'finger'.

Particle size

Particle sizes are compared to the emulsion dispersions in figures 4.7 to 4.9 (page 33 to 35). In each case, the particle size is greatly reduced (typically under 100 nm) in comparison to the emulsion system and in most cases the polydispersity is significantly narrowed (spanning approximately one order of magnitude for particles from about four orders of magnitude in the case of the parent emulsion). TEM images confirm the relatively narrow range of particle sizes (figures 4.10 and 4.11, pages 36 and 37). These results indicate that the emulsion systems are not in themselves directly templating the particle size, but instead a classical emulsion polymerisation

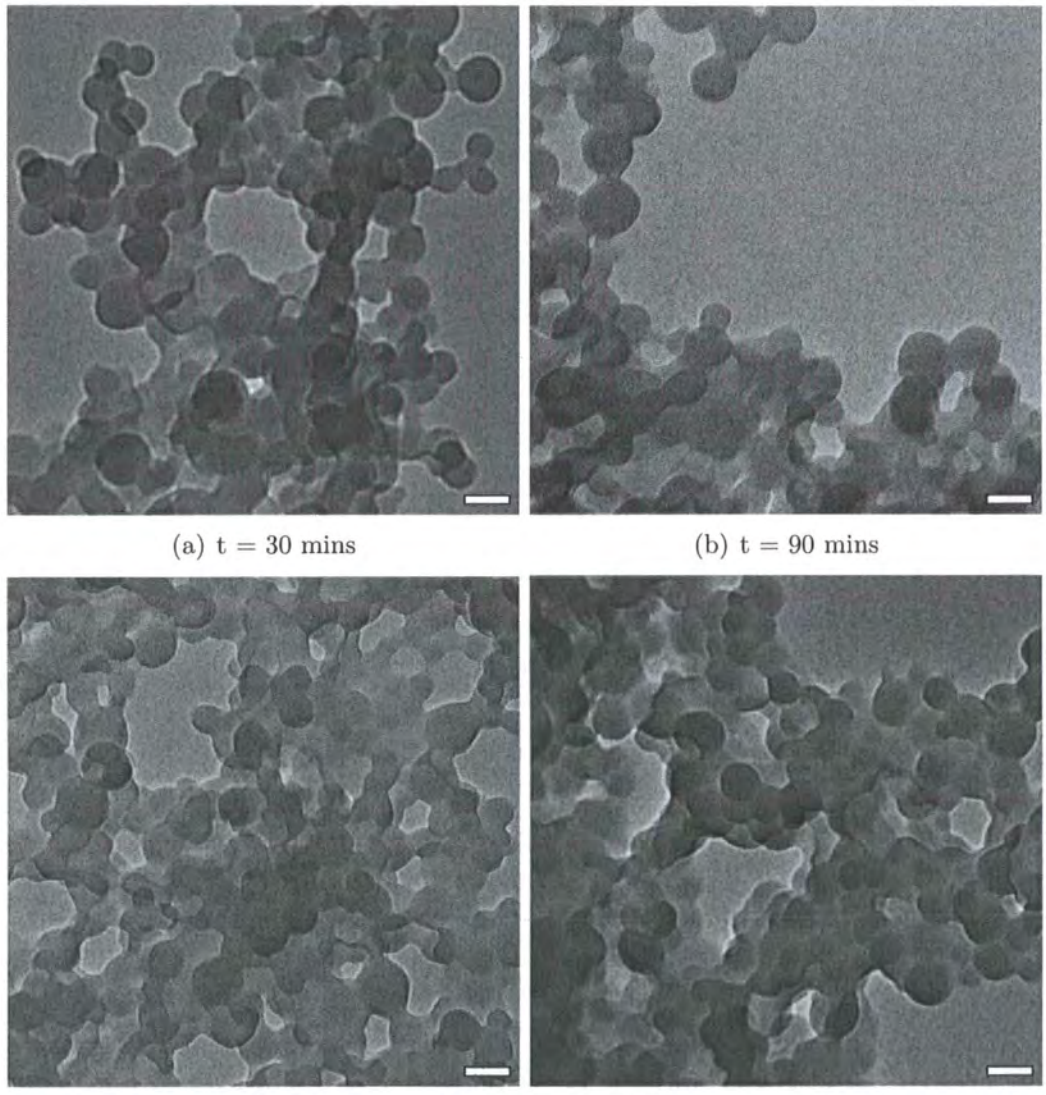

(a) t = 30 mins (b) t = 90 mins

(c) t = 300 mins (d) t = 24 hours

Figure 4.6: Time resolved TEM images of particle synthesis (emulsion comprises 90 wt% water, 5 wt% surfactant (3:1 weight ratio DTAB:DDAB), and 5 wt% monomer (98:2 weight ratio styrene:DVB)). Scale bars = 100 nm.

mechanism is most likely in action whereby larger droplets are acting as monomer reservoirs to feed the growing particles.

Maxima in populations of particle diameter fell below 100 nm for all compositions, except 98 % styrene in the presence of heptane. These maxima lie at higher diameters for lightly crosslinked particles in all cases (i.e. when prepared in both the presence and absence of solvent). Particle diameter then decreases with increasing DVB content.

It may be expected that those latex particles most lightly crosslinked would present at a higher diameter than more crosslinked particles as lightly crosslinked materials posses greater scope for swelling in good solvents. Particle size variation between the two more highly crosslinked compositions is comparatively much less pronounced (figure 4.7(b)). The DLS data corresponding to samples prepared in the presence of solvents do not appear to support this statement, and so reference is paid to TEM image analysis, in which it is clear that the particle diameters are in fact comparable (figure 4.10).

Particle morphology

Particles synthesised in both the absence (figure 4.11) and the presence of inert solvents (figure 4.10) are smooth spherical structures, lacking internal structure. The apparent core-shell morphology observed in images 4.10(a) and 4.10(b) are most likely to be artefacts of drying, in which residual THF is trapped inside the particles due to drying under slightly different conditions (an apparent core-shell like morphology is also detectable in figure 4.6(b), page 31). The alternative explanation, the formation of a core-shell structure, is extremely unlikely as this is typically observed only when a two-stage monomer addition process is used,[16] and is not observed to occur spontaneously in this way.

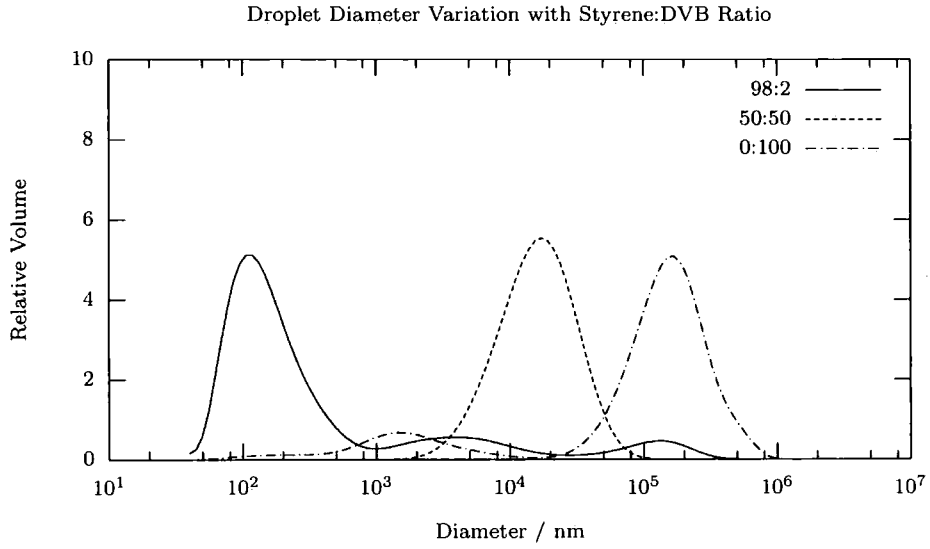

(a) Emulsion Droplet Size Distribution

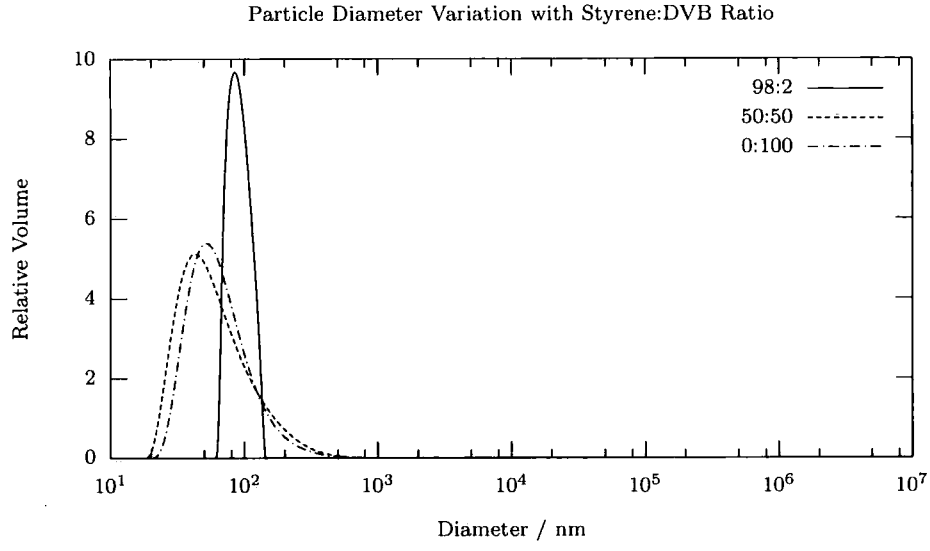

(b) Particle Size Distribution

Figure 4.7: Emulsion droplet and particle size variation with varying styrene:DVB content. Data measured by DLS (top: emulsion (90 wt% water, 5 wt% surfactant (3:1 weight ratio DTAB:DDAB), and 5 wt% monomer (composition shown)) diluted in water, bottom: particles dispersed in THF).

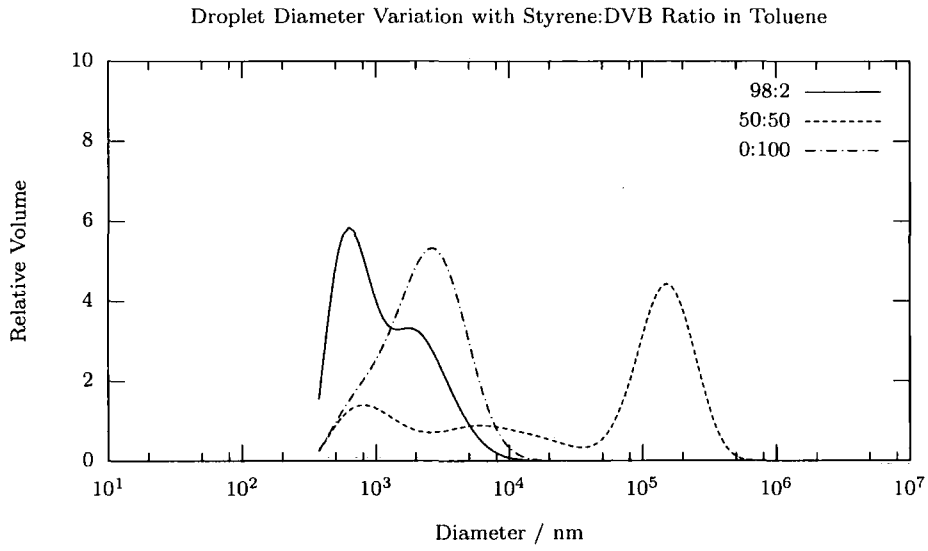

(a) Emulsion Droplet Size Distribution

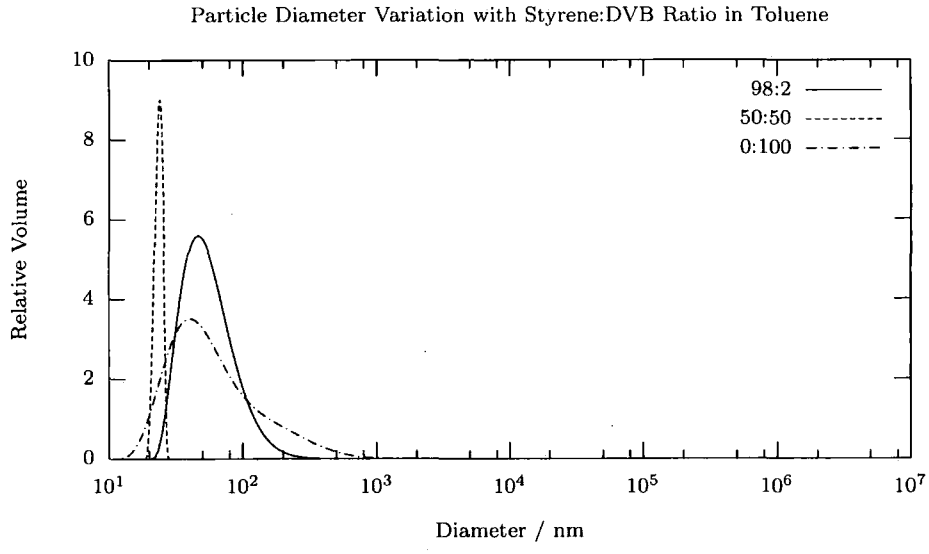

(b) Particle Size Distribution

Figure 4.8: Emulsion droplet and particle size variation with varying styrene:DVB content in toluene. Data measured by DLS (top: emulsion (90 wt% water, 5 wt% surfactant (3:1 weight ratio DTAB:DDAB), 2.5 wt% toluene, and 2.5 wt% monomer (composition shown)) diluted in water, bottom: particles dispersed in THF).

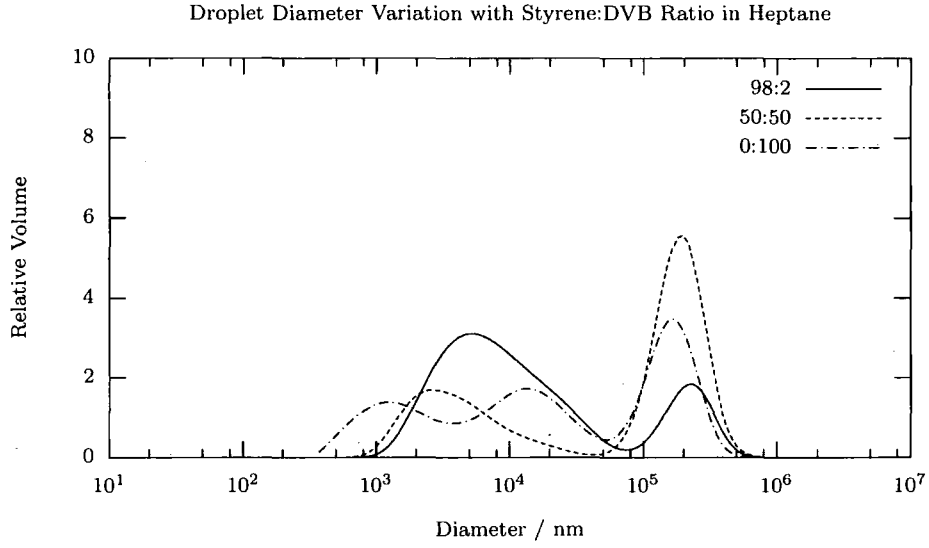

(a) Emulsion Droplet Size Distribution

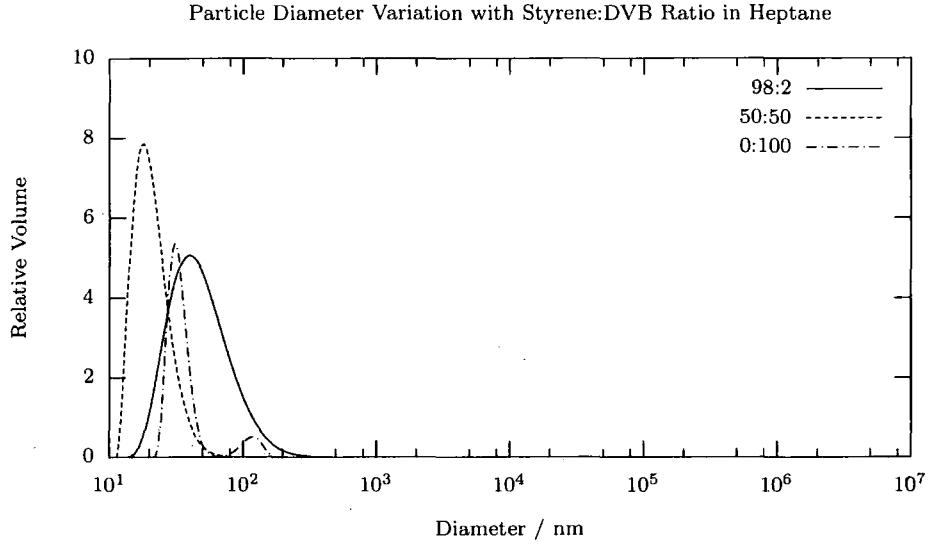

(b) Particle Size Distribution

Figure 4.9: Emulsion droplet and particle size variation with varying styrene:DVB content in heptane. Data measured by DLS (top: emulsion (90 wt% water, 5 wt% surfactant (3:1 weight ratio DTAB:DDAB), 2.5 wt% heptane, and 2.5 wt% monomer (composition shown)) diluted in water, bottom: particles dispersed in THF). Note that particles of composition 98:2 above 450 nm diameter are not displayed due to filtration.

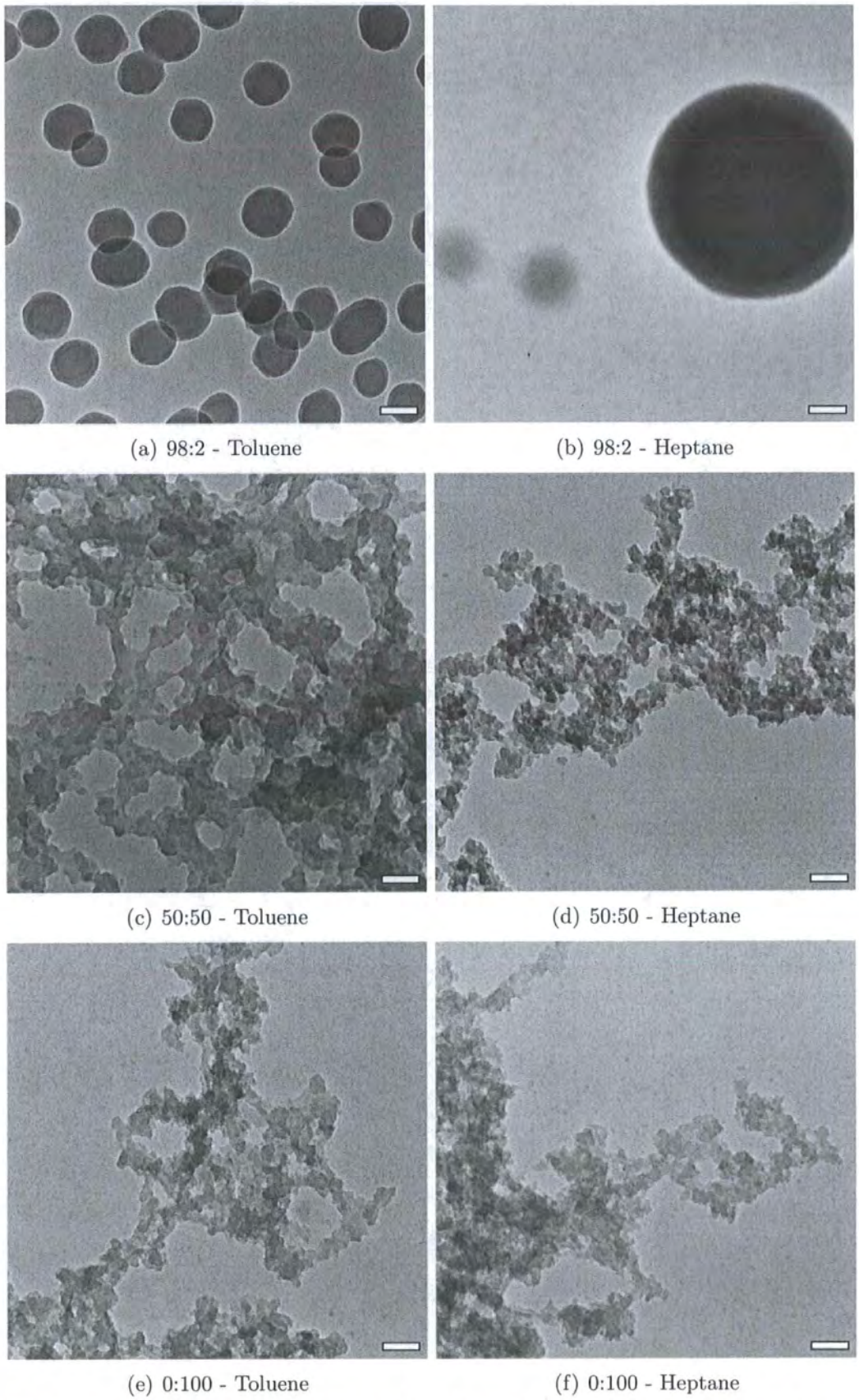

(a) 98:2 - Toluene

(b) 98:2 - Heptane

(c) 50:50 - Toluene

(d) 50:50 - Heptane

(e) 0:100 - Toluene

(f) 0:100 - Heptane

Figure 4.10: TEM images showing particle size & morpholgy variation with composition ratio styrene:DVB, comprising 50 wt%, 50 wt% solvent (as listed). Scale bars = 100 nm.

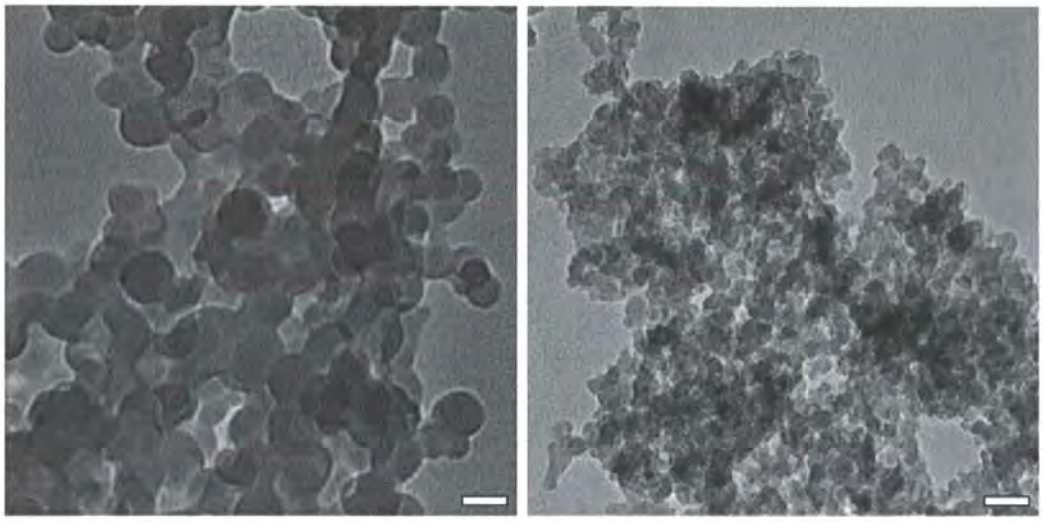

(a) 98:2 (b) 50:50

Figure 4.11: TEM images showing particle size & morpholgy variation with composition ratio styrene:DVB. Scale bars = 100 nm.

4.3.5 Surface area and porosity

A typical N_2 isotherm is shown in figure 4.12. The isotherm is most similar to a Type II isotherm by IUPAC definition.[49] The very early plateau in the adsorption isotherm shows the low monolayer coverage of the sample. The absence of a significant hysteresis is indicative of a lack of porous structure, and that small hysteresis observed is attributable to void space between particles. Consequently, the calculated surface area of the sample is a measure of the external surface only; no micropores are observed by this technique. Pores reported by the analysis are of the lengthscale of the particles, and therefore relate to the packing spaces between the particles in the dry state.

4.4 Conclusions and summary

Polystyrene particles prepared from SDS and pentanol stabilised emulsion systems were polydispersed. Equally, MMA particles from microemulsion polymerisation

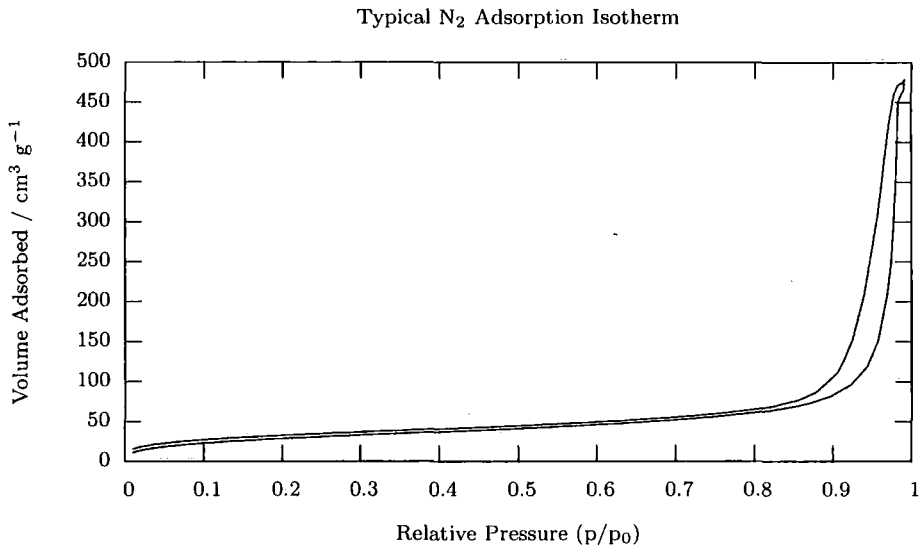

Figure 4.12: Typical N_2 sorption isotherm, specifically of 98% styrene, 2% DVB particle sample.

were also polydispersed with respect to particle diameter even though the parent emulsion was, by definition, monodispersed.

The copolymerisation of styrene with varying degrees of crosslinking DVB was carried out by a classic emulsion polymerisation mechanism, as determined by following conversion with time. Interval I was completed at low conversion, and particle size was observed to remain constant from the onset of interval II. The resulting latex particles were small (<100 nm diameter) monodispersed, non-porous microgel powders, showing no porosity in the dry state. Additional use of porogenic solvents failed to generate microporosity, and had little influence over the final properties of the latex particle, except for the case of heptane addition to 98 % styrene emulsion, in which case a bimodal particle distribution was generated. Although this solvent appeared to have a greater effect over the emulsion droplet size and polydispersity than the styrene:DVB ratio did, the particle morphologies produced from these emulsions at higher DVB content were very much comparable to the equivalent latexes prepared in the presence of no solvent, and in toluene. It is therefore concluded that the presence of solvent has little effect when crosslinker content is very high (>50 %).

Table 4.2: Summary table of poly(styrene-*co*-divinylbenzene) nanoparticles. Duplicates shown for ease of comparison.

Sample	Composition[a]				Particle Sizing[b]			Physisorption Data		
	Monomer		Solvent		DLS		TEM			
	Styrene	DVB	Toluene	Heptane	Emulsion ⊘ / μm	Particle ⊘/ nm	Particle ⊘/ nm	B.E.T. Surface Area / $m^2\ g^{-1}$	B.E.T Pore ⊘ / nm	Micropore Vol. / $cm^3\ g^{-1}$
6011001	98	2	-	-	0.1	100	100	106	11	nil
6062301	50	50	-	-	20	50	25	326	13	nil
6062701	0	100	-	-	100	50	25	494	8	nil
6011001	98	2	-	-	0.1	50	100	106	11	nil
6070701	49	1	50	-	1	50	100	130	13	nil
6081101	49	1	-	50	10	50[c]	550[c]	7	8	nil
6062301	50	50	-	-	20	50	25	326	13	nil
6080901	25	25	50	-	10	25	25	447	7	nil
6080801	25	25	-	50	100	25	25	484	8	nil
6062701	0	100	-	-	100	50	25	494	8	nil
6071901	0	50	50	-	100	50	25	518	6	nil
6072001	0	50	-	50	100	50	25	601	6	nil

[a]Compositions by weight %. AIBN : monomer ratio consistently 1:100 by weight. [b]Value listed refers to largest peak where multimodal. [c]Bimodal distribution. ⊘ denotes diameter.

All data collected on polystyrene-*co*-divinylbenzene nanoparticles are included in summary table 4.2.

Part II

Hypercrosslinked Nanoparticles

One learns by failing.

Silk Road Fortune Cookie

Chapter 5

Literature Review

The aim of this chapter is to present a summary of the literature published on the subject of porous and hypercrosslinked polymer particle synthesis and characterisation, paying particular attention to the preparation of hypercrosslinked polymer particles.

5.1 Introduction

Porous polymers have great potential in the fields of cell growth and heterogeneous chemistry. In the former case, monolithic structures have been demonstrated to have optimum pore and strut sizes for cell attachment and growth, in the latter case, again monolithic structures show promise for through-flow chemistry,[50] in which a catalyst can be anchored to the polymeric support, similar to MCM-41 and zeolite type materials. Porous polymeric beads have been employed in such applications as ion exchange resins and SEC media, and also as supports for chemical reactions such as peptide synthesis.[51] These particles are described as macroporous,[52] a definition referring to the presence of an open porous structure in the dry state and *not* relating to the size of the pores.

For the application that is the motivation for this thesis, it would be required that the particles be macroporous in the predefined sense while also having a much larger pore volume than typical of those macroporous particles previously mentioned.

5.2 Conventional networks

5.2.1 Porous gels

Microgel particles, such as described by Antonietti et al,[53,54] are intermediate between macroscopic networks and branched linear polymers, possessing properties associated with each such as a crosslinked structure and low molecular weight respectively. They are typically prepared by polymerisation in the presence of high crosslinker and porogen solvent content,[55] although it is possible to crosslink a linear or branched polymer in ultradilute conditions as an alternative method to produce a microgel.[53,56]

Due to their collapsed nature in which their polymer chains are in very close proximity to each other with little or no free volume, microgels show little appreciable pore volume in the dry state (see Part I). This feature is illustrated by relatively low specific surface areas[55] measure in the dry state, and yet such gels will swell in a good solvent.[57] As the amorphous polymer chains become solvated, so the porous nature of the particles becomes apparent, and the latent pore volume is occupied by the swelling solvent. The degree of swelling is found to be dependent upon the crosslink density, such that a linear increase in solvent uptake is observed as the statistical spacing between crosslinks increases[53,54] (indicative that swelling is restricted by the crosslinks, and thus is typically to the elastic limit of the material). By contrast, such materials show no swelling in a poor solvent[55] and thus the porous structure remains collapsed, as found in the dry state.

Gene delivery has been proposed as a future use for such gel particles,[58] among the other applications already mentioned (chromatography medium, ion-exchange resin and support for peptide synthesis). However, due to their non-porous nature in the dry state, microgel particles would not be suitable for the application at the heart of this thesis.

5.2.2 Macroporous resins

As mentioned in the introduction to this chapter, a macroporous resin has an appreciable pore structure in the dry state. However, as discussed in a thorough review of the topic by Okay,[52] the definition of 'macroporous' has been contested and that used is of Okay's review, for the reasons outlined therein (namely that most common usage dictates this to be the case). The specific surface area of macroporous resins ranges, depending upon the composition of the dispersion used in their synthesis, up to $\sim$1000 m^2 g^{-1}, and arises in part from an internal structure comprising macropores (pores >50 nm) and micropores (pores <2 nm).

Classical macroporous resins

Macroporous resins are prepared by the copolymerisation of mono- and di-functional monomers in the presence of an inert solvent; an example system would be the copolymerisation of styrene and DVB in the presence of toluene. The smallest constituent particles of macroporous resins are nuclei of $\sim$10 nm diameter, which are formed in the early stages of the polymerisation and consequently comprise a relatively large quantity of DVB (the DVB is more reactive than styrene due to its difunctional nature, hence is more quickly incorporated into the growing polymer chains). These highly crosslinked nuclei are essentially non-porous (as is the case for gel particles). Aggregation of the nuclei forms secondary particles (microspheres)

of ~100 nm diameter, which pack to form the macroporous resin. The interstitial spaces between microspheres and between the nuclei that make up the microspheres determine the pore size distribution of the particle. Typically, the packing of the nuclei generates micropores (<2 nm) and the packing of microspheres generates mesopores (2–50 nm) and macropores (>50 nm).[52]

In the formation of macroporous resin particles the nature of the porogen and the relative amount of crosslinking monomer are balanced, serving to mediate the phase separation of the crosslinked polymer and thus control the nature of the particles produced. Phase separation (precipitation of the microsphere polymer particles) occurs when the monomer and (porogen) solvent mixture can no longer support the growing crosslinked polymer phase. At the point of phase separation, both microsphere and solvent phases contain monomer and crosslinker which, after further reaction, fuse the microspheres in the approximate conformation as found at the point of phase separation. Consequently, it is apparent that the point of phase separation is crucial in determining the particle's pore structure. If a good solvent for the polymer network is used then phase separation occurs at high conversion, thus only sufficient monomer is left to fuse the microspheres and a porous structure results. If phase separation occurs early in the polymerisation then a relatively large quantity of monomer remains unreacted; unreacted monomer thus fuses the microspheres together and also fills the voids between microspheres, reducing the porosity of the particle. If phase separation is not observed at all (as may be the case if too little porogen or crosslinker is used) then a gel type resin is produced.[59]

The porogens employed in macroporous polymer particle synthesis are typically small molecules such as solvents, for example toluene. A special case of molecular porogen is supercritical carbon dioxide,[60] used to prepare sub 100 nm polymer particles with extremely high dry-state surface areas (>2000 $m^2\ g^{-1}$).

Different species have been demonstrated capable of behaving as porogens. Increased control over particle morphology has been exercised by inclusion of oligomeric poly-(propylene glycol) in combination with toluene,[61] while swollen oil-soluble surfactant micelles have a similar influence in the o/w suspension polymerisation of styrene and divinylbenzene.[62]

The properties of macroporous resins can be affected by post-synthesis treatment. The porous structure of particles was found to collapse when dried from good solvents, but then could be re-established by re-solvating and drying from poor solvents.[63,64]

Multi-hollow macroporous resins

Although a number of multi-hollow particle syntheses are reported in literature, no group appears to have studied hollow or pore structure by any intrusion technique (N_2 sorption or mercury porosimetry). Consequently, it is not possible to state whether or not such particles are macroporous with respect to having accessible porosity in the dry state, although it is arguable that an open porous structure does exist as ascertained by TEM analysis.[65–67] Other claimed multihollow particles lack supporting evidence from both intrusion measurements and TEM analysis, and can therefore only be claimed to possess pocked surfaces[68,69] as opposed to true hollows.

5.3 Hypercrosslinked polymers

In contrast to the macroporous resins discussed previously, hypercrosslinked polymer networks are prepared by a two-step reaction, and lack internal macro-structure. Instead, the porosity present in such particles comes from the locking-in of the swollen state of a gel, hence porosity is of the molecular length scale alone (i.e. only

micropores are present). The specific surface areas of such materials can measure as much as 2000 $m^2\ g^{-1}$.

5.3.1 Solution phase bifunctional hypercrosslinking

The hypercrosslinking reactions involving monomers with aromatic side groups discussed in this review require a Friedel-Crafts reaction to generate the characteristic microporous structure that is accessible in the dry state. A wide range of styrene polymer architectures and molecular weights is readily available upon which hypercrosslinking reactions can be executed, achieved using a variety of crosslinking agents. In early work, agents such as monochlorodimethyl ether in conjunction with the Lewis acid stannic chloride were used to hypercrosslink linear and lightly crosslinked polystyrenes in dilute solution.[70] Surface area and pore volume measurements showed the resulting polymers to be highly porous and possessing micropores.

Solution phase polymerisation of reactive precursors, in effect the hypercrosslinking of a hypercrosslinking agent alone, has more recently been demonstrated as a means to producing hypercrosslinked polymers.[71] An example of such a reaction is the Friedel-Crafts self condensation of *p*-xylylene.

5.3.2 Gel phase hypercrosslinking of functional precursors

Copolymers of VBC (vinyl benzyl chloride) and DVB can be prepared in much the same way as styrene-DVB copolymers, resulting in lightly crosslinked gel resins with an abundance of benzyl chloride moieties on which to affect Friedel-Crafts alkylation reactions[72–76] (reaction mechanism shown in figure 5.1). It is conceivable that a similar effect may be achieved by alternative means, e.g. through reaction of the benzyl chloride moieties with short chain diols.

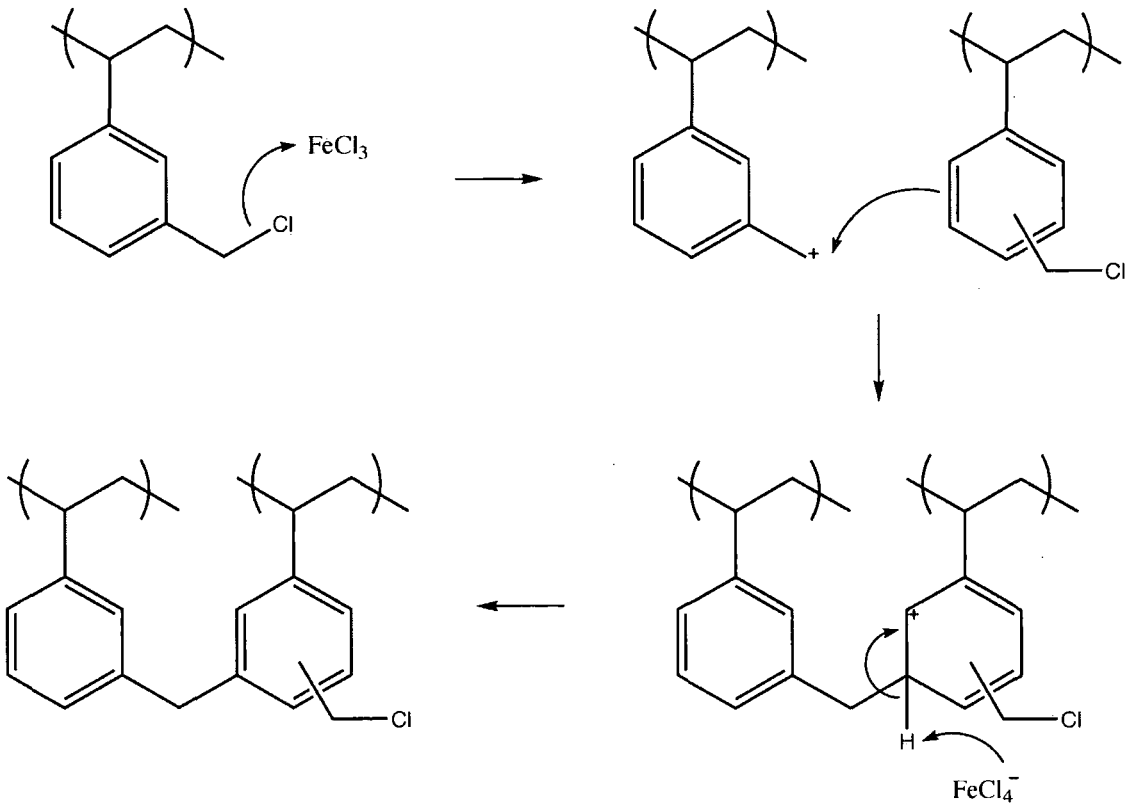

Figure 5.1: Mechanism of Friedel-Crafts alkylation (hypercrosslinking) of VBC.

This general approach removes the carcinogenic risks associated with the hypercrosslinking agents mentioned previously as the reactive moieties are built in to the polymer particle. Hypercrosslinked nanoparticles of ~400 nm diameter have been synthesised using this gel precursor and Lewis acid approach, with the precursor particle prepared in a surfactant free emulsion.[76] Although it is known that VBC undergoes hydrolysis[77] (therefore reducing the benzyl chloride content), microporosity and surface areas in excess of 1200 $m^2\ g^{-1}$ were generated. The solvent used for the hypercrosslinking step (DCE) is insufficiently reactive for it to take part in the Friedel-Crafts reaction as a reagent.

Chapter 6

Experimental

*The aim of this chapter is to explain the experimental procedures used in the synthesis of poly(vinylbenzyl chloride-*co*-divinylbenzene) particles and the subsequent hypercrosslinking thereof.*

6.1 Introduction

The synthesis of nanoparticles of $\leq$50 nm diameter was discussed (and achieved) in Part I through an emulsion-type polymerisation technique. As introduced in the previous chapter, syntheses exist whereby lightly crosslinked pVBC particles are internally hypercrosslinked through the action of Lewis acids via Friedel-Crafts alkylation, generating open porous structures and ultra-high surface areas. The aim of this work is to marry the two approaches, resulting in hypercrosslinkable nanoparticles of $\leq$50 nm in diameter.

6.2 Synthesis

6.2.1 Materials

Styrene (99%, Sigma) and DVB (80%, mixed isomers, Aldrich) were washed over basic alumina (Activated Basic, Brockmann type II, Aldrich) to remove inhibitor before use. VBC (>95%, mixed isomers, inhibitor free, Fluka), DTAB (98%, Aldrich), DDAB (98%, Aldrich) KPS (99+%, Sigma Aldrich), 2,2-azobis(2-amidinopropane) dihydrochloride (V-50, 97%, Sigma Aldrich), 1,2-dichloroethane (DCE, 99+%, Sigma), iron(III) chloride (97%, Aldrich), potassium iodide (99%, Sigma-Aldrich), DMF and THF (both Laboratory Reagent Grade, Fisher Chemicals) were all used as supplied. AIBN (Fluka) was recrystallised according to a published method.[44]

6.2.2 Surfactant-free emulsion polymerisation

Polymerisations were carried out in a baffled reactor vessel with a twin bladed impeller, similar to reported literature.[76] Distilled water (500 ml) was heated to 75 °C and under stirring at 500 rpm, then the comonomer mixture (totalling 26 ml) was added. The dispersion was stirred for ~15 minutes before addition of initiator solution (440 mg V-50, 20 ml water). The polymerisation was permitted to proceed under stirring for 18 hours before allowing to cool to room temperature (still under stirring). Once cooled the polymer latex dispersion was decanted into round bottom flasks and freeze dried. A free flowing white powder was recovered.

In testing the effect of the initiator, an equivalent molar concentration of KPS was added in place of V-50.

6.2.3 DTAB / DDAB emulsion polymerisation

Precursor particle synthesis I

Syntheses were undertaken using emulsion compositions similar to Part I. Syntheses were initially carried out in round bottomed flasks with magnetic stirrer bars as described on page 20, section 3.2. However, in this variation of the synthesis the flask was charged with 85 g of water, VBC was used for 98 wt% of the monomer phase, DVB making up the remaining monomer. Initiator (10 mg g^{-1} monomer, solution in 5 ml water) was added by syringe, and the reaction allowed to proceed for 18 hours.

Precursor particle synthesis II

The above emulsion mixture was used in a baffled reactor vessel equipped with a twin bladed impeller, stirred at 500 rpm, as for the surfactant-free emulsion polymerisation synthesis. Initiation was attempted by AIBN (which was dissolved in the monomer phase prior to its injection into the surfactant solution), and V-50 and KPS (added as solutions by syringe after a well dispersed emulsion was formed).

Particles were recovered by precipitation into methanol before centrifugation at 8000 rpm for 2 minutes. The resulting slurry was washed in the centrifuge tube by shaking in methanol until the washings were free of surfactant (determined by evaporation of the methanol). The cleaned particles were crudely dispersed by shaking in water before freeze drying.

Precursor particle functionalisation

Octadecylamine

VBC gel particles were dispersed in DMF directly from the centrifuge tube, so that the concentration was approximately 1 g in 50 ml solvent. Dispersion was assisted by low powered sonication. Octadecylamine was added in equimolar amount *cf* the VBC content of the particles. A two-fold molar excess of KI was added and the solution heated to 60 °C for 18 hours (similar to the amination of poly(vinyl benzyl chloride-*co*-divinylbenzene) polyHIPE's[78]). Products were isolated by precipitation into methanol, then recovered by centrifugation.

Oleic acid

Synthesis was as above, but with addition of oleic acid.

6.2.4 Hypercrosslinking reaction

Similar to Macintyre et al.,[76] precursor gel particles were dispersed in a baffled reactor vessel with DCE (1 g per 100 ml DCE) by continuous sonication in a low powered sonic bath until a good dispersion was achieved. The dispersion was then stirred at 500 rpm with a twin bladed impeller for 5 minutes before addition of $FeCl_3$ solution in DCE (1 g in 100 ml DCE). The mixture was heated to 80 °C in an oil bath for 18 hours to ensure complete reaction. After allowing to cool to room temperature, DCE was removed by rotary evaporation and the hypercrosslinked particles washed by sequential addition, sonication (15 minutes each) and decantation of aqueous HNO_3, methanol, acetone and water. Finally, the particles were dispersed in water and freeze-dried to yield a free flowing tan coloured powder.

6.3 Analysis

Particle size was measured by DLS as previously described, with calculations based on the assumption that the particles have a refractive index equal to polystyrene. TEM was also used, again as previously described. In this case, particles in water were dropped onto carbon coated copper grids and dried under a hot lamp.

Surface area and pore size distributions were analysed as previously described.

Elemental analysis was carried out using an Exeter Analytical E-440 Elemental Analyser.

Chapter 7

Results and Discussion

The aim of this chapter is to present and offer explanation for the observations made in the synthesis of poly(vinylbenzyl chloride-co-divinylbenzene) particles and the resulting hypercrosslinked particles.

7.1 Surfactant-free emulsion gels

Precursor nanoparticles were prepared similarly to the published work of Macintyre et al.[76] The precursor particles prepared in the work presented here differ from those reported in literature, being a little smaller in diameter, most likely due to differences in the reactor vessel and stirrer dynamics. Similarly to the published findings, a small increase in diameter is observed following the Friedel-Crafts hypercrosslinking alkylation (see figure 7.1), which would be expected of a gel-like particle locked into its swollen state by hypercrosslinks. The observed particle size increase is further supported by TEM imaging (figure 7.2).

Porosimetry measurements again reflect the findings of the published literature. Here, the precursor resin particles show very little N_2 sorption (figure 7.3), and

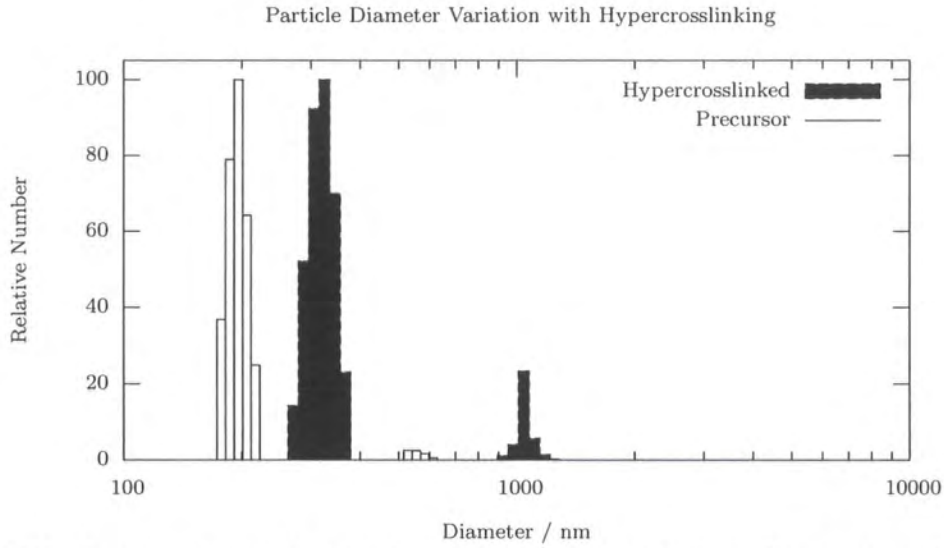

Figure 7.1: Increase in particle diameter with hypercrosslinking reaction, measured by DLS analysis of particles dispersed in THF.

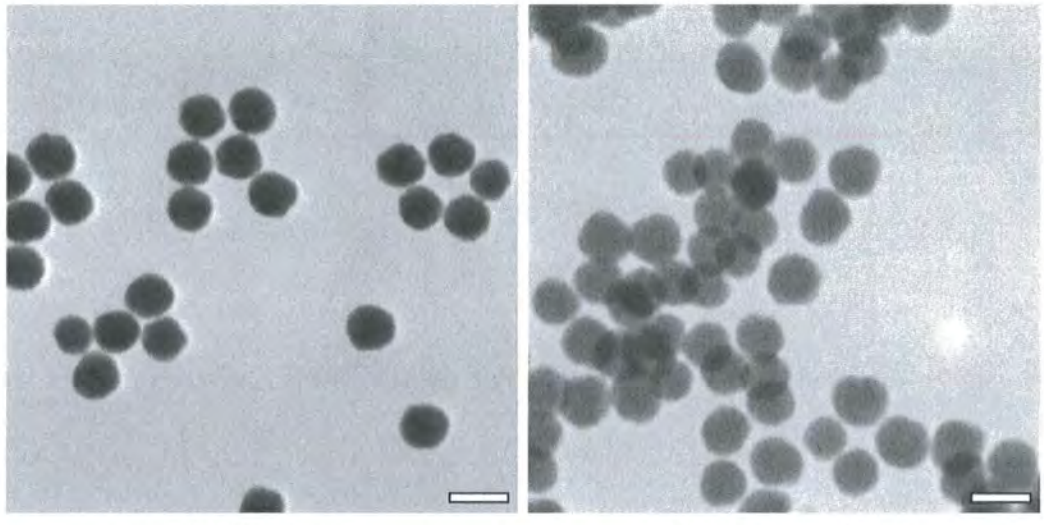

(a) Precursor (b) Hypercrosslinked

Figure 7.2: Precursor and hypercrosslinked nanoparticles imaged by TEM. Scale bars = 500 nm.

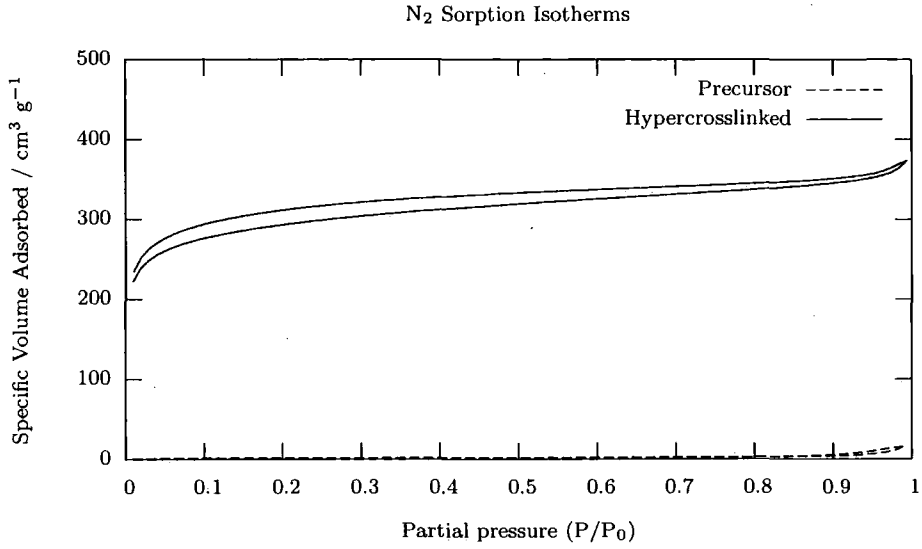

Figure 7.3: N_2 sorption isotherms of gel-like precursor and hypercrosslinked pVBC nanospheres.

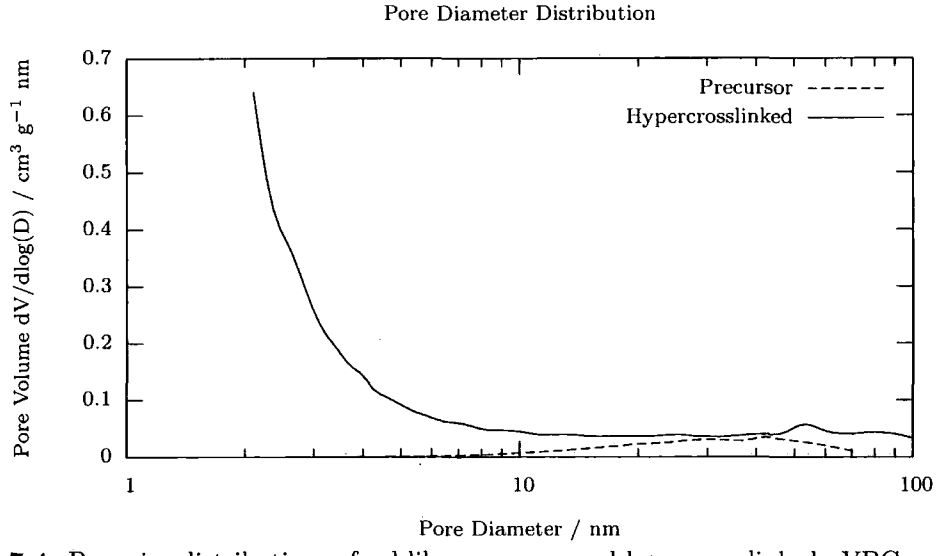

Figure 7.4: Pore size distributions of gel-like precursor and hypercrosslinked pVBC nanospheres calculated from N_2 sorption isotherms.

Table 7.1: Physical properties of precursor and hypercrosslinked pVBC nanoparticles.

Sample	Particle diameter[a] / nm	Specific surface area[b] / $m^2\ g^{-1}$	Micropore vol.[c] / $cm^3\ g^{-1}$	Density[d] / g cm^3
Precursor	200	~10	0.0174	0.0989
Hypercrosslinked	350	~1000	0.5528	0.0774

[a]Measured by DLS. [b]Measured by N_2 sorption, BET analysis. [c]Measured by N_2 sorption, BJH analysis. [d]Measured by He pycnometry.

no microporosity (figure 7.4). The specific surface area of the precursor resins was measured to be <10 $m^2\ g^{-1}$. After swelling and hypercrosslinking, the volume of sorbed N_2 (figure 7.3), microporosity (figure 7.4) and the specific surface area all increased markedly, the latter to ~1000 $m^2\ g^{-1}$. The sorption isotherm for the hypercrosslinked particles is Type I, relating to the microporous strucutre.[49] The specific density (measured by helium pycnometry) is also seen to decrease with hypercrosslinking. These data are summarised in table 7.1.

Elemental analysis showed a decrease in polymer-bound chlorine as the Friedel-Crafts alkylation reaction proceeded (see figure 7.5). The initial chlorine content appears artificially low in figure 7.5, where a value of ~4% is found *cf* an expected value of ~23%. This is most likely due to combined effects of the rapid reaction and the work-up procedure (as $FeCl_3$ was added before isolation of the 'time zero' sample to allow an equivalent comparison with other time intervals). The high rate of the reaction and the observation that the reaction fails to reach completion is in agreement with both published[75] and unpublished[79] data. Expected and measured elemental analyses listed in table 7.2 are in good agreement for nanoparticles. Photographs of the powders illustrate that the sequential washings by sonication yielded a tan powder, indicating that an appreciable quantity of iron remained trapped in the porous particles (see figure 7.6), again correlating with the published findings. The iron content of the final particle product was low, measured by elemental analysis to be <0.05 wt%.

Table 7.2: Elemental analysis of pVBC gel and hypercrosslinked nanoparticles.

Sample	% Carbon		% Hydrogen		% Chlorine		% Iron
	Calc.	Found	Calc.	Found	Calc.	Found	
Precursor	70.80	71.36	5.9	6.12	23.3	22.66	nil
Hypercrosslinked	-	77.83	-	3.86	-	4.04	<0.05

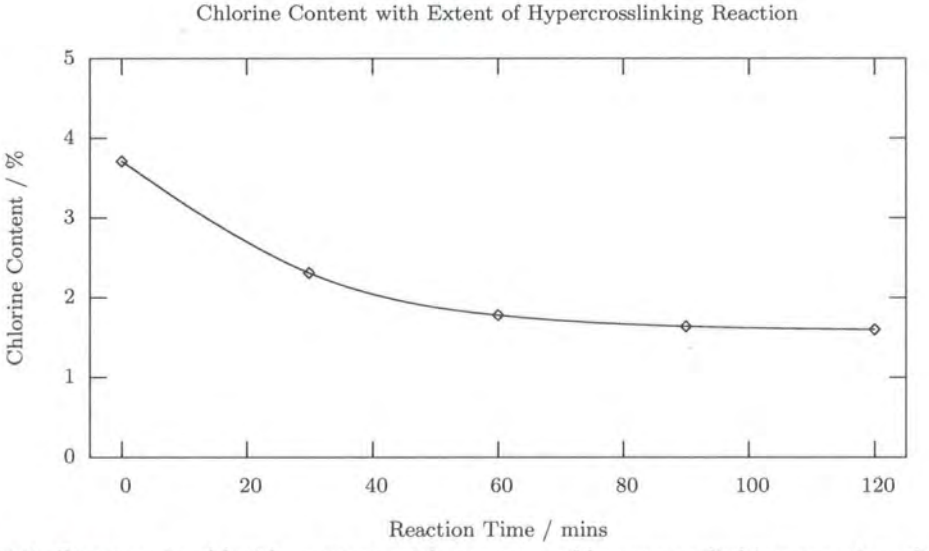

Figure 7.5: Decrease in chloride content with progress of hypercrosslinking reaction, determined by elemental analysis.

(a) Precursor (b) Hypercrosslinked

Figure 7.6: Precursor and hypercrosslinked nanoparticles imaged by photography.

7.2 DTAB/DDAB emulsion gels

7.2.1 Effects of reactor dynamics and initiator fragments

One of the aims of this project was the synthesis of porous particles of diameters less than 50 nm. The emulsion system used to prepare crosslinked polystyrene particles of such dimesions in Part I was here employed for the synthesis of similar particles, but with an appreciable VBC content. Initial attempts at such syntheses were conducted in round bottomed flasks with a magnetic stirrer bars. It quickly became evident that the direct substitution of VBC for styrene was not feasible, as large aggregates of floculum were produced by this procedure. It was rationalised that the emulsion system was unstable leading to droplet coalescence and hence the formation of the floculum. To address the issue the initiator was switched to V-50, as used in the surfactant-free emulsion system, and finally KPS. These initiator fragments possess ionisable or ionised functionality (see figure 7.7) and are aqueous soluble, and consequently would act to stabilise the hydrophobic particle in the aqueous environment. In practice none of these steps yielded any improvement, and so the emulsion was then polymerised in the high shear baffled reactor with impellar, again as used in the surfactant free system. The increased shear served to break up coalescing droplets, however this was with limited success in the case of AIBN and V-50 initiated systems, where large aggregates of polymer were still formed. Only with KPS initiating the polymerisation were stable latex nanoparticles formed, initially confirmed by the blue hue visible in the reactor vessel (figure 7.8). The failure of AIBN can be explained as the initiator fragments offer no additional particle surface stabilisation due to their low aqueous solubility; in contrast, this is provided by the persulfate fragments. It can only be guessed that the V-50 fragments failed to offer sufficient stabilisation in this system, although why this should be the

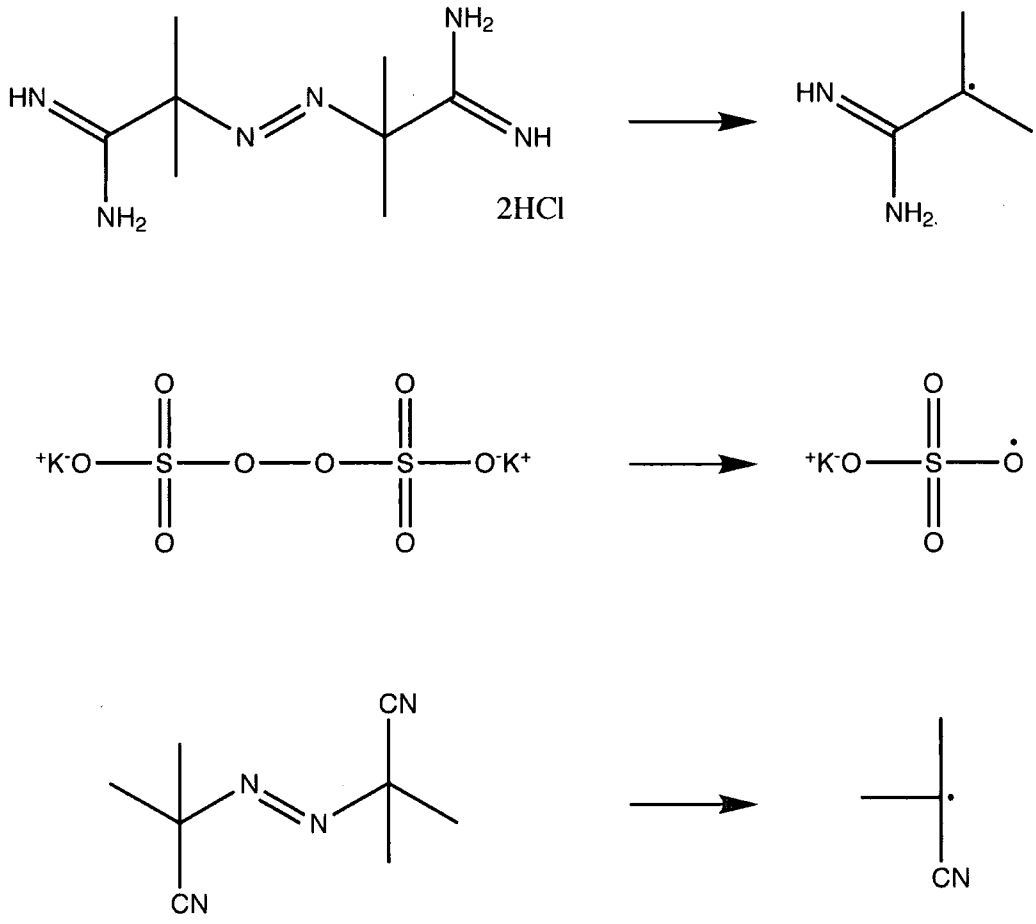

Figure 7.7: Molecular structures of initiators (left) and initiator fragments (right) resulting from thermal decomposition of the initiators. Initiators are (top to bottom) V-50 (aqueous soluble), KPS (aqueous soluble) and AIBN (oil soluble).

case is unknown (although may possibly be due to unfavourable interaction with the surfactant), particularly since the initiator serves well in surfactant-free syntheses.

7.2.2 Effects of surfactant stabiliser

Nanoparticles were prepared by a DTAB/DDAB stabilised emulsion system only when KPS was used as the free radical initiator and high shear was provided through the combination of reactor vessel and stirring method. These nanoparticles, precipitated from the parent emulsion, washed, and redispersed in THF, were analysed by DLS and TEM. Figure 7.9 shows particle size distributions measured by DLS. Particles from the DTAB/DDAB stabilised emulsion copolymerisation of DVB and

Figure 7.8: Latex particles from the emulsion copolymerisation of VBC and DVB in a baffled reactor vessel with twin bladed impellar.

VBC are shown in comparison to similar particles synthesised by the surfactant-free approach, but with KPS as the radical initiator instead of V-50. These data confirm that the surfactant is crucial in acting to stabilise and thereby facilitate the formation of small gel-like nuclei, similar in diameter to those particles synthesised in Part I. Although the composition of the two emulsions varies slightly even when the surfactant is neglected due to the different initiator to monomer ratios, it is with confidence that it is stated that the presence of the surfactant is most important in controlling the particle size (the effect of the nature of the initiator on the particle size of the surfactant-free gel particles was negligible in comparison to the effects of the surfactant (compare figures 7.10(b) and 7.2(a))).

7.2.3 Hypercrosslinking of swollen gels

The gel particles prepared by the surfactant stabilised emulsion system were freeze dried before taking up in DCE for the hypercrosslinking reaction, the same approach as employed in section 7.1. However, redispersion of the dried nanoparticles was not complete, and translucent aggregates of swollen polymer were visible in the dispersion. Similar observations were made when THF was used as the dispersive solvent. Aggregates remained visible even after high powered probe sonication, leading to the conclusion that either chemical bonding or a high degree of entanglement was likely responsible for the irreversible aggregation. It is possible that partial hydrolysis of surface oriented benzyl chloride groups would provide a potential mechanism by which interparticle crosslinking could occur, as illustrated in figure 7.11.

This irreversible aggregation was only observed when the particles were dried down; redispersion occurred readily provided that the particles were transferred to solvent without an intermediate freeze drying step. It was therefore hoped possible that the hypercrosslinking reaction could be carried out on these gel particles, provided that

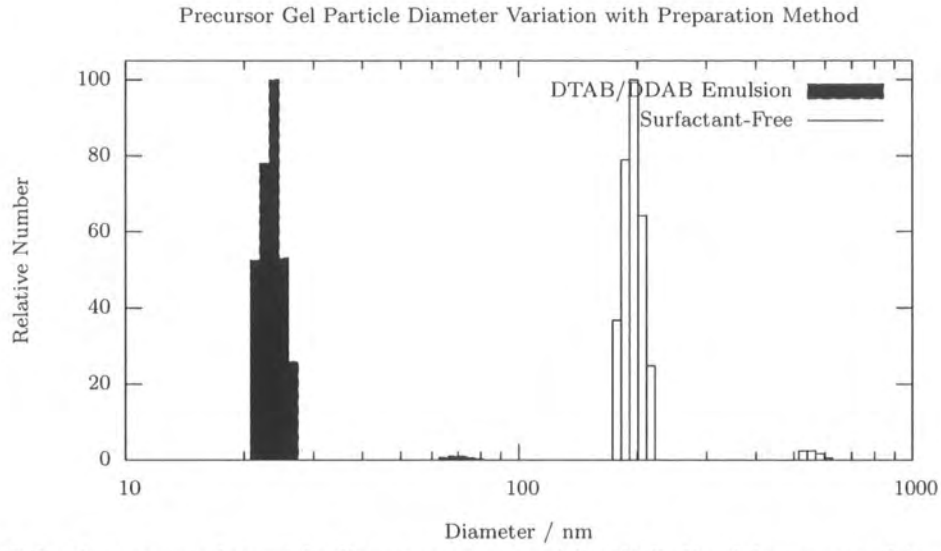

Figure 7.9: Precursor gel particle diameters measured by DLS. Particles prepared in emulsions with and without surfactant (DTAB/DDAB).

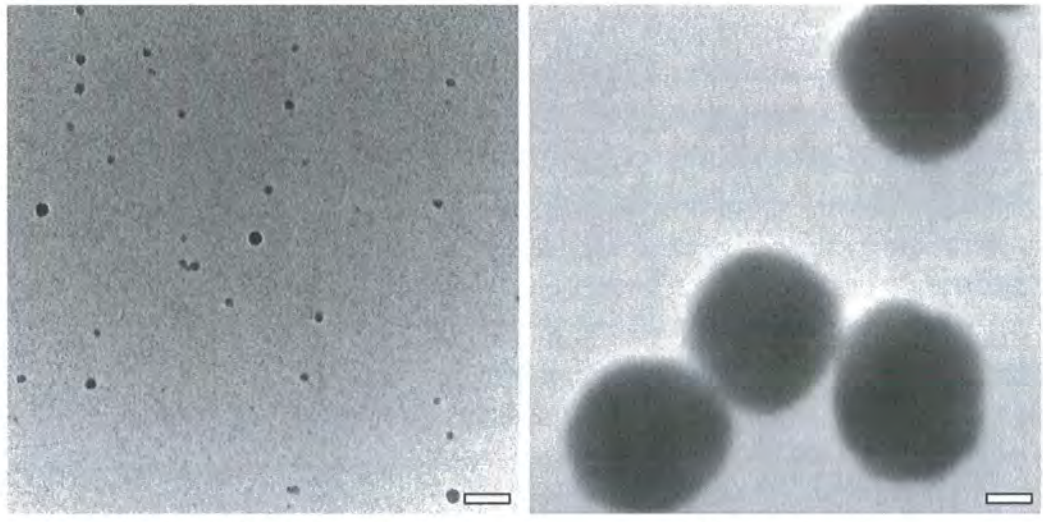

(a) DTAB/DDAB Emulsion (b) Surfactant-free

Figure 7.10: Precursor gel particles imaged by TEM prepared by surfactant and surfactant free emulsions. Scale bars = 100 nm.

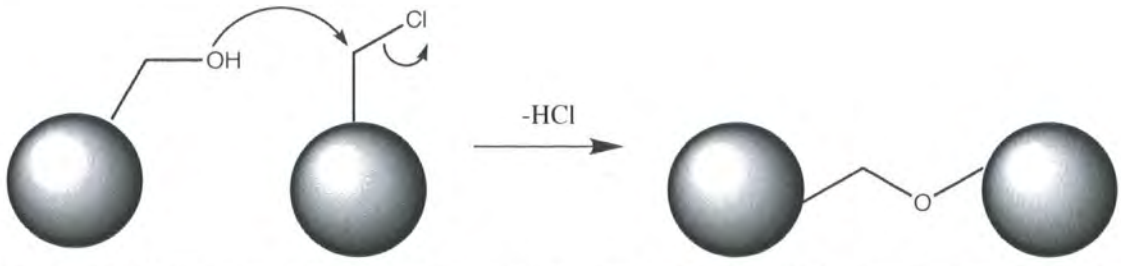

Figure 7.11: Scheme to illustrate the potential mechanism by which crosslinking of particles could occur during freeze drying.

Figure 7.12: Hypercrosslinked ~20 nm precursor gel particles imaged by photography.

they could by dried while in the solvent (to preserve the Lewis acid required for the Friedel-Crafts reaction). Accordingly, precursor gel particles of ~20 nm diameter were isolated from the parent emulsion by precipitation as before, then redispersed in DCE, stirred over a drying agent ($MgSO_4$). The dispersion and slurry were separated by filtration, and at this point the particles dried down by rotary evaporation (to allow a crude determination of the mass of pVBC present). It was determined that there was only approximately 30 % recovery of nanoparticle mass (*cf* the amount expected), the missing mass being retained in the slurry. Redispersion in DCE was successful and the hypercrosslinking reaction undertaken, the product of which is shown in figure 7.12. Ultrahigh surface area (~1000 $m^2\ g^{-1}$) and the presence of micropores were detected by N_2 sorption studies, showing the hypercrosslinking reaction was successful (figure 7.13). Pores of larger diameters were also present, symptomatic of the aggregated nature of the nanoparticles in the hypercrosslinked state.

It was concluded from these findings that the irreversible aggregation of the gel particles occurred only when dried from water, and also that the hypercrosslinking reaction was successful, but that interparticle hypercrosslinking had also occurred.

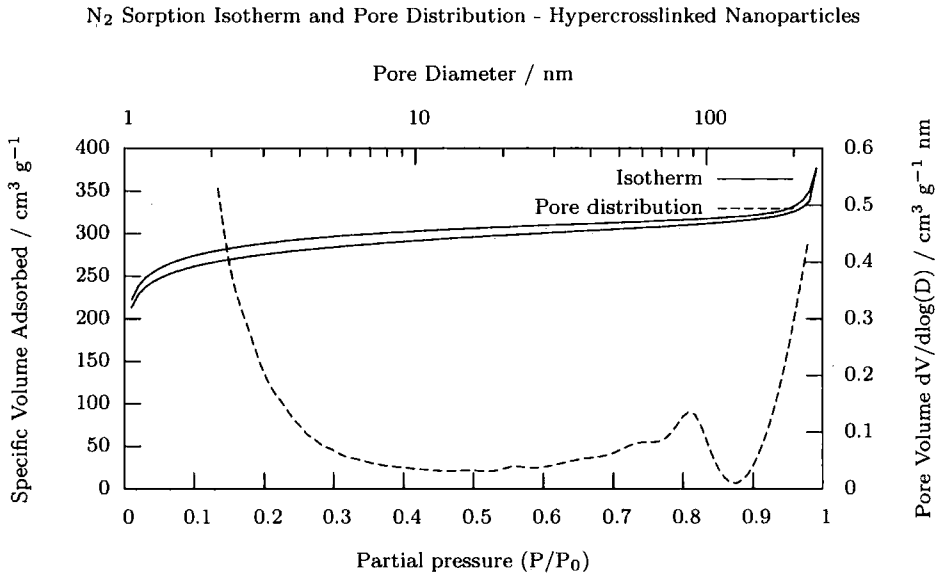

Figure 7.13: N_2 sorption isotherm and pore distribution data calculated from the isotherm. Data related to hypercrosslinked nanoparticles in their final aggregated state.

Neither of these phenomena were found to occur in the surfactant free emulsion gel particles (both V-50 and KPS initiated).

To explain the observations it was necessary to consider the differences between the products of both types of emulsion synthesis. It may be considered that the surfaces of particles prepared in the surfactant free system would be fully hydrolysed, given that they are in direct contact with water during the polymerisation reaction, and hence the coming together of such surfaces in the freeze drying and hypercrosslinking processes would not facilitate a crosslinking reaction to occur. Conversely, the surfactant stabilised particles would undergo hydrolysis at a reduced rate and so would retain an abundance of benzyl chloride groups at their surfaces. Thus, under hypercrosslinking conditions, interparticle hypercrosslinking could occur. This is presented schematically in figure 7.14. Under freeze drying it is possible that a similar crosslinking reaction could occur as illustrated previously (figure 7.11, page 62), however this is unlikely as aprotic conditions are required for such Williamson ether formation reactions to occur (which is not the case here).

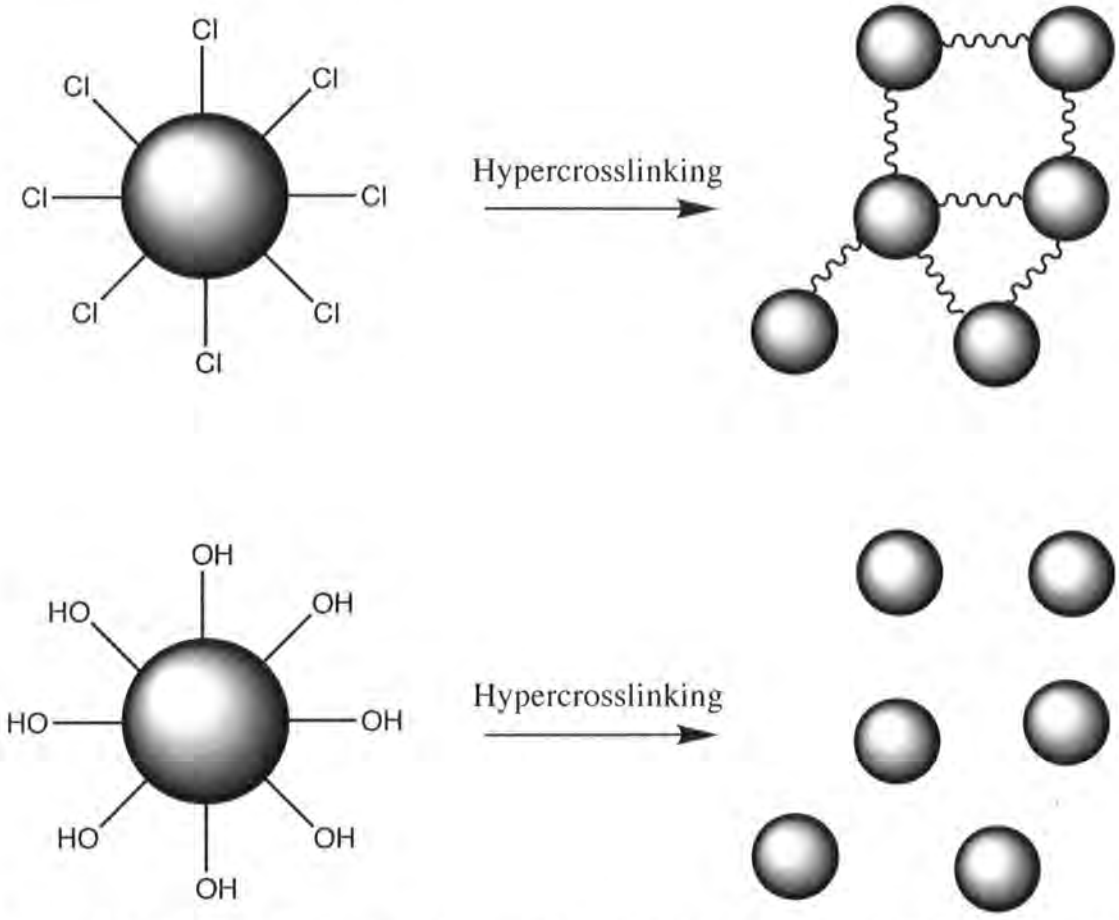

Figure 7.14: Scheme to illustrate the potential mechanism by which crosslinking of particles could occur during freeze drying.

It is necessary to also consider the possible influence of particle size. The particles are not perfect spheres, and hence can be considered to have localised flat, rough surfaces. When small spheres, such as described, come into contact with each other, the relative contact area is greater than with equivalent larger spheres. It could be argued that as a result of this increased relative contact area, the smaller spheres could experience irreversible chain entanglement and remain attached whereas with their larger size and smaller contact area, the larger spheres could, with less entanglement, redisperse.

To determine the most likely explanation, surface chemistry must be investigated.

7.2.4 Surface functionalisation of precursor gels

Hydrolysis

Working on the premise that the difference in hydrolysis rates between the surfactant-free and DTAB/DDAB emulsion syntheses caused a difference in surface chemistry, an hydrolysis of the gel particles was attempted by two approaches. In one case, particles were recovered from their emulsions as described previously and dispersed in acetone, water added to the point of the onset of clouding, and then extra acetone added to ensure a clear (discrete particle) dispersion. The resulting mixture was stirred in the baffled reactor vessel for seven days, heated to 50 °C. Recovery from the solvent and freeze drying still yielded an irreversibly aggregated polymer. The alternative hydrolysis method, the addition of KOH to the polymerised emulsion, also failed to deliver the desired product.

Octadecylamine / oleic acid coatings

It is known that VBC polymers can undergo reactions with amines by attack on the benzyl chloride residue.[78,80,81] Gel precursor particles were reacted with ODA and oleic acid, however spectroscopic evidence to support the success of the reactions was not forthcoming, largely due to the difficulty in separating excess functionalisation reagent from the ~20 nm, surface coated, nanoparticles. Qualitative evidence in support of the success of the reactions came from the redispersibility of the particles post-reaction, with DLS data displayed in figure 7.15.

Hypercrosslinking reactions of these samples were necessarily undertaken in the presence of the excess surface functionalising reagent due to the difficulties in functionalised particle purification. N_2 sorption isotherms and the pore size distribution data are displayed in figures 7.16 and 7.17. These data are at best unreliable due

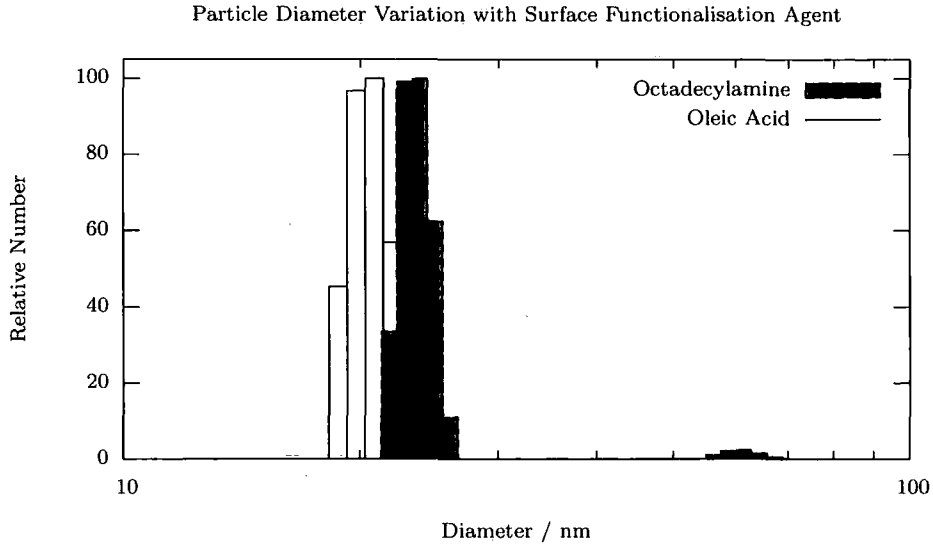

Figure 7.15: DLS data of redispersed, surface coated gel particles in THF.

to the quantity of contaminants present in the analysis, for example, of the ODA coated sample it is unknown how much of the analysis pertains to free ODA, and how much to the polymer sample. Any porous structure may be masked, or pores may be blocked by the excess ODA. It is also probable that the Lewis acid required for the Friedel-Crafts reaction would be less efficient in the presence of ODA. In the case of the oleic acid coated particles, the sample presents as a waxy solid rather than a powder and therefore the meaning of any analysis is questionable.

Although surface functionalisation appears to be a successful method for maintaining discrete particles, it is not yet proven that such an approach can lead to discrete, hypercrosslinked nanoparticles.

7.3 Conclusions and summary

Nanoparticles of ~400 nm, possessing a high VBC content, have been prepared by a surfactant-free emulsion polymerisation, similar to Macintyre et al.[76] The presence of water soluble initiator fragments formed during the polymerisation and bound

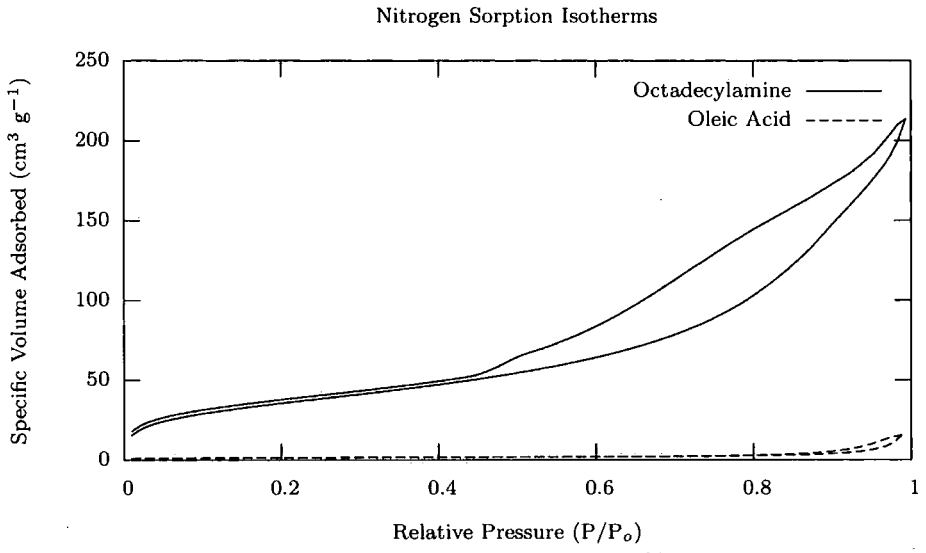

Figure 7.16: N_2 sorption isotherms of lightly crosslinked 98% VBC nanoparticles of ~20 nm diameter, surface coated with octadecylamine and oleic acid.

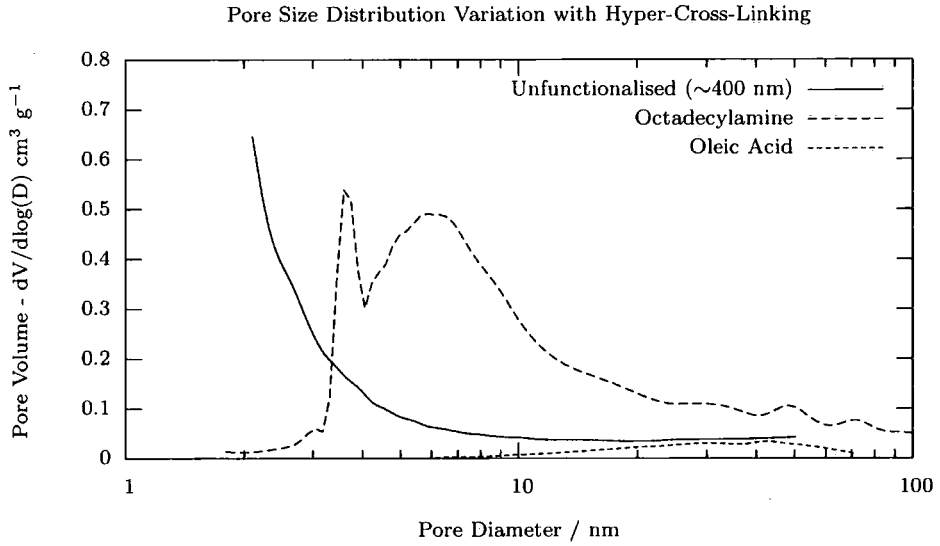

Figure 7.17: Pore size distribution data of surface coated particles calculated from the sorption isotherms in figure 7.16. Data from the unfunctionalised, larger particles (section 7.1) included for comparison.

to the particle surface provides the particle with surface stabilisation required for the formation of discrete, water miscible pVBC nanoparticles. These precursor gels were swollen in DCE and hypercrosslinked by intraparticle Friedel-Crafts alkylation to yield microporous, ultrahigh surface area particles. These syntheses show a viable method by which porous nanoparticles can by prepared.

Surfactant (DTAB/DDAB) stabilised emulsion copolymerisation of VBC and DVB yielded ~20 nm nanoparticles which were unstable with respect to irreversible aggregation under freeze drying and hypercrosslinking. The irreversible aggregation of the particles resulting from the drying process is explained as most likely arising from interparticle chain entanglement as opposed to the formation of ether linkages (as previously proposed). This argument is based on the fact that attempts to force the hydrolysis of surface bound benzyl chloride moieties to completion was apparently unsuccessful in preventing irreversible aggregation.

Precursor gel particles dried from dry organic solvent were redispersible, and subsequent reactions could be carried out. It has been shown that surface functionalisation of these nanoparticles by the reaction of surface benzyl chloride groups with a long-chain primary amine or caboxylic acid produces redispersible, discrete particles, but the success of subsequent hypercrosslinking reactions remains unproved. Hypercrosslinking reactions with the dried, unfunctionalised discrete gel particles yielded large aggregates, attributed to the formation of interparticle methylene bridges.

With further development, it should in future be possible to produce ultra-high surface area nanoparticles of less than 50 nm, with appreciable open microporous structure in the dry state.

Part III

Polymeric Nanocapsules

Do, or do not; there is no try.

Yoda

Chapter 8

Literature Review

The aim of this chapter is to present a summary of the literature published to date regarding the synthesis, characterisation and uses of hollow polymeric particles.

8.1 Introduction

The majority of approaches taken toward the synthesis of hollow particles are broadly divisible into two camps. These are the core-shell templating (hereafter CST) and self-assembly or surfactant templated methods. Both synthetic routes have advantages and disadvantages, each of which is discussed below. Various review articles have previously been published relating to the preparation and potential uses of such particles.[82–87]

8.2 Core-shell templating

This approach to the preparation of hollow nanospheres requires first the ability to synthesise a suitable core template, then to precipitate or grow a shell layer about

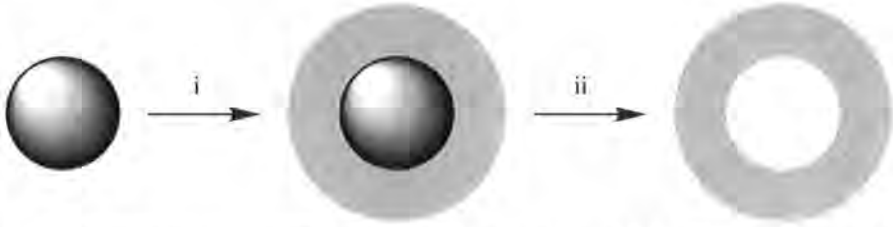

Figure 8.1: Schematic of CST synthesis of hollow nanoparticles. The process involves i. shell deposition about a core particle, and ii. core removal to leave a hollow particle.

that core prior to core removal, leaving the hollow shell capsule (illustrated in figure 8.1). The majority of literature relating to the synthesis of core-shell particles includes the use of polymers as either the core or shell component, owing to the suitability of polymers for each of these applications. Uniform polymeric core particles can be synthesised in abundance relatively easily (see part I), additionally polymeric shells can be added to cores in a controlled manner to produce layers of controlled thickness (see later in this section). Where polymers are used as neither the core nor shell component in the synthesis of core-shell particles, the reaction conditions required for the synthesis become more extreme[88] and the issue of material compatibility becomes of greater importance, often requiring an additional functionalisation of the core particle to allow deposition of the chemically dissimilar shell component.[89]

8.2.1 Inorganic core templates: Polymer shell layers

Inorganic core templates provide well defined structures on which, or from which, to form polymer shells. Inorganic templates may be smaller than the smallest organic or polymeric equivalent, e.g. gold clusters, and therefore provide a route to the smallest of voided particles. The difference in reactivity of core and shell often allows relatively passive core removal, even if extreme conditions are required.

The strength of the thiol-gold interaction has been exploited by a number of groups for the growth of polymers from,[90] or the attachment of polymers to,[91] gold surfaces. More specifically, this has been developed to the attachment of monomers (and other vinyl bearing moieties)[92–95] and polymers[96] to gold nanoparticles. By extension, this could lead to hollow nanoparticle synthesis by removing the gold core particle following the formation of a crosslinked oligomer / polymer shell.[97]

Gold has also been used as an inert core particle in the synthesis of hollow polypyrrole nanocapsules of ~50 nm, achieved by Marinakos et al.[98] In this synthesis the gold nanoparticles were incorporated into a membrane, to which initiator was then added. Monomer deposited below the membrane was allowed to evaporate and diffuse into the support where it polymerised upon contact with the initiator coated particles. It was reported that 'very few' polymeric particles were found not to contain gold cores. The gold was then removed by treatment with CN^-. The advantage of thiol-gold bonding was not taken as previously, although was recognised by the authors as a possible mechanism by which thiol bearing species could be encapsulated within the hollow spheres. Similar syntheses have been undertaken using different metal core and polymer shell materials, for example CuO CST of ~300 nm hollow polyaniline spheres.[99] Alternative particle morphologies were then obtained with different core materials, namely spindles (Fe_2O_3) and ellipsoids (Fe_2O_3 / SiO_2).

Other examples of gold-core-polymer-shell particles exist, but in these cases the gold was not required for templating.[100,101] So called "rattle" particles[100,101] are prepared to contain small, mobile gold nanoparticles within the hollow cavity of the shell, synthesised in these cases by first encapsulating the gold within a larger silica particle: it is this silica that templates the formation of the polymer shell. Carbonised polymer shells have been produced by a similar approach,[102] and also a method for preparing copper in silica and silver in silica rattle particles by encap-

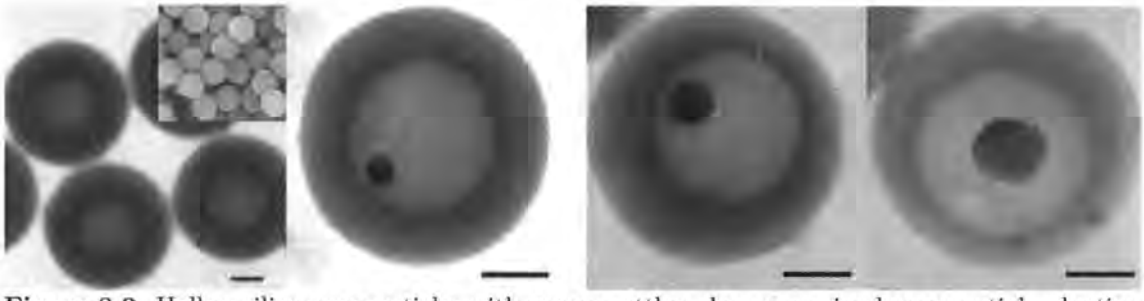

Figure 8.2: Hollow silica nanoparticles with copper rattles, shown growing by sequential reduction of infused copper salts. Scale bars = 100 nm. Images by electron microscopy, reproduced from Hah et al.[103]

sulation post hollow particle synthesis is reported,[103] in which the size of the rattle core can be controlled (see figure 8.2).

Silica has been studied extensively in the field of porous monolithic materials since 1992[104–106] and now is also widely found in the porous[107,108] and hollow[109–111] particle literature. The mesoporous (2–50 nm) nature of silica particles makes the material well suited to the formation of porous-shelled hollow polymer structures,[101,102] while its ability to be etched chemically makes it an ideal core material for CST synthesis of hollow capsules. Silica also lends itself to simple functionalisation allowing bonding of various moieties, some suitable for subsequent polymerisation reactions.[112]

As was seen in the case of gold, silica has been used as a template from which to grow polymers[100,113–117] and to which to attach polymers.[118] Controlled free radical polymerisation from functionalised silica particle surfaces by ATRP[100,113,115,117] and NMP[114] has yielded core-shell particles of 50 – 600 nm in diameter. Crosslinking of shells and removal of cores has produced hollow capsules, the largest of which collapse upon removal of the core;[114] the smaller hollow particles appear to retain their shape upon core removal.[100,113]

Only one report[118] of attachment of polymer to functionalised silica was found, in which micron-sized silica particles were decorated with polystyrene nanoparticles, forming an uniform shell upon subsequent solvent treatment. Chemical etching of

the silica produced hollow spheres which showed signs of collapse, again, probably due to their large size.

8.2.2 Polymer core templates: Inorganic shell layers

The synthesis of well defined latex polymer particles is well documented (see Part I), giving many possible routes to a range of suitable monodispersed polymeric core templates. Aside from size, the choice of polymeric cores in CST syntheses of inorganic hollow shell materials is supported by ease of removal of the core by simple calcination, which acts both to remove the core and in many cases also to fuse or set the shell material. Alternatively, polymeric cores can be removed by dissolution or chemical etching.

Hollow silica nanospheres (~0.7–1 μm diameter) have been produced by decorating core polymer particles with silica[110] (see figure 8.3), analogous to the materials previously discussed where the role of the materials was reversed (silica particles were decorated with polymer)[118] . A similar decorating synthesis has also been reported although in this case the core was not removed,[119] leaving a core-shell solid micro-particle. Presumably, in this and in other such reported syntheses of polymer coated silica nanoparticles,[120] it would be possible to remove completely the core templates. Work by other groups[121,122] has shown that development of the CST technique to involve the polymerisation of the templating core in the presence of the decorating inorganic colloid was successful in producing core-shell particles. In the former work[121] core-shell particles were formed only in the presence of cationic azo-initiator; the anionic equivalent gave no particles whereas the non-ionic initiator (AIBN) gave only lightly decorated polymer cores. Calcination produced hollow spheres of 500 nm, later reduced to a lower limit of ~250 nm through compositional adjustments.[123]

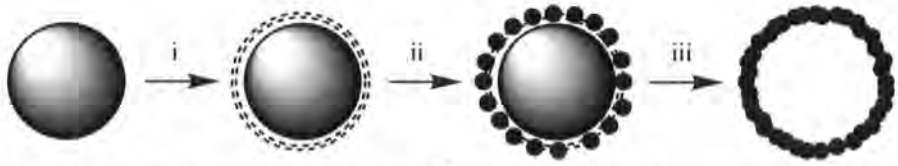

Figure 8.3: Schematic to show the synthesis of hollow silica spheres produced by i. coating a polystyrene latex particle with a cationic polymer, ii. decorating with silica nanoparticles and iii. calcination facilitating latex and polymer removal. Adapted from Caruso et al.[110]

Analogous to the growth of polymers from core surfaces (previous section) is the growth of silica around a polymeric core. This is achieved by the hydrolysis of tetraethoxysilane (TEOS) in the presence of the core to yield SiO_2,[124] with growth nucleated about the seed core. Particle size and shell thickness can be controlled by selection of appropriate core latex particles together with factors such as TEOS concentration and shell growth time.[125,126] In this way, hollow silica spheres of as little as 100 nm diameter[125] have been prepared. Porous hollow shells are reported in some cases owing to the intrinsic porosity of such silica particles.[126] A similar approach has also been applied in the reduction of silver on polymer cores, with etching to produce hollow capsules.[127]

8.2.3 Polymer core templates: Polymer shell layers

Polymeric material employed as both core and shell materials potentially allows the greatest degree of control over core and shell dimensions, and possibly provides the most highly tailorable chemistry. Such syntheses are typically based upon latex core particles, however hollow nanocapsules have been prepared via a controlled radical polymerisation about a hyperbranched polymeric core.[128]

The synthesis of polymer-polymer core-shell nanoparticles is reported by both sequential layering and decoration approaches. The decoration of large, negatively charged polymer core particles with smaller positively charged polymer particles,[129] and the reverse arrangement,[130] has been shown to be a successful method of prepar-

ing core-shell nanoparticles, however in these cases no attempts were made to etch the cores. Hollow shells prepared by this approach[131] have necessarily been large (microns in diameter) due to the limits imposed by the smaller decorating particle's diameters.

In the case of sequential layering, it may be expected that polymerisation of monomer in the presence of an existing latex may not lead to the formation of a shell. Indeed, there are circumstances under which the addition of a second batch of monomer into what is then effectively a seeded polymerisation does not produce a shell layer about the existing latex, leading to the formation of a mixture of discrete latexes of types A and B.[132–135] Core-shell formation was found to be more likely to occur when the second (i.e. shell) monomer was added at approximately 60% conversion of the core (as compared to addition to a pre-formed latex). The rationale behind this is that the core is still swollen with monomer A at the time of the addition of B, and so monomer B migrates to the area where growing radicals (of polymer A) are already present.[132]

Predicting the outcome of sequential addition polymerisations is not trivial, as highlighted by the production of unexpected morphologies. For example, under conditions expected to give PPy coated polystyrene particles,[136] discrete PPy particles of ~30 nm were observed, adsorbed onto the larger polystyrene seed particles, leading to heteroflocculation;[135] only reducing the concentration of pyrrole and polystyrene particles gave core-shell particles, probably due to kinetic effects. Additional to this case, attempted addition of a polystyrene shell to a PMMA core in an emulsion actually resulted in the inverse morphology as the less polar styrene diffused into the core, giving the more thermodynamically stable product.[137] It has since been shown possible to prepare the less thermodynamically stable polystyrene shell particle with a highly crosslinked poly(^{t}butyl acrylate) core, but that the core-shell boundary is much less well defined than in the inverse, thermodynamically stable,

arrangement.[133] This approach appears unfavourable for the formation of hollow particles by CST due to the required high degree of crosslinking of the core, rendering its removal more difficult. In attempting copolymerisation of MMA, acrylic acid and a fluorinated methacrylate monomer, the spontaneous formation of core-shell particles has been observed where mixed latex particles had been expected, due to a thermodynamically driven phase separation.[138]

Core-shell particles have been prepared by the designed sequential layering of polymers. Addition of functionality bearing shells to inert cores by this means has yielded particles with reactivity for subsequent reactions,[139,140] while PMMA coated particles were prepared by a two step addition process in which PMMA served to promote compatibility between the core and other materials,[141,142] and multi-layer coated cores of polystyrene have increased the processability of conductive polymers.[143,144] In these final two examples, core etching yielded hollow particles.

Other successful routes to polymer-polymer CST of hollow spheres have been found. Jang and Ha[145] offer a route to hollow polystyrene nanospheres of 20–30 nm diameter with shell thickness of 2–5 nm, by CST around a PMMA core, despite the difficulties encountered previously.[137] In this case, an ABA triblock copolymer surfactant was used throughout the process to stabilise the particles at each stage, this likely overcoming the thermodynamic rearrangement seen previously in PMMA core/polystyrene shell particles[137] by providing a more hydrophobic surface. The core was reportedly removed by dissolution with methylene chloride to leave the hollow spheres. Further work by Jang shows similarly proportioned nanocapsules of PPy also prepared by CST, but using PPy as both core and shell.[146] In this case, N_2 sorption isotherm analysis showed the presence of 2 nm pores in the shell walls.

Hollow particles with functionalised interior surfaces have been synthesised by a CST approach in which a PMAA core particle was coated with 4-vinylpyridine before DVB was added to complete a shell. Dissolution of the core particles left the

vinylpyridine interiorly coated hollow particles.[147] Inner-surface functionalisation such as this could provide a means by which material could be selectively encapsulated within hollow particles.

8.3 Surfactant self-assembly methods

8.3.1 Micellar structures

Amphiphilic block copolymers are known to aggregate in solution to form a variety of micellar structures, from rods to spheres.[86,148] Crosslinking the internal moieties of amphiphilic micelles produces stabilised core-shell type particles;[149–152] crosslinking the external moieties produces shell-crosslinked particles, and this provides a route to hollow particle synthesis.

The difference between this and the core-shell methods discussed previously is subtle. Particle size is determined by the molecular weight of the amphiphilic polymer used to compose the particle, and is as such set at the beginning of the synthesis. Equally, the core and shell functionality is determined at the beginning of the synthesis, according to the make up of the polymer amphiphile used. In both of these cases, there is a balance between the properties desired of the particles and the requirements necessary for particle synthesis. For example, in the use of diblock copolymers for the synthesis of shell-crosslinked particles, varying the relative molecular weights of the hydrophilic/phobic blocks affects both particle size (in part due to the relative molecular weights of the blocks in question, in part due to variation in micelle aggregation number) and the stability of the diblock surfactant with respect to sedimentation.[153] There must also be consideration of the chemical nature of each block, especially if used for biological (drug delivery) applications. The shell must be biocompatible and the core must be suitable for solubilising and releasing the

encapsulated drug.[154] Controlled polymerisation methods are typically employed for the preparation of the amphiphilic diblock copolymers used for such syntheses due to the requirements for controlled compositions with respect to block lengths in order that surface activity be controlled. A review has recently been published covering shell-crosslinked micelle particle synthesis.[86]

The micellisation and shell-crosslinking of diblock copolymers containing peptide blocks has recently been published, with the potential for drug delivery applications,[155] and the claimed possibility of targeted delivery. Core-shell micelles can also be shell functionalised by the same chemistry used to crosslink the shells, giving rise to great possibilities for compatibilisation, particularly important if drug delivery applications of such micelles are to be pursued.[156] Similarly, multilayered core-shell-corona (CSC) particles can be prepared by an amphiphilic block copolymer self-assembly approach by addition of a second block copolymer to an existing block copolymer micellar solution.[157] CSC type aggregates have also been reported from the self-assembly of triblock copolymers, with the middle block being reversibly photo-crosslinkable.[158] In this case, PEG was used as the outermost (corona) layer.

Shell-crosslinked particles from micelles can be hollowed provided that a suitable block copolymer is employed in their synthesis (various reviews have been written covering this type of synthesis).[159] A diblock composed of poly(*cis*-1,4-isoprene) (PI) and poly(acrylic acid) (PAA) was prepared by Huang et al,[160] micellised in aqueous solution and shell-crosslinked by addition of a diamino terminated PEG. Degradation of the PI block by ozonolysis left hollow nanospheres of ~130 nm (measured by AFM). Figure 8.4[161] depicts this process for similar nanoparticles made by the same approach. Similar syntheses with differing diblocks prepared by more elaborate routes have been reported.[162] Hollow spherical particles with PAA shells have recently been reported to be pH sensitive, varying in diameter with pH and salt concentration, attributed to the alteration in electronic interactions between PAA

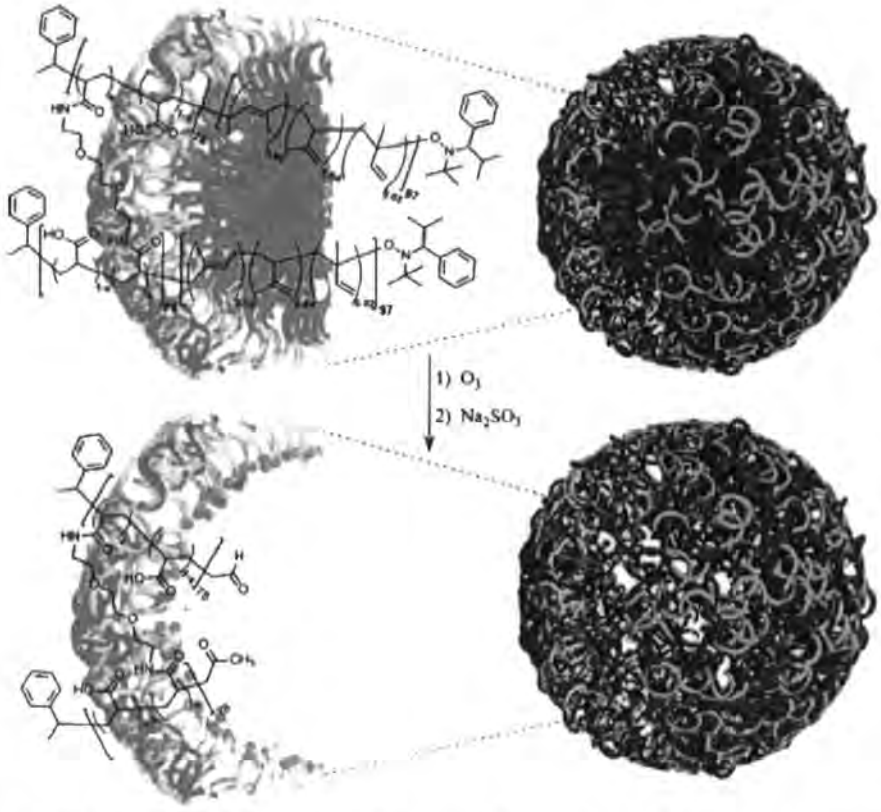

Figure 8.4: Synthesis of shell crosslinked nanocages by surfactant self assembly, crosslinking and ozonolysis. Reproduced from Turner and Wooley.[161]

moieties in the presence of ionic species (lipase was employed to degrade selectively a poly(ϵ-caprolactone) core in this synthesis).[163]

8.3.2 Vesicular structures

Vesicles are self assembled bilayer structures, and have been the subject of recent reviews.[164,165] Vesicles typically comprise an amphiphile bilayer with identical media on both internal and external sides of the bilayer. Ion exchange and facilitated diffusion can be used to generate concentration gradients across these interfaces, thus altering the internal and external media compositions. Liposomes are a special class of vesicle, being comprised specifically of lipid bilayers. Otherwise, liposomes are similar to other types of vesicle excepting in that they are typically larger (of the order of microns) than others, as those prepared from block copolymers can

be of the nanometer scale, although extrusion and ultra-sonicaton techniques have recently made possible the formation of nanoscale liposomes.

In the case of block copolymers, the transition from micellar to vesicular structures can be observed by increasing the concentration of the block copolymer in solution, or by changing the relative volume fractions of the hydrophilic and hydrophobic segments. Zhang et al[166] observed micelles at lower concentrations (0.1 mg mL^{-1}) of block copolymer surfactant (PS-*b*-P(AA-*co*-MA)) which increased in diameter with increasing concentration, up to 2.0 mg mL^{-1} at which point hollow vesicle aggregates were observed. Complementary publications by Ding and Liu demonstrate the capability to both prepare diblock copolymer vesicles[167] and use them for guest encapsulation and release.[168] In this work, vinylic moieties present on the internal blocks were gelated to produce stabilised, crosslinked vesicles. Triblock copolymers have more recently been employed and crosslinked in the same manner.[169]

More recently still, Du et al.[170,171] reported the preparation of hybrid hollow particles from diblock copolymer vesicle systems. In this work, a diblock copolymer comprising PEO and silyl-bearing blocks was prepared, dispersed to form vesicles and gelated by hydrolysis of the silyl moieties in the presence of base. In studying the effects of solvent, polymer concentration and block lengths, and the gelation time, hollow particles were prepared with variable size and size distribution, and tunable wall thicknesses.

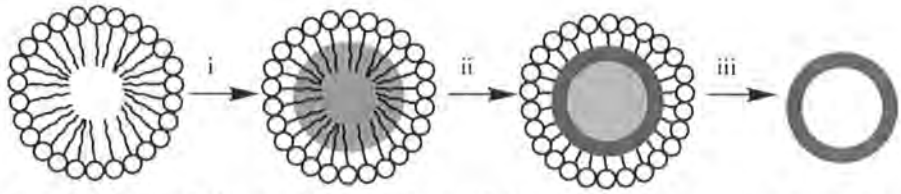

Figure 8.5: Schematic of phase separation in emulsion-type polymerisation to produce a hollow particle. i. A micelle is swollen with monomer and solvent, which ii. phase separates during polymerisation, yielding a hollow particle, iii. after washing and drying.

8.4 Alternative methods

8.4.1 Phase separation in emulsion type systems

Phase separation of polymers in solution occurs due to thermodynamics, explicitly because the free energy of the discrete polymer and solvent phases (or some combination away from homogeneity) is less than the free energy of the homogeneous mixture. Reports of the synthesis of hollow particles by spontaneous phase separation (illustrated in figure 8.5) are found for emulsion,[172] miniemulsion[173] and microemulsion[174,175] systems.

The study of the miniemulsion polymerisation of both methyl methacrylate (MMA) and styrene monomers in the presence of hexadecane gave rise to the spontaneous formation of hollow capsules in the case of MMA, facilitated by the thermodynamically controlled phase separation of the growing polymer from the hydrophobic oil.[173] This was not observed to occur in the styrene system as the relative polarities of the hydrophobe and the polymer were insufficiently different to drive the phase separation. The same phase separation phenomenon was used by Jang and Lee in the microemulsion polymerisation of DVB crosslinked styrene nanospheres of 20–50 nm in the presence of isooctane.[175] The shell thickness was reported to be 3 nm, and the particle void diameter was controlled by varying the length of the surfactant's aliphatic component, to give total particle dimensions within the stated range.

Work on predicting the morphology of nanocapsules formed by these means has shown that it is likely that the phase separation is not entirely governed by thermodynamics, and that kinetics may play a role, specifically in cases where the rate of polymerisation is low[176] or polar radicals are used (which are unable to diffuse into the oil core of the droplet).[177]

8.4.2 Interfacially restricted polymerisation

Initiator controlled interfacial polymerisation

Restricting polymerisation to the interfaces of droplets is largely achieved through thermodynamic control, e.g. use of aqueous soluble initiator species in o/w systems. For example, by using block copolymer surfactant, hollow polyaniline nanoparticles can be formed by interfacial polymerisation,[178] where the aqueous soluble initiator and oil soluble monomer meet only at the surfactant interface. Differences in micelle size were reported to influence particle morphology. By altering the relative molecular weights of the hydrophilic and hydrophobic blocks, smaller micelles could be formed resulting in solid particles as the initiator was able to propagate polymerisation to greater relative depths in the smaller micelles. It was only from larger micelles that hollow particles were formed.

Thermodynamic control of the RAFT-mediated miniemulsion polymerisation of styrene was firstly demonstrated by altering the initiator species. When initiated by KPS hollow particles could be produced, whereas under initiation by AIBN such morphologies were never observed, due to the lack of thermodynamic drive for surface anchoring of the propagating polymer.[179] Kinetic control can also be influential with respect to particle morphology. The effect of the kinetics over particle morphology was demonstrated through employing different RAFT agents. A RAFT agent providing rapid polymerisation gave hollow particles whereas an agent lead-

ing to a slower rate of polymerisation did not. Rapid polymerisation allowed the formation of long, entangled chains, trapping the propagating radicals at the interfacial region. With the RAFT agent providing a slower rate of polymerisation, the reduced occurrence of chain entanglement and lower viscosity associated with the shorter polymers allowed polymerisation of monomer throughout the whole droplet, as propagating radicals were not trapped at the interface, and could enter the core of the particle by unhindered diffusion.

Transurfs, surfmers and inisurfs

An alternative RAFT mediated polymerisation strategy was employed by Luo and Gu, and also lead to hollow spheres.[180] The polymerisation in this case was restricted to the interface by using a surface active RAFT agent (RAFT agent capped oligomeric poly(styrene-*co*-maleic anhydride)). This type of reagent is termed a 'transurf', derived from the fact that it is both a '*trans*fer agent' and a '*surf*actant'. Radicals could only propagate from the interfacial region, where the RAFT agent was anchored, and in this way a hollow particle formed.

Polymerisable surfactants ('surfmers' from '*surf*actant agent' and 'mono*mer*') are another means to drive the formation of hollow polymeric spheres (see section 8.3). The majority of those examples previously mentioned concern the crosslinking of self-assembled structures. The miniemulsion synthesis of nanocapsules reported by Crespy et al.[181] differs in that the polymerisation of a monomer / hydrophobe droplet was carried out in the presence of a surfmer. Hollow spheres of ~200 nm were prepared, driven by a phase separation between the hydrophobe and the polymer, the latter being anchored to the surfmer.

Surfactants with the ability to act as initiators are termed 'inisurfs', their names derived by amalgamation of the two classes of molecule which they embody. The

most commonly used inisurf is KPS, which by decomposition generates two persulfate radicals. When used to initiate o/w emulsion polymerisations, the persulfate fragments tend to reside at the o/w interface, and as a result possess surfactant properties. Another similar example is V-50, used in the surfactant-free polymerisation of VBC, and in which the surface restricted fragments stabilise the latex particles.[76] A clearer example comes from the controlled polymerisation of butyl acrylate and butyl methacrylate in miniemulsion systems to form triblock copolymers from inisurf diblock copolymers, here by ATRP.[182] In this synthesis a diblock copolymer is firstly prepared by bulk phase ATRP initiated by a macroinitiator (a methoxy terminated PEG, capped with a halide bearing agent). A third block is added by emulsification of butyl acrylate or butyl methacrylate stabilised by this surface active diblock copolymer, with no additional surfactant. Finally, AGET ATRP is undertaken in the miniemulsion system, producing ABC triblock copolymers with PDI <1.5, in the form of stabilised particles of $\leq$200 nm in diameter.

Monomer restricted interfacial polymerisation

The copolymerisation of hydrophilic and hydrophobic monomers has been employed in order to ensure that polymerisation can occur only at the interface. In their synthesis, Co et al.[183] use a miniemulsion system with both aqueous soluble (PEG divinyl ether) and oil soluble (dibutyl maleate) monomers, initiated by a surface active azo-initiator. This is illustrated in figure 8.6. Uniform shell thicknesses result from this approach as the limited solubilities of the monomers in the contrasting phases prevent diffusion into and out of the droplets beyond a thermodynamically dictated optimum. Homopolymerisation of either monomer is not possible, resulting exclusively in alternating copolymer capsules of $\sim$ 200 nm diameter. A similar approach has been used to yield hollow particles via inverse (w/o) emulsions[184] and

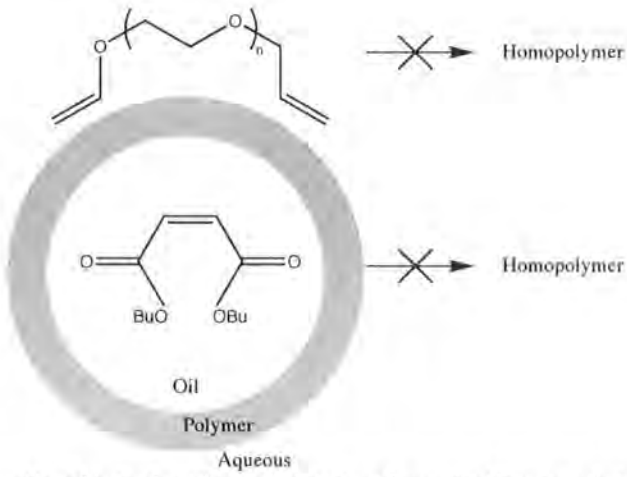

Figure 8.6: Schematic of interfacially restricted polymerisation in miniemulsion polymerisation, to produce a liquid-core nanocapsule. Homopolymerisation is not observed, and copolymerisation is possible only at the droplet interface. Adapted from Scott et al.[183]

miniemulsions.[185] In the latter case, a variety of solvents and monomers were used in the study, producing a variety of hollow and solid sphere morphologies.

8.4.3 Other notable methods

Oil-in-water-in-oil emulsion-type systems have been employed to prepare multihollow particles, possessing large hollows similar to the morphology of Swiss-cheese, from dispersed polymer.[186]

The synthesis of hollow polymeric particles by osmotic swelling has been reviewed elsewhere.[83] In brief, the method requires the synthesis of a core-shell particle of which the core is able to induce an osmotic pressure. For example, a polyelectrolytic core when ionised by a pH change in the surrounding solvent will require additional solvent to enter the core region, swelling the particle and creating a void. Removal of the core by dissolution can thus produce a hollow particle.

Chapter 9

Experimental

The aim of this chapter is to outline the experimental procedures employed in the synthesis of nanoparticles mediated by ATRP, and to introduce the analytical techniques used in their characterisation.

9.1 Introduction

Many methods exist for producing hollow nanocapsules, as reviewed in the previous chapter. Briefly, these tend to comprise core-shell templating or surfactant micelle crosslinking for smaller particle synthesis, or solvent swelling methods. While maintaining the biphasic (emulsion) based approach of Parts I and II, controlled radical polymerisation was used for the work presented in this part in the aim of producing hollow capsules. Controlled polymerisation has been demonstrated effective in the preparation of hollow nanocapsules in the case of RAFT,[179] and literature has been published showing emulsion based ATRP to be possible,[182,187–193] and so the question to be answered was: Can ATRP be used in emulsion systems to synthesise hollow nanocapsules?

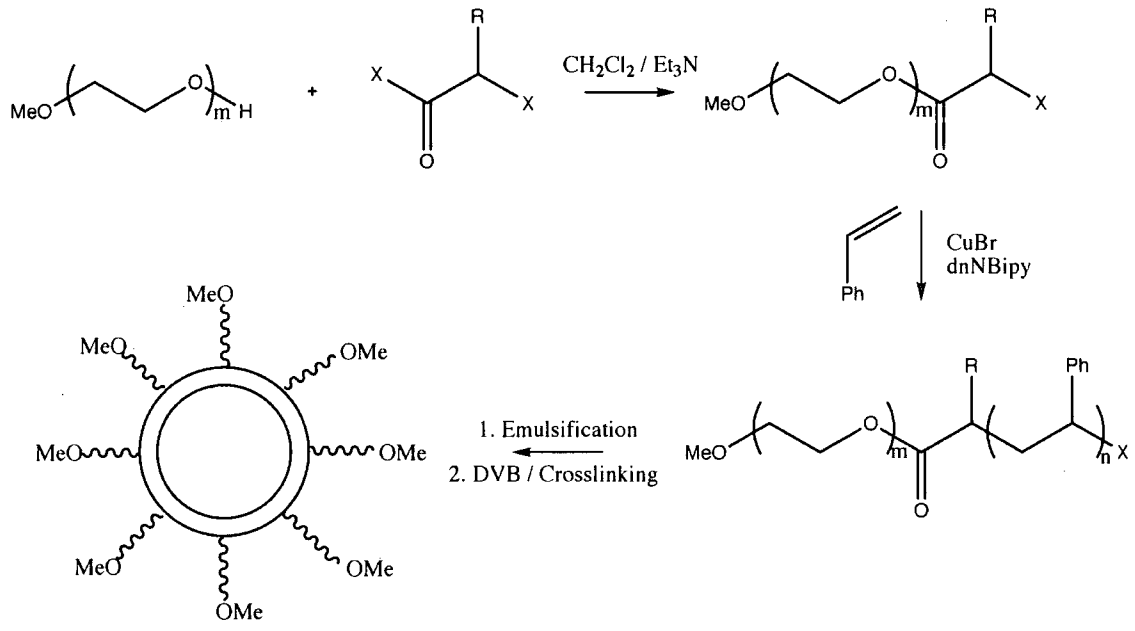

Figure 9.1: Proposed scheme for hollow nanocapsule synthesis mediated by ATRP, where: R_1 = Me, X_1 = Br; R_2 = Ph, X_2 = Cl.

The synthetic scheme (figure 9.1) illustrates the proposed route to hollow particle synthesis. The synthesis requires three steps: the functionalisation of a mono methoxy terminated PEG (to form a macroinitiator), the growth of a diblock from that macroinitiator (to form an inisurf) and finally, emulsification and subsequent polymerisation of the emulsion, initiated by the inisurf.

9.2 Synthesis

9.2.1 Materials

Styrene (99%, Sigma) and DVB (technical grade, 80%, Aldrich) were washed over basic alumina to remove inhibitor before use. Triethylamine (99%, Aldrich) was dried and stored over molecular seives. DCM (dichloromethane) was dried to 16.1 ppm water content with Innovative Technology Inc. solvent purification system.

Brij 98 (Aldrich), mPEG (mono-methoxy terminated polyethylene glycol, M_n 550, 750, 2000, Aldrich), dnNBipy (4,4'-dinonyl-2,2'bipyridyl, 97%, Aldrich), Cu(I)Br (99.999%, Aldrich), (1-bromoethyl) benzene (97%, Aldrich), α-chloroacetylphenyl chloride (technical garde, 90%, Aldrich), 2-bromopropionyl bromide (97%, Aldrich), toluene (99.8%, Aldrich), THF (tetrahydrofuran, laboratory reagent grade, Fisher), HCl (laboratory reagent grade, Fisher) and $NaHCO_3$ (99.5%, Sigma) were all used as supplied.

9.2.2 Standard initiator ATRP

Bulk phase ATRP

In a typical synthesis, initiator was weighed into a round bottomed flask (with high vacuum line attachments and rubber seal port for syringe entry) together with monomer sufficient to achieve DP 20 at 100 % conversion (i.e. a 20:1 molar ratio of monomer to initiator). The solution was deoxygenated by three sequential freeze-pump-thaw cycles, under vacuum of $\leq$0.05 mBar. In a second equivalent vessel, Cu(I)Br and ligand were weighed out to give the overall molar ratio of 1:1:3 with respect to initiator:copper:ligand respectively. This was deoxygenated by three cycles of evacuation (vacuum of $\leq$0.05 mBar) and back-filling with N_2. The degassed monomer and initiator solution was added by degassed syringe to the flask containing the catalyst and ligand, chilled in liquid nitrogen and one freeze-pump-thaw cycle completed. After thawing, the reaction vessel was back filled with N_2, and equilibriated to atmospheric pressure.

Kinetics were measured by extraction of $\sim$0.1 ml aliquots by degassed syringe at specified time intervals which were transferred to clean NMR tubes and diluted with $\sim$0.6 ml $CDCl_3$ before shaking then storing at 4 °C until the NMR experiment was run. Conversion was calculated from the decrease in the vinylic styrene protons

(an average of the integrals of the two doublets between 5–6 ppm) relative to the corrected aromatic signal (between ~6.4–7.6 ppm); correction by subtraction of signal intensity equivalent to the contribution of one proton is necessary due to the broadening of the aromatic signal (observed in this region as the polymerisation of the monomer progresses) overlapping the similarly broadened signal of the remaining vinyl proton doublet of doublets at ~7.8 ppm. After the NMR experiments, samples were subsequently prepared for SEC analysis by firstly diluting with DCM and passing over activated basic alumina to remove copper complexes. Evaporation of $CDCl_3$ and DCM left a residue, this then dissolved in THF to approximately 1 mg per ml of solvent.

Emulsion phase ATRP

Brij 98 was used for the preparation of emulsion systems as there is literature precedent suggesting non-ionic surfactants (and specifically Brij 98) to be superior for controlled ATRP in emulsion systems.[187,190] In the current work, the surfactant (0.33 g) was dissolved in distilled water (24 g) in a 100 ml round bottomed flask with high vacuum line attachments and rubber seal port for syringe entry. The solution was degassed by repeated freeze-pump-thaw cycles until no appreciable increase in pressure upon pumping was detected (typically around 5–7 cycles).

In a second similar vessel, monomer (0.172 g, DP 50 at 100% conversion) and initiator (6 mg) were weighed out and degassed by three freeze-pump-thaw cycles. In a third vessel, the Cu(I)Br and dnNBipy were degassed by evacuating and back filling with N_2 three times.

The monomer and initiator solution was added to the catalyst and ligand by degassed syringe and stirred to dissolve the solids. A second degassed syringe was then used to extract the monomer, initiator, catalyst and ligand solution before addition to

the surfactant in water solution. The resulting mixture was gently shaken to assist dispersion of the oil phase before sonication for 5 minutes in a low powered sonic bath. The resulting emulsion was then stirred while heated to 90 °C by oil bath.

The polymeric product was recovered by freeze-drying the emulsion after the reaction period, this was then dissolved in THF and analysed by SEC.

9.2.3 Macroinitiator ATRP

Macroinitiator synthesis

Different methods towards the functionalisation of mPEG by reaction with acyl chlorides for macroinitiator synthesis are described in the literature.[194,195] In a typical synthesis in this work, 1 g of mPEG was added to a round bottomed flask with high vacuum line attachments and small rubber septum. Azeotropic drying was carried out with toluene. Dry DCM was distilled into the reaction flask under high vacuum conditions and warmed to allow dissolution of the mPEG. Fine control over the volume of added solvent was not possible by this technique, however concentrations of mPEG were typically around 10^{-3} mol dm^{-3}. The flask was then back filled with N_2 before addition under stirring of a 3:1 molar excess of TEA (relative to mPEG), added by degassed syringe. After cooling in an ice bath to 0 °C, a 3:1 molar excess (again, relative to mPEG) of acyl chloride was added by dropwise addition under stirring by degassed syringe. The resulting solution was left to stir overnight, gradually equilibriating to room temperature.

Macroinitiator was purified by washing alternately with aqueous $NaHCO_3$ (0.1 M) and aqueous HCl (0.1 M) in a separating funnel, before the organic phase was concentrated by rotary evaporation. Approximately 50 ml of distilled water was added to the concentrated products and the mixture shaken to facilitate dissolution

of the water soluble macroinitiator. This was then centrifuged at 8000 rpm for five minutes. The supernatant was retained and freeze dried to give the purified macroinitiator; the oily residue was discarded.

Inisurf synthesis

Diblock copolymers were prepared as follows: Macroinitiator was added to a round bottomed flask equipped with a high vacuum line attachment and rubber septum. To this was then added the required mass of styrene (for low M_n macroinitiator, molar ratio 50:1, for high M_n macroinitiator, molar ratio 110:1), which was then degassed by three freeze-pump-thaw cycles. In a second vessel the required mass of Cu(I)Br was weighed out with the ligand (dnNBipy) in the required molar ratios (such that macroinitiator:Cu:ligand was 1:1:3). The solids vessel was purged of oxygen by evacuation and back filling with N_2 three times. The vessel was then chilled in liquid nitrogen.

The macroinitiator in styrene solution was added to the chilled solids vessel by degassed syringe, and a single freeze-pump-thaw cycle completed. The reaction vessel was back filled with nitrogen, the excess pressure released (to atmospheric pressure) and the flask heated to the required temperature (90 °C to 110 °C) by oil bath.

For kinetic studies, aliquots of approximately 0.1 ml were extracted from the reaction vessel by degassed syringe at suitable time intervals, and transferred into a clean NMR tube. Approximately 0.6 ml of $CDCl_3$ was added and the tube shaken before storing in a refrigerator at 4 °C until the NMR experiment was run (to determine conversion). Following acquisition of the NMR spectrum, the contents of the NMR tube was diluted with DCM, filtered through basic alumina (to remove copper (II) complexes), and the block copolymer isolated by rotary evaporation.

This product was dissolved in THF and analysed by SEC (to determine apparent molecular weight).

Otherwise, the diblock copolymer was purified by passing through basic alumina in DCM solution before concentration by rotary evaporation. Low molecular weight diblock copolymers were not purified further. High molecular weight diblock copolymers were further purified by dissolving in water, and filtering through syringe filters to remove the majority of the dnNBipy (5.0 μm pore size) before freeze drying.

Emulsion based ATRP

The process for the inisurf emulsion ATRP was similar to that described previously. However, in this case the inisurf was dissolved in the aqueous phase (no Brij 98 was used), and DVB was used as the monomer phase also in the presence of toluene (50:50 by weight).

9.3 Analysis

9.3.1 Macroinitiator synthesis

NMR

Macroinitiator synthesis was confirmed by ^{1}H NMR spectroscopy, undertaken using a Varian Unity NMR spectrometer at 300 MHz.

Macroinitiator molecular structures are shown in figure 9.2, and the corresponding quantitative NMR shifts are listed below for 550 M_n; other molecular weights appear with equivalent shifts and integrals with the exception of the integral value at 3.52–3.64 ppm, which increases with increasing PEG M_n.

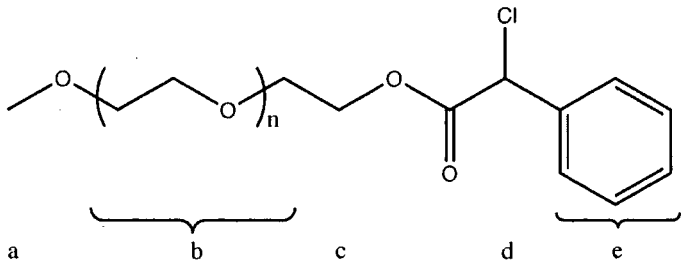

(a) Acyl chloride macroinitiator

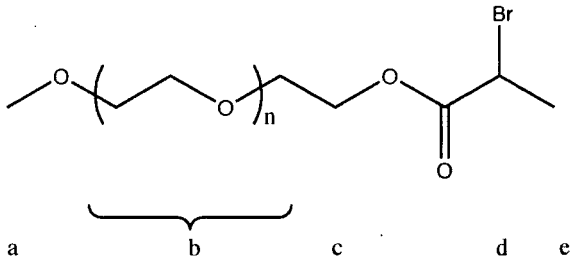

(b) Acyl bromide macroinitiator

Figure 9.2: Macroinitiator molecular structures, labelled for NMR interpretation such that (a) chemical shift environments show increasing shift from a–e, (b) chemical shift environments show increasing shift from e, a–d.

Acyl chloride macroinitiator,[195] figure 9.2(a);

δ_H(300 MHz, $CDCl_3$) 3.36 ppm (3H, s, CH), 3.52–3.64 ppm (46H, m, CH_2), 4.20–4.40 ppm (2H, m, CH_2), 5.39 ppm (1H, s, CH), 7.35–7.50 ppm (5H, m, aromatic).

Acyl bromide macroinitiator,[196] figure 9.2(b);

δ_H (300 MHz, $CDCl_3$) 1.78 ppm (3H, d, J = 6.9 Hz, CH_3), 3.36 ppm (3H, s, CH), 3.52–3.64 ppm (46H, m, CH_2), 4.27 ppm (2H, m, CH_2), 4.36 (1H, q, J = 6.9 Hz, CH).

Mass spectroscopy

Electrospray mass spectroscopy (Thermo-Finnigan LTQ FT) was used to confirm the formation of macroinitiators from 550 and 750 M_n mPEG, and MALDI-ToF mass spectroscopy (Applied Biosystems Voyager-DE STR) in the case of 2000 M_n mPEG. A partial list of characteristic peaks follows:

Electrospray MS, $mPEG_{550}OH$ M/z:

$[M+Na]_n^+ = 319_6, 363_7, 407_8, 451_9, 495_{10}, 539_{11}, 583_{12}, 627_{13}, 671_{14}, 715_{15}, 759_{16}, 803_{17}, 847_{18}, 891_{19}, 935_{20}, 979_{21}$. $[M+NH_4]_n^+ = 358_7, 402_8, 446_9, 490_{10}, 534_{11}, 578_{12}, 622_{13}, 666_{14}, 710_{15}, 754_{16}, 798_{17}$. $[M+K]_n^+ = 468_9, 512_{10}, 556_{11}, 600_{12}, 644_{13}, 688_{14}, 732_{15}, 776_{16}$.

Electrospray MS, $mPEG_{550}$-R-Cl M/z:

$[M+Na]_n^+ = 471_6, 515_7, 559_8, 603_9, 647_{10}, 691_{11}, 735_{12}, 779_{13}, 823_{14}, 867_{15}, 911_{16}, 955_{17}, 999_{18}, 1043_{19}, 1087_{20}$. $[M+NH_4]_n^+ = 466_6, 510_7, 554_8, 598_9, 642_{10}, 686_{11}, 730_{12}, 774_{13}, 818_{14}, 862_{15}, 906_{16}, 950_{17}$.

Electrospray MS, $mPEG_{550}$-R'-Br M/z:

$[M+Na]_n^+ = 453_6, 497_7, 541_8, 585_9, 629_{10}, 673_{11}, 717_{12}, 761_{13}, 805_{14}, 851_{15}, 895_{16}, 939_{17}, 983_{18}, 1027_{19}$. $[M+NH_4]_n^+ = 448_6, 492_7, 536_8, 580_9, 624_{10}, 668_{11}, 712_{12}, 756_{13}, 800_{14}, 844_{15}, 888_{16}, 932_{17}, 976_{18}, 1020_{19}$.

Electrospray MS, $mPEG_{750}OH$ M/z:

$[M+Na]_n^+ = 583_{12}, 627_{13}, 671_{14}, 715_{15}, 759_{16}, 803_{17}, 847_{18}, 891_{19}, 935_{20}, 979_{21}, 1023_{22}$. $[M+NH_4]_n^+ = 578_{12}, 622_{13}, 666_{14}, 710_{15}, 754_{16}, 798_{17}, 842_{18}, 886_{19}, 930_{20}, 974_{21}, 1018_{22}$. $[M+K]_n^+ = 687_{14}, 731_{15}, 775_{16}, 819_{17}, 863_{18}, 907_{19}, 951_{20}$.

Electrospray MS, $mPEG_{750}$-R-Cl M/z:

$[M+Na]_n^+ = 735_{12}, 779_{13}, 823_{14}, 867_{15}, 911_{16}, 955_{17}, 999_{18}$. $[M+NH_4]_n^+ = 730_{12}, 774_{13}, 818_{14}, 862_{15}, 906_{16}, 950_{17}, 994_{18}$.

Electrospray MS, $mPEG_{750}$-R'-Br M/z:

$[M+Na]_n^+ = 717_{12}, 761_{13}, 805_{14}, 849_{15}, 893_{16}, 937_{17}, 981_{18}$. $[M+NH_4]_n^+ = 712_{12}, 756_{13}, 800_{14}, 844_{15}, 888_{16}, 934_{17}, 976_{18}$.

MALDI-ToF MS, $mPEG_{2000}OH$ M/z:

$[M+Na]_n^+ = 1815_{40}, 1859_{41}, 1903_{42}, 1947_{43}, 1991_{44}, 2035_{45}, 2079_{46}, 2123_{47}, 2167_{48}$,

2211_{49}, 2255_{50}. $[M+K]_n^+$ = 1831_{40}, 1875_{41}, 1919_{42}, 1963_{43}, 2007_{44}, 2051_{45}, 2095_{46}, 2139_{47}, 2183_{48}, 2227_{49}, 2271_{50}

MALDI-ToF MS, $mPEG_{2000}$-R-Cl M/z:

$[M+Na]_n^+$ = 1967_{40}, 2011_{41}, 2055_{42}, 2099_{43}, 2143_{44}, 2187_{45}, 2231_{46}, 2275_{47}, 2319_{48}, 2363_{49}, 2407_{50}. $[M+K]_n^+$ = 1983_{40}, 2027_{41}, 2071_{42}, 2115_{43}, 2159_{44}, 2203_{45}, 2247_{46}, 2291_{47}, 2335_{48}, 2379_{49}, 2423_{50}

9.3.2 Diblock copolymers & kinetics

Inisurf synthesis and kinetics were measured by ^{1}H NMR spectroscopy. Molecular weight analysis was carried out by size exclusion chromatography (SEC) on a Viscotek TDA 302 with refractive index, viscosity and light scattering detector (with a 690 nm wavelength laser). A value of 0.185 mL / g (obtained from Viscotek) was used for the dn/dc of polystyrene. 2 x 300 mm PLgel 5 μm mixed C columns (with a linear range of molecular weight from 200–2,000,000 g mol^{-1}) were employed; Tetrahydrofuran (THF) was used as the eluent with a flow rate of 1.0 ml / min at a temperature of 30 °C. Molecular weights are reported as 'apparent' molecular weights due to the discrepancies between polystyrene standards and PEG samples.

Emulsions and emulsion latexes were characterised by DLS (Brookhaven Instruments Zetasizer).

9.3.3 Nanoparticles

Latex particles were characterised by SEC, TEM (Mitsubishi 7600, 100 kV accelerating voltage) and SEM (Mitsubishi S-5200, 1.5 kV, in lens field emission).

Chapter 10

Results and Discussion

The aim of this chapter is to present and rationalise the observations made in the controlled polymerisation of styrene via ATRP, the synthesis of macroinitiators, the bulk phase polymerisation of styrene initiated by the macroinitiators to yield insurfs, and finally the emulsion polymerisation of DVB initiated by inisurfs, again via ATRP.

10.1 Standard ATRP

ATRP experiments using a standard initiator, (1-bromoethyl) benzene, were undertaken to determine the plausibility of using ATRP in an emulsion system. The ligand dnNBipy and Cu(I)Br were used to control the polymerisation of styrene, as described in section 9.2.

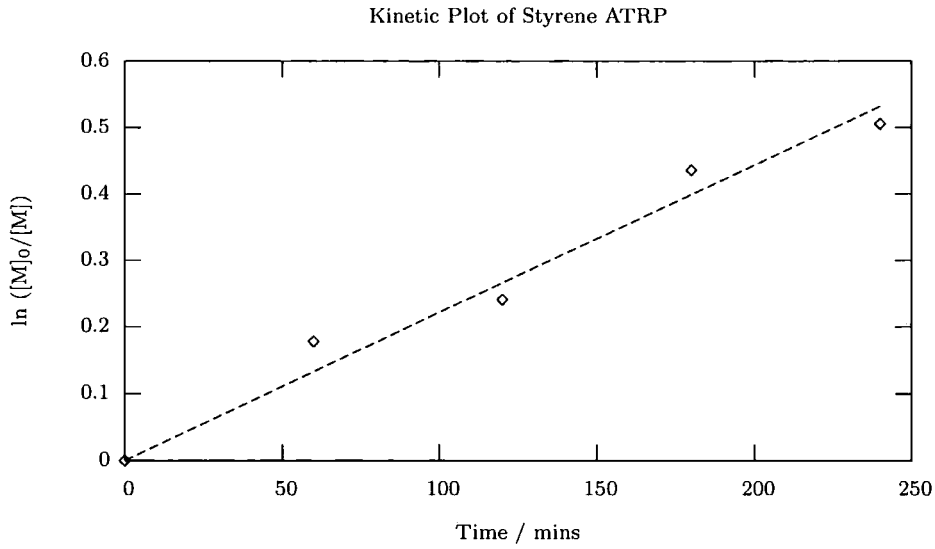

Figure 10.1: Kinetics of (1-Bromoethyl) benzene initiated ATRP of styrene in bulk, measured by NMR spectroscopy.

10.1.1 Bulk phase ATRP

The kinetics of the polymerisation of styrene in bulk were first order, as illustrated in figure 10.1. The polydispersity of the polymer was less than 1.1, molecular weight increased linearly with conversion, coinciding with a decrease in polydispersity (figure 10.2). Together these data confirm the controlled nature of the polymerisation, as defined by Matyjaszewski.[197]

10.1.2 Emulsion phase ATRP

It has been reported possible to polymerise both MMA and styrene in microemulsions by ATRP.[190] A bimodal distribution of molecular weights was reported in the paper pertaining to PMMA products: the only result reported for the polymerisation of styrene was for AGET ATRP conditions (M_n 17800, PDI 1.33). The emulsion phase polymerisation of styrene by ATRP reported in this section shows a monomodal distribution of molecular weights (although differences exist between the synthetic methods, and so results are not directly comparable).

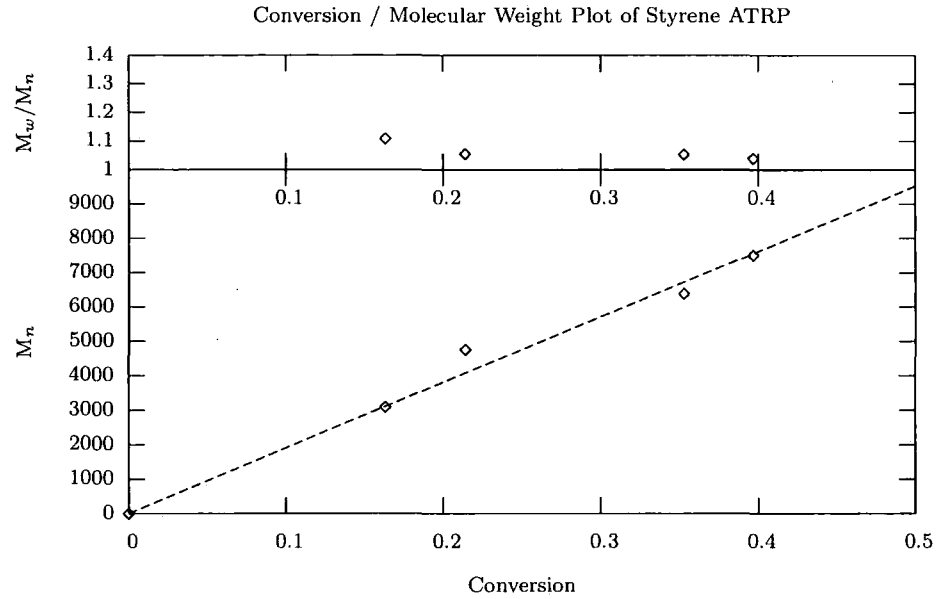

Figure 10.2: Kinetics of (1-Bromoethyl) benzene initiated ATRP of styrene in bulk. Conversion measured by NMR spectroscopy; molecular weight and PDI measured by SEC.

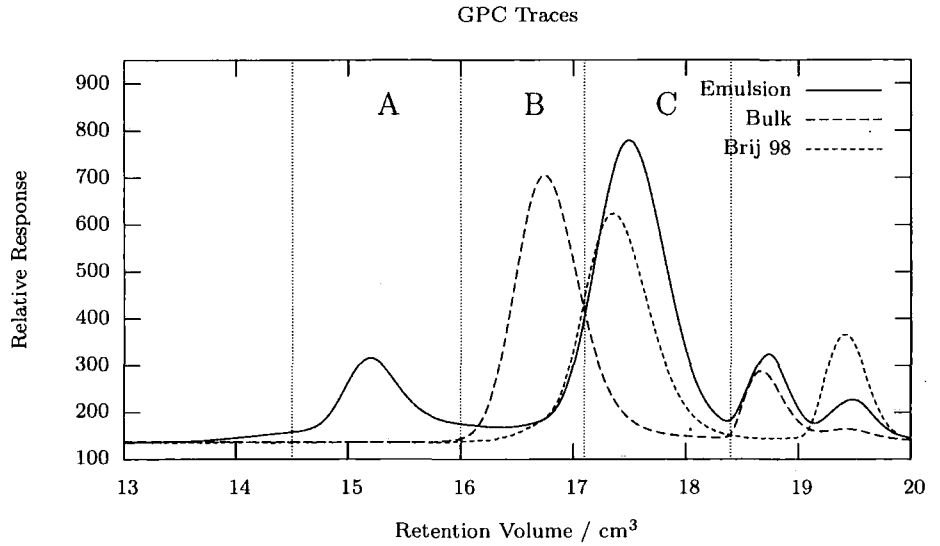

Figure 10.3: SEC traces of surfactant, bulk and emulsion phase ATRP polymerisation of styrene.

Figure 10.3 illustrates the molecular weight distributions, measured by SEC, of the products of emulsion polymerisation and the corresponding bulk polymerisation of the same monomer / initiator system solution. The SEC trace of the emulsion polymerisation shows a peak at low retention volume (region A), plus another at high retention volume (region C) corresponding to Brij 98 (trace also shown). The corresponding bulk phase polymerisation, conducted at the same temperature and for the same duration as the emulsion polymerisation, presents at an intermediate retention volume (region B), meaning a lower molecular weight polymer was produced than in the emulsion system. The number average molecular weights were ~21k (PDI 1.23) and ~5k (PDI 1.11) for the emulsion and bulk polymerisations respectively. The suggested explanation for this observation is that in the emulsion phase ATRP reaction there is likely to be incomplete solubilisation of the copper within the oil droplets. Due to the partitioning between the two phases (aqueous and oil), there is likely to be a higher monomer:initiator ratio in the emulsion system, giving a higher molecular weight product than expected and achieved in the bulk system. The emulsion polymerisation reported here yields a higher molecular weight polymer with a lower PDI than the microemulsion AGET ATRP product reported by Min and Matyjaszewski.[190]

10.2 Macroinitiator synthesis

10.2.1 Low molecular weight mPEG's

Low molecular weight mPEG's of M_n 550 and 750 were taken through the synthetic process (illustrated on page 89) to the point of diblock formation using both an acyl chloride and an acyl bromide end-capping agent. A number of procedures for the acylation of mPEG have been reported,[194,195,198] but the method outlined in

the experimental section was found to be simpler, and successful. The successful acylation was proven by quantitative NMR, where for the acyl chloride a 3:1 ratio is observed for protons relating to the MeO terminating group of the mPEG, and the proton alpha to the chloride moiety of the acylating group (see section 9.3.1), and for the acyl bromide a 1:1 ratio is observed between the same MeO of the mPEG, and the methyl group alpha to the bromide moiety of the acylating group.

Electrospray mass spectroscopy also proved acylation; mass spectra for the acyl chloride capped mPEG macroinitiator are shown in figure 10.4. The interval of peaks seen in the mPEG (starting material) sample corresponds to the addition of ethylene oxide units of forty-four a.m.u., as chain length increases by incremental additions of ethylene oxide monomer unit. The absolute values of the highest intensity series of peaks correspond to the sodium salt of the molecular ion (Na^+(mPEG-OH)), whereas the lower intensity envelope corresponds to the ammonium salt (NH_4^+(mPEG-OH)). An even lower intensity envelope can be detected (with a peak at M/z 600), corresponding to the potassium salt (K^+(mPEG-OH)).

The envelope of peaks shifts to higher mass when end-capped with the acyl chloride. There is also an increase in the number of peaks in the macroinitiator spectrum, arising from the isotope pattern of chlorine (3:1 ^{35}Cl to ^{37}Cl); this adds additional patterns to the sodium and ammonium patterns already present, resulting in a more crowded and complicated spectrum. Peaks are also present at low intensity corresponding to unreacted mPEG, even though NMR analysis showed quantitative results. Again, these peaks are detected as both sodium and ammonium salts. The key observation is the increase in molecular weight of the highest intensity envelope by 153 a.m.u., the molecular weight of the end-capping group (COCH(Ph)Cl). Similar results were observed for the acyl bromide end-capped macroinitiator.

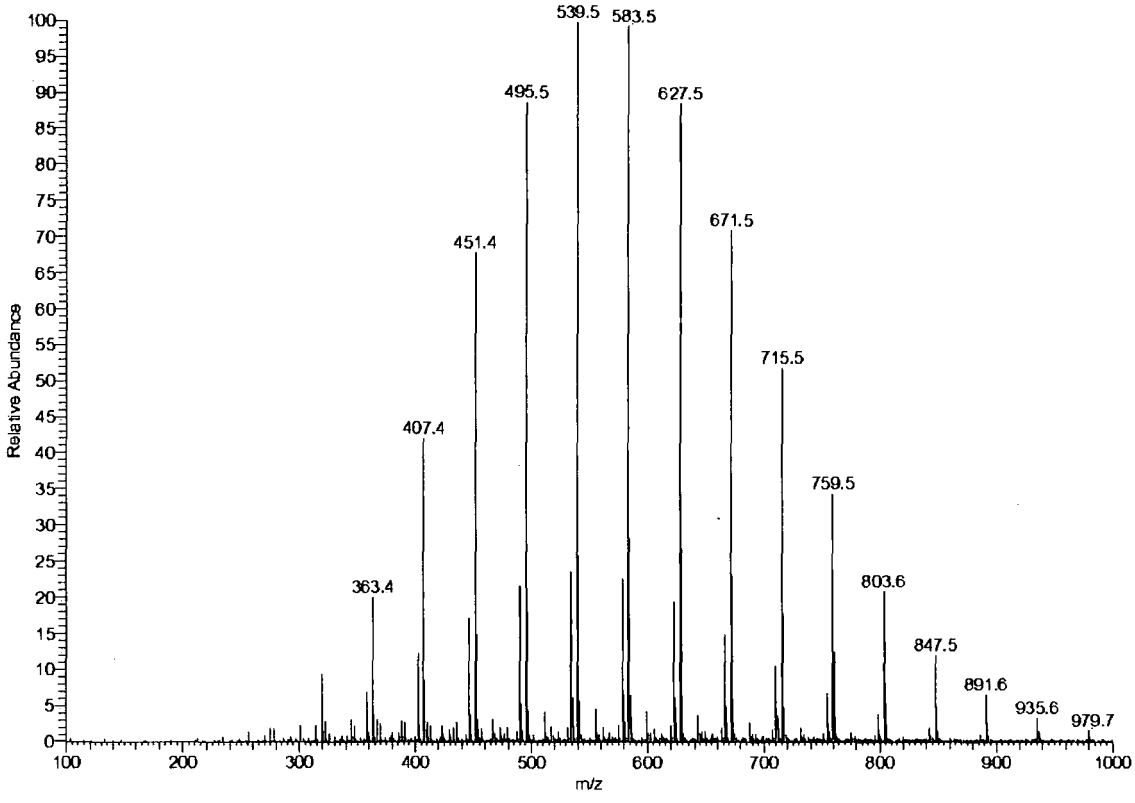

(a) mPEG

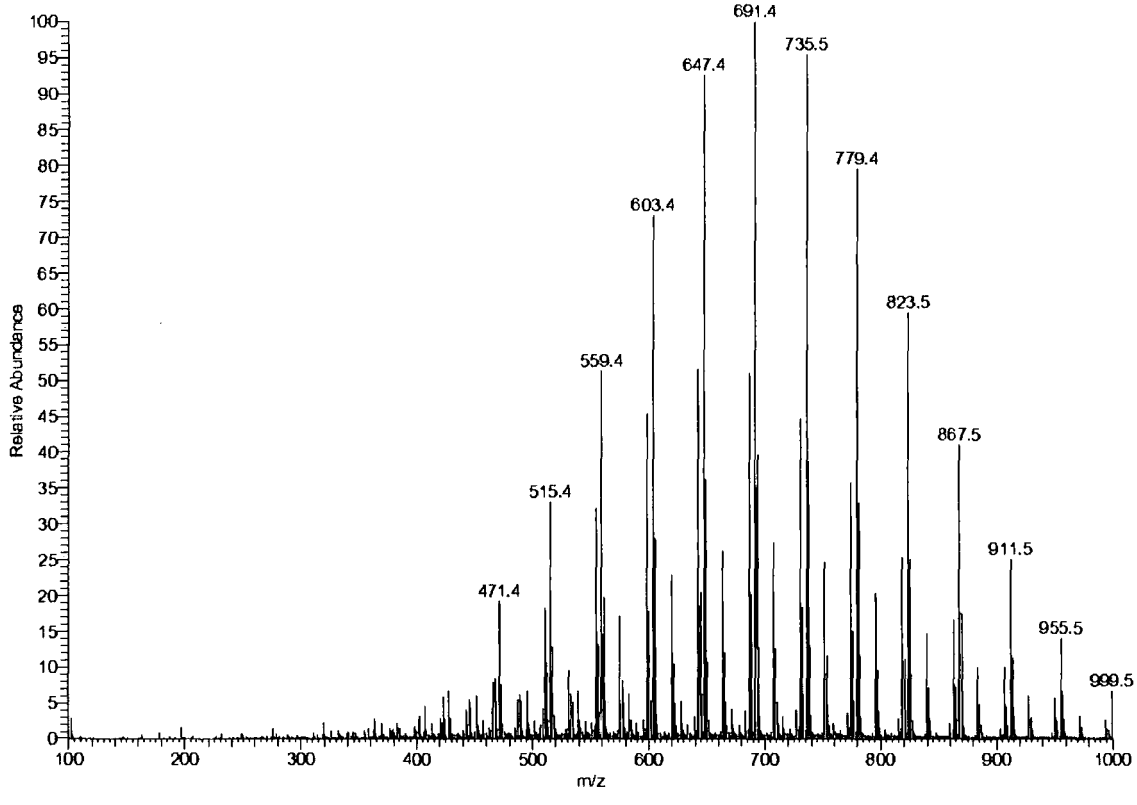

(b) Macroinitiator

Figure 10.4: Electrospray mass spectra of mPEG and acyl chloride capped macroinitiator, 550 M_n mPEG.

10.2.2 High molecular weight mPEG

An equivalent analysis was undertaken for the acyl chloride end-capping of high molecular weight mPEG, but in this case using ^{1}H NMR in conjunction with MALDI-ToF mass spectroscopy. Quantitative NMR results were recorded, and similar increases in mass were observed by MALDI-ToF *cf* electrospray mass spectroscopy analysis of the smaller mPEG based samples (see section 9.3.1 for detailed information).

10.3 Inisurf synthesis

The growth of polystyrene from the macroinitiator block was achieved by ATRP in bulk polymerisation conditions. The kinetics of polymerisation were measured by two techniques as described in the Experimental section (conversion was measured by NMR and apparent molecular weight by SEC). The kinetics of the polymerisation of styrene in bulk were measured for each molecular weight mPEG and for both bromo- and chloro- end-capped macroinitiators.

Once the kinetics were determined for each case, diblock copolymers of controlled molecular weight (and hence architecture) could be synthesised. A DP of ten was targeted to ensure achieving the desired amphiphilic properties; any lower and the PDI would be broad (which may be undesirable for control over the emulsion droplet size), any higher and a water soluble diblock would be unlikely to be achieved.

10.3.1 Low molecular weight macroinitiator

Effect of end group on kinetics

The end group used to initiate the polymerisation had a marked effect on the kinetic behaviour. This is illustrated in figure 10.5, where it can be seen that the increased lability, and hence reactivity, of the bromide has the effect of increasing the observed rate constant of the polymerisation due to the number of active chain ends being greater at any time than is the case for the less labile chloride species which has a greater number of dormant chain ends. The influence of electronic effects of the residual group alpha to the halide (methyl or phenyl) would likely be minimal, only significant for the first styrene monomer addition. Therefore, it is stated that the difference in kinetics arises from the nature of the halide alone.

A direct comparison between the data of the chloro- and bromo- end-capped macroinitiator kinetics at 110 °C shows deviation from linearity of the latter at ~50 % conversion (120 minutes), whereas the former maintains linearity to at least 51% conversion (although requires 300 minutes to achieve this conversion (data point not plotted)), showing that the chloro- species gives the greater controlled polymerisation. Supportive of this assertion is the polydispersity, as assessed by SEC. Data relating to the bulk phase polymerisation of styrene by ATRP for both types of macroinitiator synthesised from 550 M_n mPEG are listed in table 10.1.

Figure 10.6 is the SEC trace of the bromo-macroinitiator polymerised at 90 °C, evolving with time. The growth of polymer is confirmed by the shift to lower retention volume, however it is clear from the appearance of the shoulder that the polymerisation is poorly controlled. No such shoulder is observed under identical polymerisation conditions using the chloro-macroinitiator. The shoulder most likely arises due to polymer-polymer termination, possible when the concentration of active radicals is too high, and also when conversion is high. The higher reactivity

Table 10.1: Conversion, molecular weight and PDI data from the bulk polymerisation of styrene by ATRP, initiated by macroinitiators of end-capped 550 M_n mPEG.

Macroinitiator[a]	Temp. / °C	Conversion[b] / %	M_n[c]	PDI[c]	DP[d]	
					SEC	NMR
$mPEG_{550}$-R-Cl	90	7.7	1170	1.09	3.91	3.83
$mPEG_{550}$-R'-Br	90	39	2559	1.15	16.5	19.7
$mPEG_{550}$-R-Cl	110	20	1687	1.11	8.87	10.2
$mPEG_{550}$-R'-Br	110	-	3634	1.19	26.7	-

[a]R = -COCH(Ph)-; R' = -COCH(Me)-. [b]Measured by NMR. [c]Measured by SEC. [d]Degree of polymerisation measured by SEC and NMR.

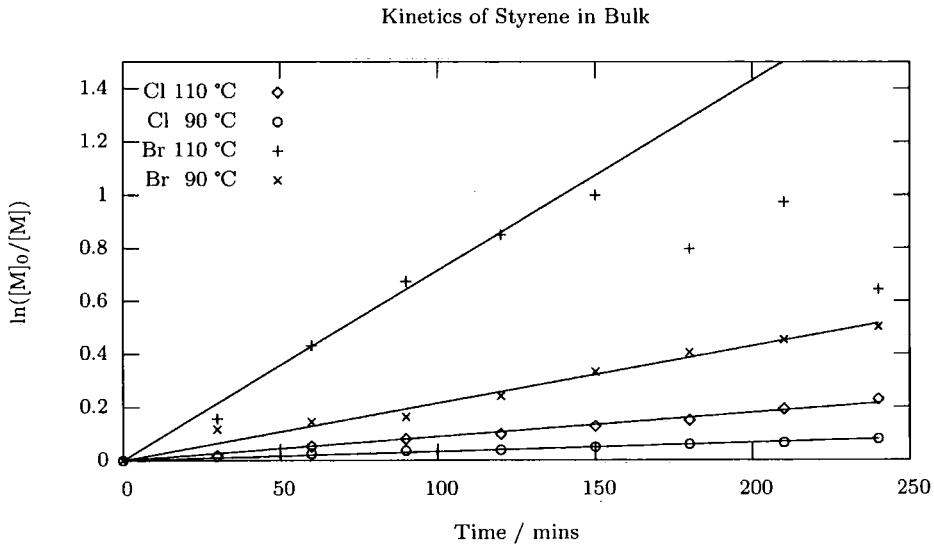

Figure 10.5: Variation of styrene polymerisation rate with temperature, measured by NMR spectroscopy.

of the bromide allows for both of these possibilities, and consequently the chloro-end-capped species appears most attractive for further study.

Effect of temperature on kinetics

Referring back to figure 10.5 and the data in table 10.1, it is apparent that, as expected, higher temperatures give faster growth. However, the deviation from linearity mentioned previously suggests that greater control is achieved with a slower polymerisation, and hence at lower temperatures. It is expected that the deviation from linearity observed in the kinetic plot (figure 10.5) would result in a plateau

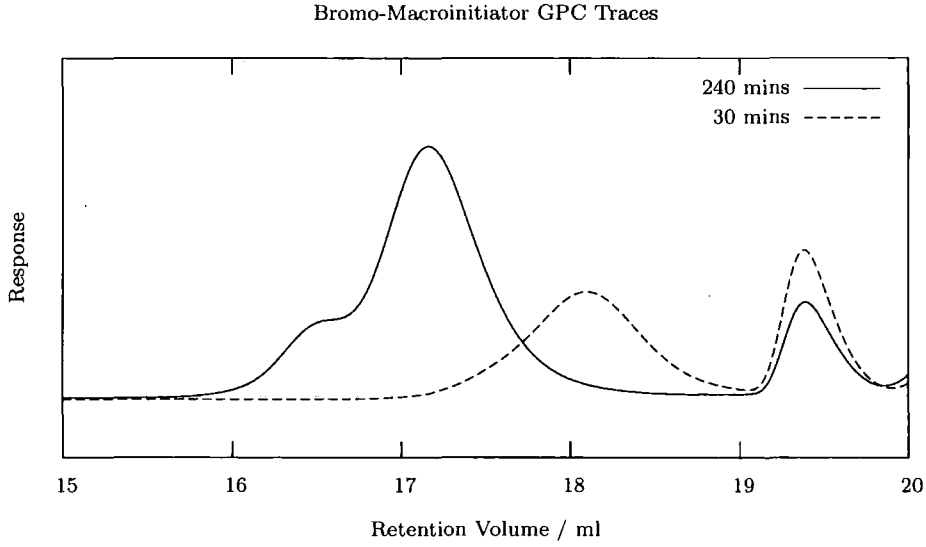

Figure 10.6: Bromo-macroinitiator SEC traces with time through reaction at 90 °C.

region; the apparent decrease in conversion is explained as arising from a sampling error due to the high viscosity of the reaction mixture.

The increase in molecular weight with conversion together with PDI are used in conjunction with the kinetic plot to assess qualitatively the level of control in the polymerisation.[197] The data displayed in figure 10.7 relate to the chloro- macroinitiator, 550 M_n mPEG. It is the case that no variation in apparent molecular weight nor PDI is detected with the increasing conversion achieved at the two temperatures in question, and this result is typical of both 550 M_n and 750 M_n mPEG macroinitiators. Consequently, it can be stated that the chloro- end-capped macroinitiator (already indicated superior to the bromo-) can be used to initiate diblock synthesis equally well at both temperatures under examination. Bulk phase ATRP can thus be carried out at 110 °C to form the inisurf diblock copolymers, followed by the ATRP of DVB in emulsions stabilised by the inisurf, at 90 °C (it is preferential that the emulsion polymerisation in water be conducted below 100 °C, negating the necessity to use pressure vessels).

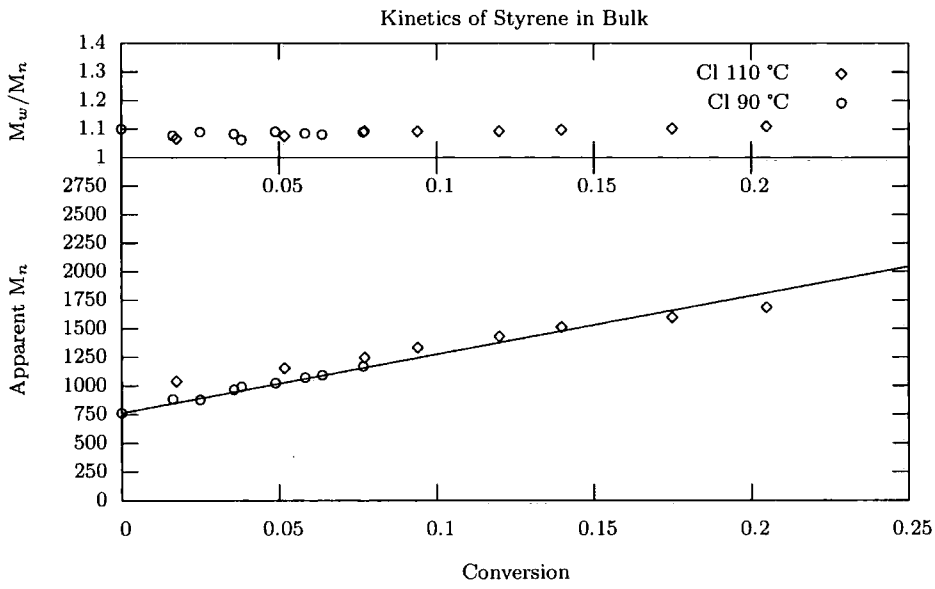

Figure 10.7: Apparent molecular weight and PDI variation with conversion at two temperatures, chloro end-capped macrointiator (M_n 550 mPEG). Conversion measured by NMR, molecular weight information by SEC.

Inisurf properties

As mentioned in the experimental section, macroinitiator was dissolved in styrene sufficient to give a DP 50 styrene block at 100 % conversion. Once the kinetics were determined inisurf was prepared by targeting 20 % converision.

From macroinitiators of low molecular weight (550 and 750 M_n), inisurfs with styrene blocks of DP ~10 were prepared. These were found to be insoluble in water even when sonicated, and consequently were unsuitable for the formation of o/w emulsion systems. For this reason the relative molecular weight of the hydrophilic over the hydrophobic region was required to be increased, and mPEG 2000 used for the macroinitiator synthesis.

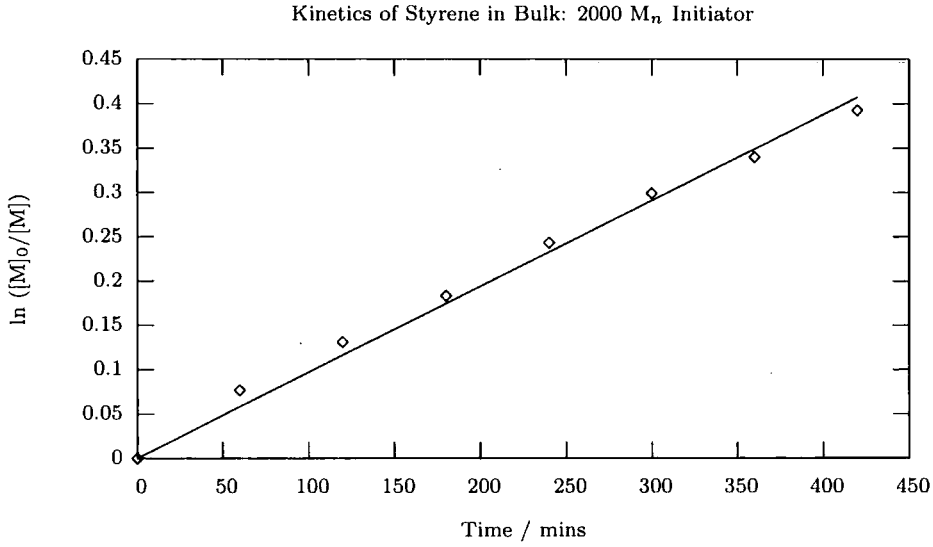

Figure 10.8: First-order kinetics of 2000 M_n macroinitiator bulk phase ATRP of styrene at 90 °C, measured by NMR spectroscopy.

10.3.2 High molecular weight macroinitiator

Kinetics

As mentioned in the experimental section, macroinitiator was dissolved in styrene sufficient to give a DP 110 styrene block at 100 % conversion (a greater volume of monomer was required to dissolve the higher molecular weight mPEG *cf* the lower molecular weight macroinitiators).

Having previously determined the preferred end-group moiety to be the chloro-species, acyl chloride was singularly used in studies relating to the preparation of high molecular weight macroinitiators. Due to the necessity in the final synthetic step of the scheme (page 89) for polymerisation in the aqueous emulsion environment, and time constraints, kinetics of polymerisation were determined solely at 90 °C. As previously in the cases of low molecular weight chloro- macroinitiators, linear kinetics were observed for f(conversion) against time, molecular weight against conversion and M_n against conversion plots (figures 10.8 and 10.9).

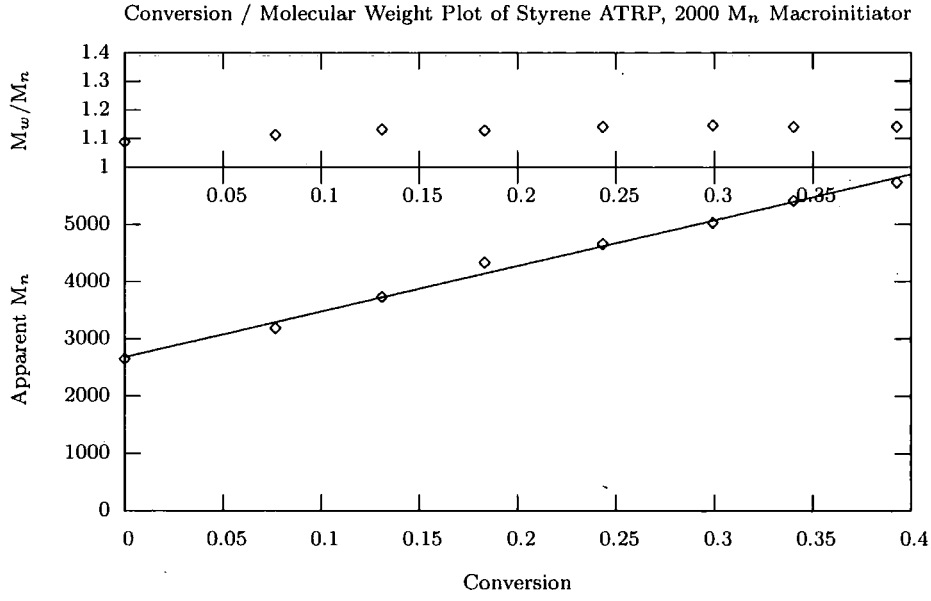

Figure 10.9: Molecular weight and PDI variation with increasing conversion of bulk phase ATRP of styrene at 90 °C, initiated by ~2000 M_n mPEG-COCH(Ph)Cl macroinitiator.

Inisurf properties

Once the kinetics were determined, inisurf was prepared by targeting 9 % conversion by stopping the polymerisation after the required time. This low conversion ensured a DP sufficiently low to produce a water soluble inisurf. Inisurf of $mPEG_{2000}$-*b*-PS_{925} (molecular weight by NMR), corresponding to a DP of 8.9, was prepared and used for the o/w emulsion ATRP polymerisation of DVB.

The surfactant properties of the inisurf were tested by dispersing toluene, used as a model for DVB. It was found that the dispersion was opaque, and still so after sonication for 15 minutes in a low powered sonic bath. A blue nanoemulsion was formed only after heating to 70 °C followed by 5 minutes sonication. The droplet size distribution was measured by DLS, in figure 10.10.

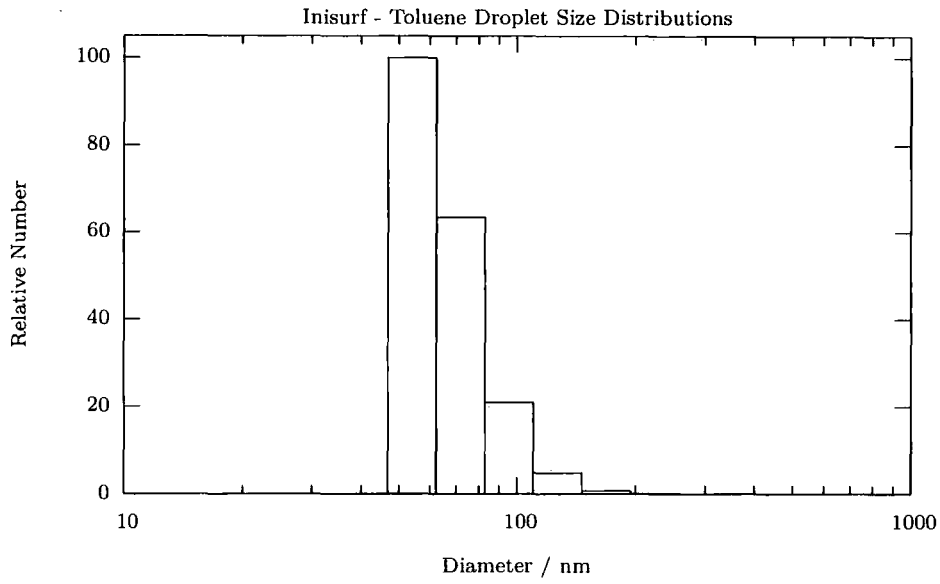

Figure 10.10: Inisurf-toluene droplet size distributions measured by DLS.

10.3.3 Inisurf emulsion polymerisation

Incomplete dispersion was observed when DVB, metal catalyst, ligand (and solvent, where used) were dispersed in equivalent emulsion systems: Milky brown dispersions were formed with dark brown oil floating on the emulsion surface, which the application of heat and sonication could not solubilise. The polymerisation was carried out regardless, and following the 24 hour reaction period the product was recovered, requiring centrifugation to remove large (visible) polymer particulate. The resulting emulsion phase was syringe filtered to remove species greater than 5 μm, diluted with water for DLS (figure 10.11) and TEM analyses and finally freeze dried.

TEM and SEM images of the products of the emulsion polymerisation of DVB by Cu(I)Br/dnNBipy mediated ATRP initiated and stabilised by mPEG-*b*-PS inisurf are shown in figure 10.12.

It is important to reiterate that the emulsion systems used to produce these particles had limited stability, requiring a filtration step before the images of figure 10.12 were taken. Accordingly, the following discussion refers to the information obtained from

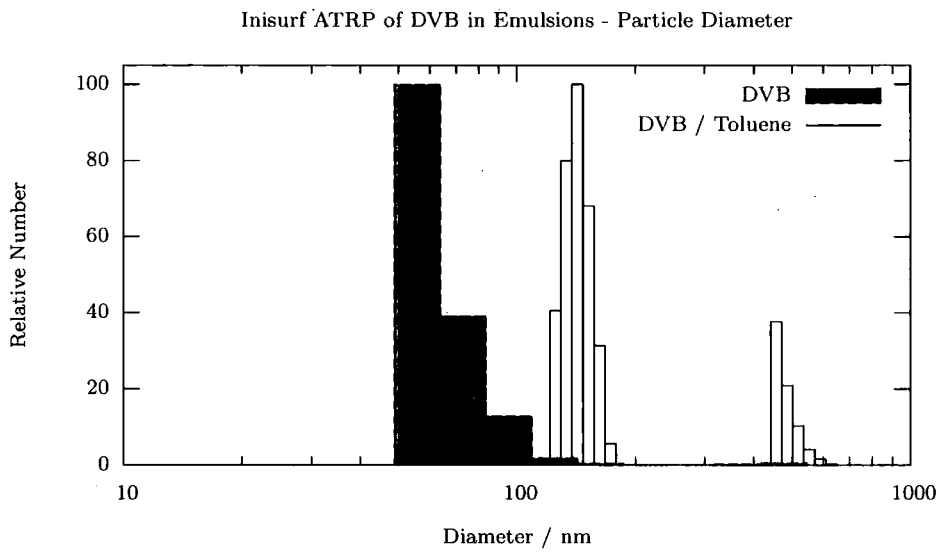

Figure 10.11: Particle size distributions (measured by DLS) of nanoparticles prepared by ATRP in emulsions in the presence of inisurf. Emulsions comprised 100% DVB and 50:50 DVB:Toluene.

these images and so neglects any products of polymerisation that failed to pass through the 5 μm filter.

The particles prepared in the absence of solvent appear more uniformly distributed with respect to particle diameter. In addition to this, the particles are smaller with no apparent structure visible by either TEM or SEM. In contrast, particles prepared with toluene in the dispersed phase are polydispersed, the largest of which appear to be hollow structures which are of the order of 200 nm to 1 μm in diameter, whereas the smaller particles are similar to those produced in the emulsion containing only monomer (lacking any visible structure, being uniform, smooth particles). The SEM image, figure 10.12(d), best illustrates the apparent bimodal distribution. The large particle in the centre of the image has a crumpled surface, indicative of collapse made possible by the void in the centre of the particle. It is also suggested that the particle to the bottom left of figure 10.12(c) shows evidence of this dimpled structure, with the dimple depressed from the top left of the particle. The resulting folding of the shell would lead to the dense band seen bisecting that region of the image of the particle.

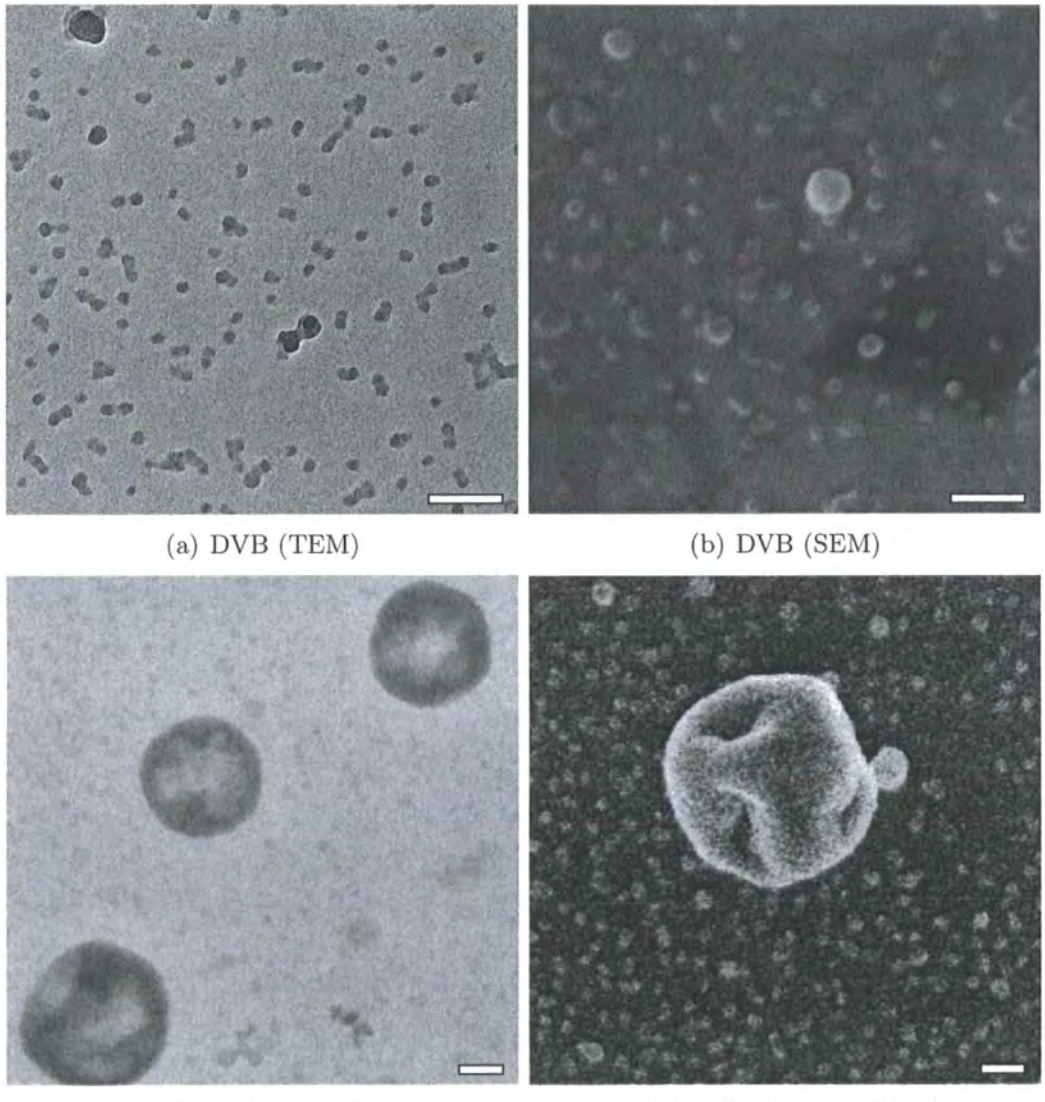

(a) DVB (TEM) (b) DVB (SEM)

(c) DVB / Toluene (TEM) (d) DVB / Toluene (SEM)

Figure 10.12: Inisurf DVB particles prepared in the absence and presence of solvent (toluene), imaged by TEM and SEM. Scale bars = 100 nm.

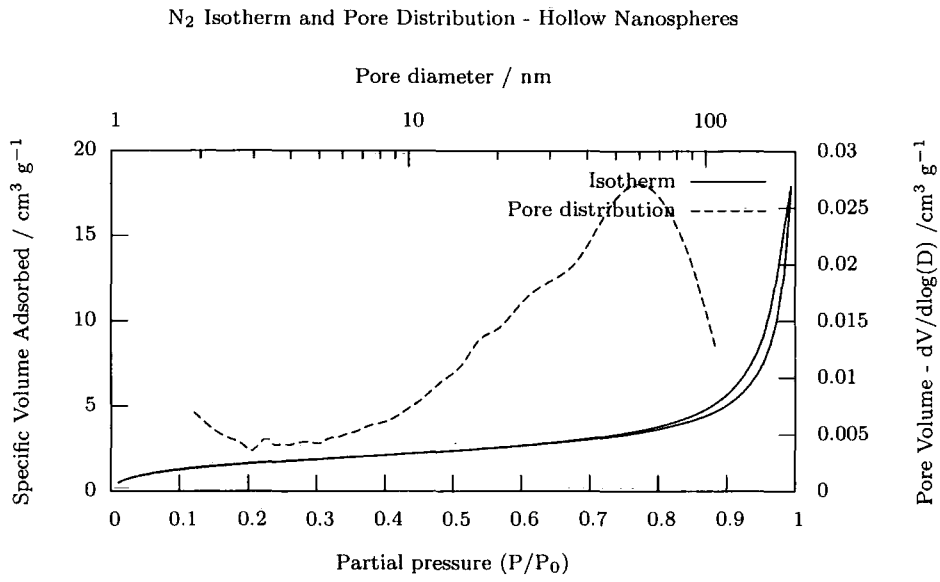

Figure 10.13: N_2 sorption isotherm and pore data of DVB nanoparticles prepared by ATRP in an emulsion (50:50 DVB:Toluene) stabilised by an inisurf.

N_2 sorption study of the products of ATRP in the absence and presence of toluene were carried out to determine whether any porosity was present. The data presented in figure 10.13 pertains to particles prepared in the presence of toluene. Data for the equivalent polymerisation was not forthcoming due to the very low surface area of the sample: although both samples were of approximately equal masses (~0.15 g), the sample prepared in the absence of solvent failed to adsorb sufficient nitrogen to produce an isotherm. The data in figure 10.13 in isolation is insufficient to determine the presence or absence of a hollow structure, with the isotherm are pore distribution data appearing similar to those samples of Part I. However, when considering that the samples were of approximately equal masses and that the particles prepared in the absence of toluene are smaller (and as such should provide a larger specific surface area), it is argued that the relatively larger sorption of N_2 by particles formed in the presence of toluene is indicative of a hollow nature. Additionally, the samples in Part I were of a different nature (crosslinked polystyrene) from the particles discussed here (with surfaces rich in mPEG), and so drawing comparisons between them may be inappropriate.

With this evidence it is concluded that the use of inisurf in the ATRP emulsion phase polymerisation of DVB allows polymerisation to be restricted to the interfacial region. It is necessary to conduct the polymerisation in the presence of an inert hydrophobic solvent in order that hollow structures be formed, else the polymerisation can propagate into the core of the particles. The emulsion system used in this case was not ideal as incomplete dispersion of the monomer was observed. Tailoring the system, either by adjustment of the inisurf diblock composition or by adjusting the emulsion composition (e.g. through using Brij type surfactants with a varied percentage of inisurf), could lead to better defined products.

10.4 Conclusions and summary

It has been demonstrated that the polymerisation of styrene can be achieved in biphasic media by ATRP when carried out using an oil soluble ligand. A comparison of bulk phase and biphasic polymerisations showed that the emulsion system provided a compartmentalisation effect, accelerating the rate of the reaction.

Macroinitiators based on mPEG starting materials were prepared by end-capping with acyl halides. Bulk phase ATRP suggested that the more reactive bromide species lacked control *cf* the chloride initiator, attributed to its higher reactivity. Inisurfs with polystyrene blocks of ~DP 10 were synthesised from mPEG macroinitiators of 550, 750 and 2000 M_n, the polymerisation of which was controlled when the chloride initiator was used. Only the macroinitiator from the 2000 M_n mPEG showed the desired water solubility, allowing the formation of o/w dispersions.

The inisurf was then used to disperse DVB, from which solid particles were synthesised. Inclusion of toluene at 50 wt% of the dispersed phase yielded polydispersed

hollow capsules of ~250 nm and up, also in the presence of smaller solid latexes. Future development should provide a more controlled synthesis.

Part IV

Nanocomposite Films

The great tragedy of Science - the slaying

of a beautiful hypothesis by an ugly fact.

Thomas H. Huxley

Chapter 11

Literature Review

The aim of this chapter is to introduce some of the current range of polymer matrix materials and composites used in the packaging industry, as well as associated technologies such as fillers and their effects on film permeability.

11.1 Introduction

The purpose of packaging is to protect a product prior to its consumption, and when appropriate, to present the product in a way that maximises salability. To meet these criteria in the meat packaging industry, the packaging film must be strong enough to withstand knocks inflicted during distribution and storage. Transparency is required to allow the product to be visible to the potential consumer.

11.2 Diffusion through films

The two main industrial applications for films in gas applications are barrier and membrane-based. A distinction is made between barrier and membrane properties:

a barrier serves to restrict the transfer of all species, whereas a membrane amplifies the separation inherent in the transfer of two or more species by selectively inhibiting the transfer of one species more greatly over another.

The mechanism by which gas is transferred across a membrane was first proposed by Graham[200] in 1866 to be independent of the gas's bulk diffusion coefficients. The rate of diffusion of different gases through films could therefore not be dictated by the macroscale defects of the film (which would render rate dependent upon diffusion coefficients), but instead must be dictated by the restrictive rate of diffusion through the polymer matrix itself. These observations lead to the development of the solution-diffusion model.

When a concentration gradient of a gas is applied across a film, the pressure difference is equilibriated by dissolution of the gas into the matrix polymer, diffusion through the thickness of the matrix film, and then release on the other side.[201,202] The permeability of the film, P, is therefore dependent upon the solubility, S, of the diffusive in the matrix polymer and the diffusion coefficient, D, through the matrix:

$$P = SD \tag{11.1}$$

Of these terms, the solubility, S, is thermodynamically controlled while the diffusion, D, is under kinetic control. The permeability coefficient, P, can be found from the rate of diffusion of a gas across a film, J, if the pressure difference across the film $(p_1 - p_2)$ and the film thickness, x, are known, using the relationship:

$$J = P\frac{(p_1 - p_2)}{x} \tag{11.2}$$

And consequently, the permeability coefficient can be defined in terms of Barrer:

$$P_{[Barrer]} = 10^{-10} \frac{V[\mathrm{cm}^3]x[\mathrm{cm}]}{A[\mathrm{cm}^2]t[\mathrm{s}]\Delta p[\mathrm{Torr}]} \tag{11.3}$$

An alternative, widely used unit for the permeability coefficient is reached by the conversion (in which a 'mil' is 10^{-3} inches):

$$1 \text{ Barrer} = \frac{1}{166.67} \cdot \frac{\text{cc mil}}{100\text{in}^2 \text{ day atm}} \tag{11.4}$$

The solubility coefficients, S, of diffusives in polymers are dependent upon the interactions of the polymer with the diffusive molecule and the competing interactions of the polymer with the polymer.[202] The case of water entering polyethylene would be thermodynamically unfavourable due to poor diffusive-polymer interactions, however water entering ethylene-vinyl alcohol would be much more favourable, and S would be larger. Water entering polyvinylidene chloride would again be unfavourable due to the strong polymer-polymer interactions. A large free volume within the film (typically present from rapid cooling to below T_g) would increase S, however crystalline regions would have a negative impact on the solubility coefficient.[202]

The gas is dissolved in regions of free volume (i.e. spaces present between polymer chains due to conformational constraints limiting packing efficiency). Thermal motions facilitate the temporary separation of polymer chains that link pockets of free volume, creating 'tunnels' of free volume along which the gas can diffuse (see figure 11.1). Computer simulations show diffusion over lengths of the order of 5 Å in ~10 ps.[201] Surprisingly, the diffusion coefficient, D, appears not to be related to the T_g or to the density of the polymer matrix.[48,201] The diffusion coefficient is affected by the free volume and the connectivity or distribution of that free volume,[201] hence it should be possible to increase D, and consequently P, by incorporating free volume.

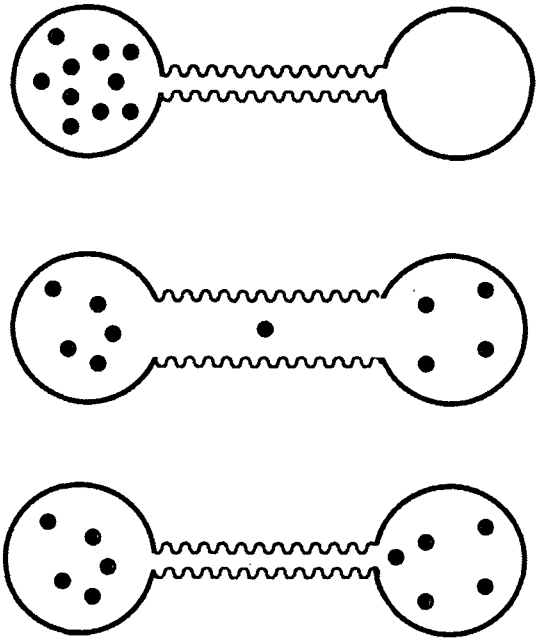

Figure 11.1: Model of gas diffusion through polymer matrices. Top: regions of free volume with concentration gradient. Middle: diffusion of single species through flexible regions of polymer chains, facilitated by thermal motion and polymer chain separation. Bottom: regions of free volume, no concentration gradient.

11.3 Film materials

In constructing a polymer film for packaging applications, the biggest factor affecting the film's characteristics is the selection of the core polymer matrix. Factors such as permeability and mechanical strength of polymer film packaging materials are measured against the standard of aluminium as this traditional packaging material is impermeable to gas and water, aromas, chemicals and bacteria, as well as UV light (against which protection is sometimes required). In moving to polymeric packaging materials, the packager seeks to benefit from product visibility while lowering packaging weight and cost, and yet retaining the barrier benefits of aluminium.

Many films are laminate composites of thinner polymer films, each with particularly good properties in different fields (e.g gas barrier, tensile strength).[202] Rather

than selecting a compromise material, a composite allows all the properties to be incorporated into one film.

11.3.1 Barrier polymers

The barrier properties of polymers to different penetrant species is difficult to predict, and so materials have been selected by empirical studies.

Oxygen barrier matrixes

Examples include polyacrylonitrile (also a sealant, ~24 mBarrer) and ethylene vinyl alcohol (1–20 mBarrer), which is also reported to be an excellent odour and aroma barrier, although as humidity increases all barrier properties decrease.[203] Poly (vinyl chloride) has an oxygen permeability of 0.09 Barrer, and polypropylene 0.9 Barrer.

Moisture barrier matrixes

These are typically cyclic olefin copolymers[203] (up to ~33 mBarrer). Polychlorotrifluoroethylene (~2.5 mBarrer) is much less permeable, but is more costly and processing is more difficult.

11.3.2 Permeable polymers

As mentioned previously, permeability comes from the thermodynamic and kinetic factors unique to each matrix-penetrant combination. Those polymers with greatest free volume are generally most permeable, for example linear low density polyethylene (LLDPE) has an oxygen permeability of ~3 Barrer.

11.4 Nanocomposite films

Inclusion of nanoscale fillers into polymer films influences a range of properties, including mechanical strength and permeability.[204]

11.4.1 Mechanical Properties

A large amount of work has been published relating to the inclusion of nanoparticles,[205] especially carbon nanotubes,[206–208] into polymer films. Briefly, the most interesting area of this research is in the mechanical properties of the composites, with large increases in tensile strength observed with carbon nanotube loading, however typically this is coupled with decreased flexibility and toughness.

A particular issue recognised with the inclusion of nanoparticles in polymer film composites is particle aggregation.[209,210]

11.4.2 Permeability

Filler particles can be used to increase permeability by dispersing them in polymer films, then stretching the films to encourage particle-film debonding. This creates void spaces around the particles, increasing film permeability.[211,212]

Fillers can be added to films to reduce permeability.[202,213] These fillers can act as either passive or active barriers, depending on their mode of action.

Passive barriers restrict the transfer of gas through the film by diffusion control.[202] The rate of diffusion decreases as the particle filler generates an increase in the effective path length that the gas must travel through the film.[214] This path length increases with increasing particle aspect ratio, and more so again when particles

with high aspect ratios are aligned perpendicular to the transient axis. Layered silicates are typical examples of passive barrier fillers.[215]

Active barriers are chemically reactive toward the diffusive species.[213] This can be by catalytic action, in which case the material maintains its barrier properties (unless saturation is reached). Scavengers also behave as active barriers, but in this case the reaction with the diffusive is irreversible and so the material has a limited scavenger lifetime. Scavengers for oxygen are typically species with unsaturated carbon-carbon bonds, coextruded with catalytic transition metals,[203] or oxidisable iron complexes.[213]

Chapter 12

Experimental

The aim of this chapter is to introduce the experimental procedures employed in the preparation of nano-composite films, and the analytical techniques utilised in their characterisation.

12.1 Introduction

The motivation behind this thesis was to determine the effects of the addition of nanoscale filler particles on the properties of polymer films. To that end, samples of hypercrosslinked porous nanoparticles and the corresponding lightly crosslinked precursor gel-like particles (discussed in Part II) were taken to Cryovac's R&D facilities in Duncan, SC., where they were mixed into polymer melts, and then pressed into films. The oxygen gas permeability of the resulting films was measured at the facility; other film properties were investigated upon returning to Durham.

12.2 Synthesis

12.2.1 Materials

Polystyrene nanoparticles of ~50 nm diameter (90% styrene, 10% DVB) were prepared as described in Part I. Amalloy B1199 (a styrene based copolymer) was used as supplied by Amco Plastic Materials, Inc.

Precursor gel and hypercrosslinked poly(vinylbenzyl chloride-*co*-divinylbenzene) particles of ~400 nm diameter were prepared by surfactant free emulsion polymerisation, as discussed in Part II. Linear low density polyethylene (LLDPE, DOWLEX™ 2045 pellets (M_n 27100), Dow Plastics) was used as provided.

12.2.2 Film formation

Optical properties study

Amalloy was melted in a Brabender mixer at 180 °C, and the filler added to comprise a loading of 5%, mixed for ten minutes. Films were pressed in a 30 tonne Carver press at 160 °C to ~175 μm thickness.

Permeability study

LLDPE was melted in a Brabender mixer (20 g capacity) at 150 °C, mixed at 30 rpm. The required mass of particle filler was added (totalling 20 g of material) and mixed for ten minutes before the blended mixture was removed and cooled to form casts. Typically, 1.2 g of cast material was placed between PTFE sheets separated by brass shims (0.15 mm thickness) and pressed in a Carver press (up to 8 tonnes at ~190 °C)

for up to five minutes. The films were removed from the press and cooled rapidly by heat sinking between aluminium blocks.

12.3 Analysis

12.3.1 Optical properties study

Gloss, haze, and transmission were measured at Sealed Air's R&D facility in Duncan, SC., by Steven Ensley.

12.3.2 Permeability study

Film thickness was gauged by averaging ten measurements across the film area.

Oxygen transmission rates (OTR) were measured by Illinois Instruments Model 8001 Oxygen Permeation Analyser, measuring over a one hour period. Three films were pressed from each cast and OTR measured for each.

Young's modulus was calculated from stress / strain curves, measured by dynamic mechanical analysis (DMA, TA Instruments, Q800 using a film tension clamp). Samples were prepared as 6.34 mm wide strips; sample length and thickness varied by sample. Samples were equilibrated at 25 °C for 5 minutes under a loading of 0.0500 N before the force was increased at a rate of 3 N min^{-1}, to a maximum of 18 N.

Optical microscopy was employed to observe film clarity, and to assess qualitatively aggregation and the level of inclusion of foreign matter. Particle distribution and film-particle cohesion were assessed by TEM, carried out on microtomed samples of

80–100 nm thickness, sectioned under cryogenic conditions (−110 °C). Images were acquired using a Hitachi 7600 TEM at 100 kV accelerating voltage.

Chapter 13

Results and Discussion

The aim of this chapter is to present and account for the observations made in the formation and testing of filler-containing films.

13.1 Optical properties study

Nanoparticles of ~50 nm were incorporated into films in order to test whether the use of such small particles would allow retention of optical properties. Table 13.1 shows the data collected on these films. These data suggest that gloss, transmission and haze are unaffected by the inclusion of ~50 nm nanoparticles. It is possible that an equivalent study with hypercrosslinked nanoparticles of 50 nm diameter would not produce the same findings as the residual iron content may reduce transmission. According to the engineer's report, there was a slight decrease in the permeability with the inclusion of these nanoparticles.[216]

Table 13.1: Optical properties of Amalloy and nanoparticle composites. Filler composition 90:10 by weigh ratio styrene:DVB.

Sample	Thickness / μm	Gloss %	Transmission %	Haze / NTU
Amalloy	186	27.2	91.9	31.9
5% Filler	155	32.6	91.2	29.6

13.2 Permeability study

13.2.1 Film preparation

It was qualitatively observed that the viscosity of both hypercrosslinked and precursor particle melts increased with particle loading, with the viscosity of the hypercrosslinked particle melts being the greater at each loading in comparison with precursor particle melts. This trend was repeated in the cutting of the resulting casts prior to film pressing: the casts containing higher filler contents were tougher, with hypercrosslinked filler particle casts requiring more effort to cut than the equivalent precursor particle containing casts. Additionally, the samples containing precursor gel particles produced the strong aroma of VBC monomer, probably due to residual monomer trapped inside the gel particles being released as the melt temperature was above the particle T_g. No monomer was detected in this way when hypercrosslinked particles were added to the melts.

Casts of LLDPE and precursor particles at lower filler content (especially 5% – 10%) were inhomogeneous, with aggregates of filler clearly visible to the naked eye. Longer mixing times appeared to yield no better homogeneity, and it is hypothesised that the gel particles fused together to some extent during the mixing process due to the thermally stimulated release of small quantities of unreacted monomer. Conversely, no such effect was observed in the case of hypercrosslinked particle fillers and apparently homogeneous casts were produced. In this case, no particle fusion would be expected as no residual monomer was detected.

Table 13.2: Sample film thickness by micrometer. Composition by wt % of Precursor and Hypercrosslinked particles, each film an average of ten measurements, final average of three films.

Sample	Thickness / μm			Average / μm
LLDPE	150	165	168	161
5% Precursor	180	182	185	182
10% Precursor	178	185	189	184
20% Precursor	164	167	176	169
40% Precursor	163	189	203	185
5% Hypercrosslinked	163	179	205	182
10% Hypercrosslinked	154	182	197	178
20% Hypercrosslinked	161	166	205	178
40% Hypercrosslinked	208	210	214	211

The increased viscosity of composites with higher loadings required increased pressures to press thin films, and the resulting films were still typically thicker than films of lower filler content (film thickness data shown in table 13.2).

13.2.2 Particle distribution

Optical microscopy

The distribution of particles and the presence of foreign substances in the films (inclusions) was investigated by optical microscopy. Figure 13.1 shows the optical micrographs of each film variant with the exception of the 40 wt% hypercrosslinked sample, this due to insufficient light transmission to enable the acquisition of a photograph.

The LLDPE virgin film shows foreign inclusions most clearly, although these are present in all of the films, and it is assumed that any affect on physical properties arising from these is equal to each film. The highly coloured patterning, made visible in the micrograph through the combination of crossed-polarisers and tint plate, is indicative of crystalline structure. It can be seen that increased loading of

particle filler decreases the occurrence of spherulites and therefore reduces the total crystalline structure due to the reduction in volume of LLDPE free from particles.

As the particle loading decreases so the formation of larger discrete regions of particles appears to become more favourable, as seen in figures 13.1(f) and 13.1(h). Hypercrosslinked particles appear more uniformly distributed.

Electron microscopy

Sectioned films containing precursor gel particles are shown in figure 13.2. Large sections of aggregated particles were found throughout the samples, supporting the findings from optical microscopy. The rafts of particles appear closely packed and well bonded to the matrix film (especially evident in figure 13.2(b)). Small regions of better dispersed particles are also evident, but no particles appear to be discretely distributed. The films of precursor particles therefore have what amount to plates of non-porous filler, and so it may be expected that these would decrease permeability[202] (provided that the permeability of the plates is lower then the matrix polymer).

Sectioned films containing hypercrosslinked particles are shown in figure 13.3. The lower magnification images (figures 13.3(a) and 13.3(b)) show the reasonably even dispersion of filler particles within the polymer matrices.

The films were affected by the sectioning process, and damage is observed as indicated by the white arrows superimposed over these images. This damage arose where particles were pulled out of the film or where the particles pulled and tore the film by the sheering action of the microtome. Also highlighted in figure 13.3(a) is a region of closely packed particles, observed in all images, suggesting particle loading to be reaching a limiting volume. It is still possible to observe regions of LLDPE between particles, better illustrated in figure 13.3(c). Here again, film damage is

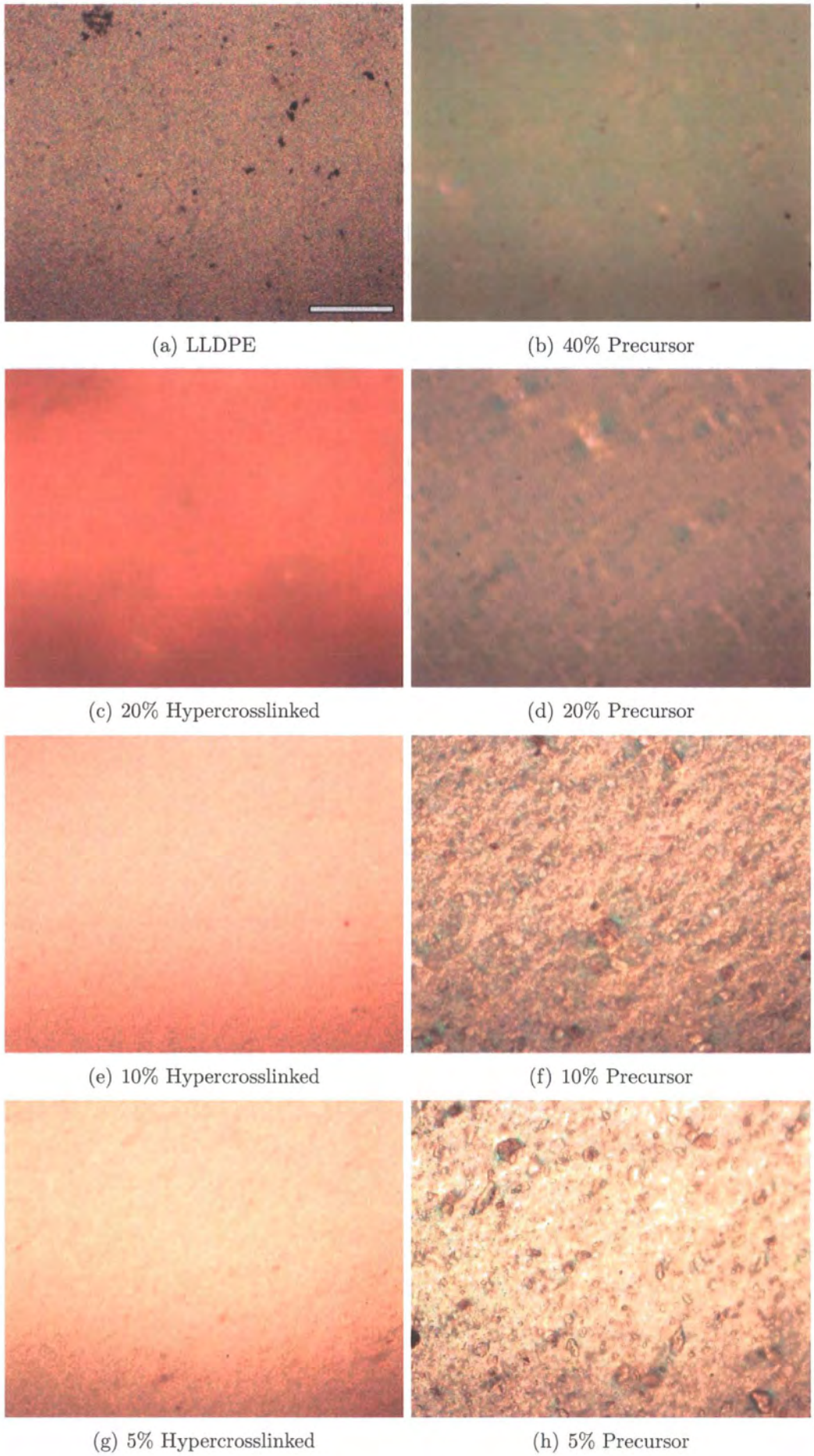

(a) LLDPE (b) 40% Precursor

(c) 20% Hypercrosslinked (d) 20% Precursor

(e) 10% Hypercrosslinked (f) 10% Precursor

(g) 5% Hypercrosslinked (h) 5% Precursor

Figure 13.1: Films imaged by optical microscopy under crossed polarisers, through 530 nm tint plate. Scale bar = 250 μm (all images to scale).

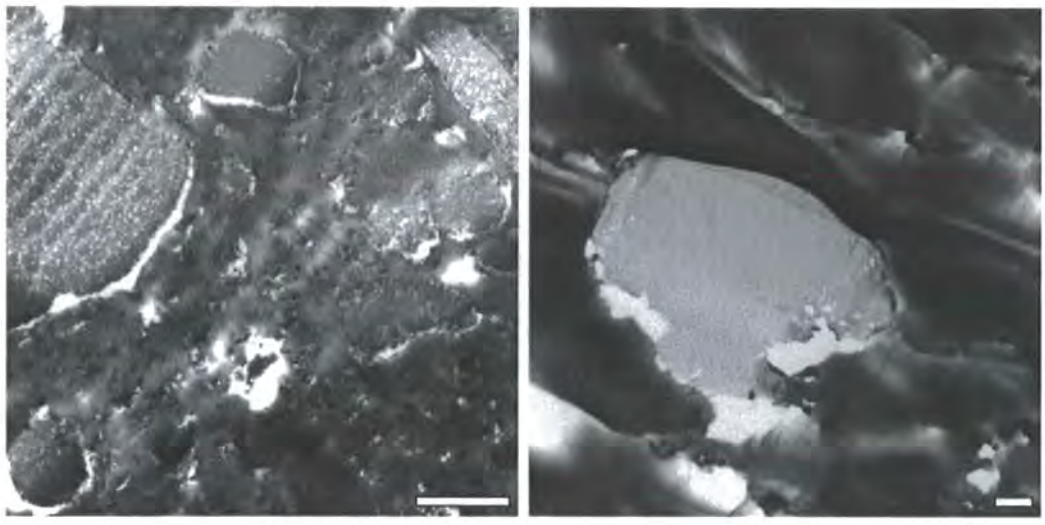

(a) 40% (b) 20%

Figure 13.2: Cryogenically sectioned composite films containing gel precursor particles (loading by weight) imaged by TEM. Scale bars = 10μm and 2 μm.

observed as a consequence of sample preparation for TEM. In both high magnification images, many particles appear to be well bound by LLDPE. This indicates good matrix-filler compatibility, and suggests that debonding at the matrix-filler interface is not significant, if present at all in the unsectioned films.

13.2.3 Physical properties

Oxygen transmission rate

The transmission rate variation of oxygen with film particle loading is shown in figure 13.4. Addition of gel-like precursor particles decreases film permeability as expected based on the evidence from optical and electron microscopy. Large plate-like non-porous aggregates increase the path length and therefore reduce the rate of oxygen diffusion across the film.[214] There is a linear decrease in the permeability with particle loading.

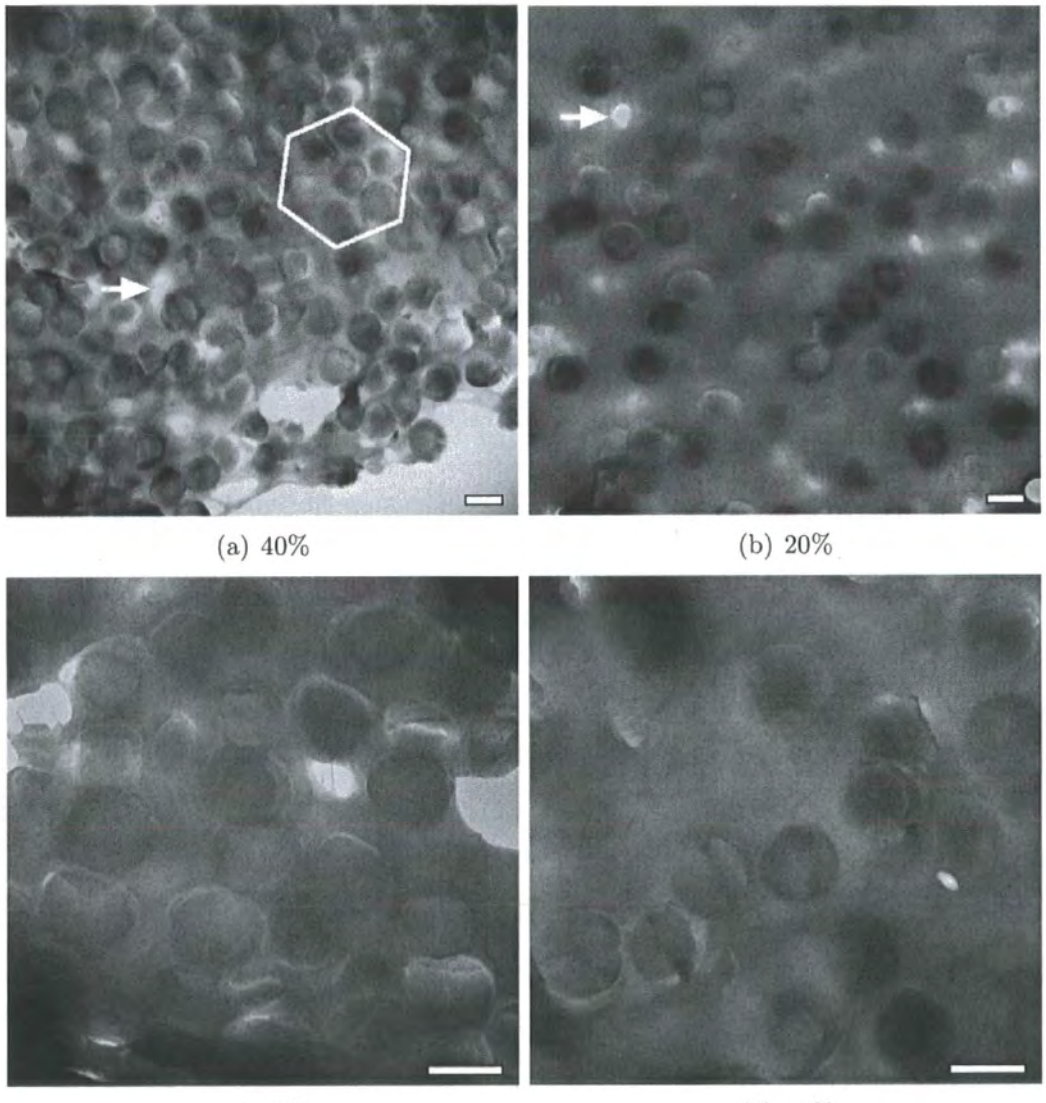

(a) 40% (b) 20%

(c) 40% (d) 20%

Figure 13.3: Cryogenically sectioned composite films containg hypercrosslinked particles (loading by weight) imaged by TEM. Scale bars = 500 nm.

By contrast, addition of microporous nanoparticles introduces free volume into the film and this is reflected with an increase in oxygen permeability. The required loading of particles to see an appreciable increase in permeability excludes this material from industrial scale applications. The fit on this data is less reliable. The closest model available[214] to assist with this analysis considers films and fillers with significantly different permeabilities, and shows an approximately linear increase in permeability with loading. It is not known whether the system presented here meets this criterion, and so applying a linear fit may not be appropriate.

An alternative argument that accounts for the increased permeability may be proposed. On that basis that the addition of the porous particles resulted in a more uniform composite material than the addition of nonporous precursor particles (figures 13.2 and 13.3), it may be expected that the total degree of crystallinity was less for the porous particle composite (as the material with the gel particles may have unadulterated crystalline regions). The lower crystallinity and greater free volume that results would therefore provide a more permeable film in the case of the composite with the more evenly dispersed filler. It is therefore possible that the same increase in film permeability could have been achieved with non-porous particles provided that they were equally well dispersed throughout the matrix.

Mechanical properties

The increase in Young's modulus (E) with particle loading is shown in figure 13.5. The value of E increases approximately linearly with low particle loading, deviating from linearity at high loading in the case of hypercrosslinked filler particles. This finding is similar to published data on the inclusion of multiwalled carbon nanotubes at up to ~9% loading.[217] The increase in modulus with the precursor particle filled films can be attributed to the transfer of stress to the nanoparticles: the relative Young's moduli of polystyrene (similar to pVBC) and polyethylene are ~3000–

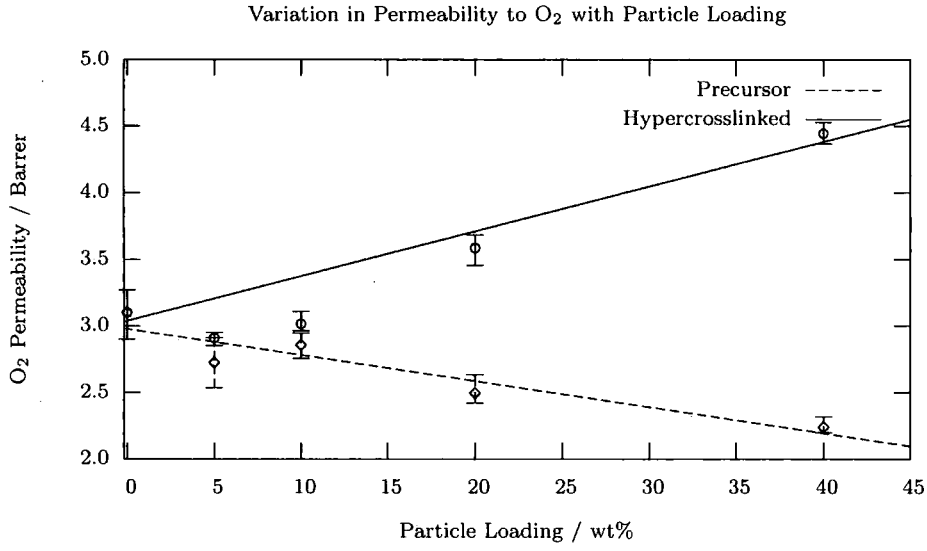

Figure 13.4: O_2 Permeability variation with particle loading.

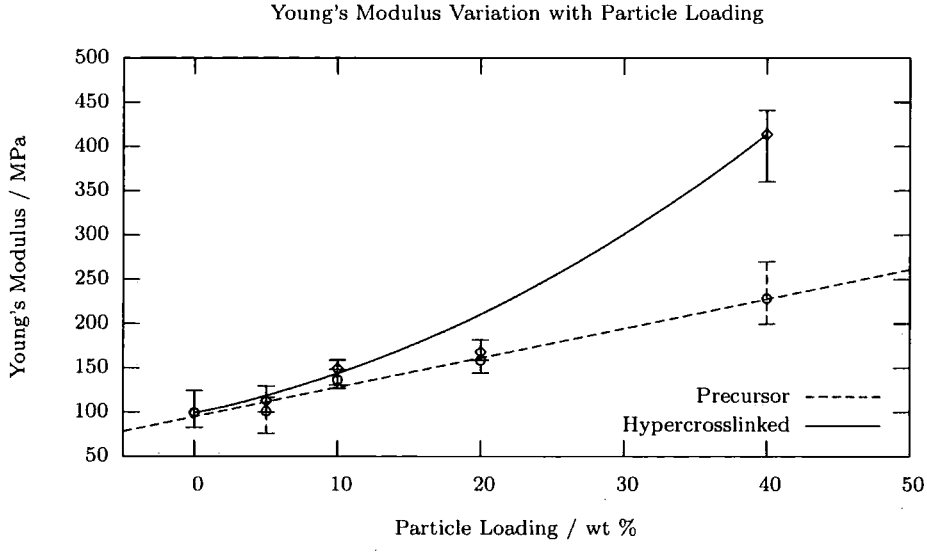

Figure 13.5: Young's modulus variation with particle loading, measured by DMA at 20 °C.

3600 MPa and 50–170 MPa respectively.[48] The further increase in E observed in the hypercrosslinked nanoparticle filled material comes from the high degree of crosslinking, with a stiffer filler producing a stiffer composite material.

13.3 Conclusions and summary

In this chapter it has been demonstrated that the addition of gel nanoparticles, with even small amounts of excess monomer, to polymer melts results in the formation of large aggregates, and these aggregates inhibit the diffusion of oxygen across the composite polymer film. A linear correlation between loading and decreasing permeability was observed.

Addition of hypercrosslinked particles to the same molten polymer produced an homogeneous dispersion. It is possible that the porous nature of the filler introduced free volume to the films and so increased the permeability, however it is more likely that the increase in permeability was due to a decrease in film crystallinity, arising from a more even dispersion of the particles. A linear correlation is claimed between particle loading and permeability.

The limited study of the optical properties indicates that inclusion of 50 nm nanoparticles has minimal negative impact on optical properties, and by extension, the use of 50 nm hypercrosslinked nanoparticles may increase permeability while having a lesser adverse effect on optical properties *cf* ~400 nm hypercrosslinked particles.

These data are summarised in table 13.3.

Table 13.3: Summary table of composite film physical properties.

Sample	Loading / wt%	O_2 Permeability / Barrer	Young's Modulus / MPa
LLDPE	-	3.101	99.50
Precursor	5	2.725	100.93
	10	2.857	136.43
	20	2.495	158.50
	40	2.240	228.40
Hypercrosslinked	5	2.908	112.99
	10	3.016	149.23
	20	3.585	168.10
	40	4.444	413.57
Amalloy	-	7.500	-
90% Sty, 10% DVB	5	6.836	-

Part V

Future Work

It's time that we began to laugh and cry

and cry and laugh about it all again.

Leonard Cohen

Chapter 14

Overall summary and future work

14.1 Summary

Nanoparticles of ~50 nm diameter were prepared from o/w emulsions comprising DTAB/DDAB surfactants, styrene and DVB with or without toluene or heptane. These particles were reasonably monodispersed, despite the parent emulsion being polydispersed, and were observed to decrease in diameter with increasing DVB content. The presence of hydrophobic solvent appeared to have negligible influence over the particle size and specific surface areas. High crosslinker contents and the use of porogen solvents failed to produce porous nanoparticles by this route. However, when these particles were added to Amalloy, no significant change in optical properties was observed, showing that, as hypothesised, the inclusion of <50 nm nanoparticles can produce a film with unspoiled optical properties. From this it is suggested that the use of other 50 nm nanoparticles would also have limited impact on the optical properties of other composite films. The effect of these particles on film permeability was limited (see table 13.3, page 139), and no firm conclusions can be drawn from this limited study.

Hypercrosslinked nanoparticles were prepared similarly to published literature.[76] Inclusion of these particles (of ~400 nm diameter and with specific surface areas of approximately 1000 $m^2\ g^{-1}$) increased the permeability of LLDPE composite films by ~50% at a loading of 40 wt%. TEM imaging showed the particles were well dispersed and well bonded to the LLDPE polymer matrix, and as such it was concluded that the increase in permeability was not due to void space arising from particle-matrix debonding, and was instead attributed to either the free volume introduced within the particles or, more likely, due to a decrease in film crystallinity. These results demonstrate that the inclusion of porous nanoparticle filler materials does increase film permeability. Together with the increase in permeability, the Young's modulus of the composite films increased with particle loading, resulting in stiffer films. The optical clarity of the films decreased significantly, rendering the product unsuitable for food packaging applications.

Large (~400 nm in diameter) gel particles were also blended into LLDPE to produce reference composites. In these cases the particles fused together, visible by optical and TEM imaging, into large aggregates. These acted similarly to clay platelets used to increase barrier properties, with a decrease in permeability measured with increased particle loading. The composite films again showed increased Young's modulus and reduced optical clarity.

Finally, hollow nanoparticles were prepared by an emulsion ATRP synthesis. In this work, inisurf block copolymers were prepared from end-capped mPEG starting materials by ATRP in bulk styrene. It was determined that a diblock with a hydrophilic:hydrophobic weight ratio of 2:1 was required to produce a water soluble inisurf for this synthesis. Once prepared, emulsification of DVB using this inisurf allowed the synthesis of solid nanoparticles of ~40 nm in diameter, where emulsification of DVB and toluene (1:1 by weight) produced polydispersed ($\geq$250 nm

diameter) hollow nanoparticles in addition to more solid nanoparticles. Thus, a novel synthesis of hollow nanoparticles has been devised.

14.2 Suggestions for future work

It is proposed that nanoparticles similar to those prepared in Part I, but without crosslinker, may be used as cores for a CSTed preparation of hollow nanoparticles. It may be possible to deposit a lightly crosslinked pVBC shell around such a core particle which, once the core is removed, could be hypercrosslinked by Friedel-Crafts alkylation, as in Part II, to yield a hypercrosslinked hollow particle. This particle would possess a void of controlled diameter (approximately 50 nm, according to the results presented in Part I) with a microporous shell. This particle may maximise the O_2 permeability of a composite film material while the film retains its optical clarity (or at least it should possess better optical properties than observed in the films containing hypercrosslinked particles reported in Part IV).

It is unlikely that hollow pVBC nanoparticles could be prepared via the ATRP route outlined in Part III as the benzyl chloride moiety would be free to initiate ATRP of the monomer within the core of the emulsion droplets. However, it is possible that an inisurf may have an anchoring effect to drive a phase separation. For this reason, it would be of interest to conduct this experiment. It may prove possible to use a similar controlled-free-radical-polymerisation-in-emulsion approach with a RAFT agent to prepare ultra-porous hollow nanoparticles. Such an approach would be unlikely to be commercial due to the necessity for greater control over the reaction, however would be of academic interest.

Regarding the ATRP synthesis reported in this thesis, study of inisurf/surfactant content, inisurf composition, and emulsion composition (possibly with the aim of

developing a nanoemulsion polymerisation) should be undertaken. Similarly, the body of work regarding the synthesis of hypercrosslinked <50 nm nanoparticles could yet be completed. To achieve this, the tendency towards particle aggregation during the hypercrosslinking reaction must be overcome.

The mechanism by which the permeability of the film was increased could be elucidated by completion of two further experiments: a study of the film crystallinity by WAXS and a similar study to that which was carried out in part IV using the non-porous particles prepared in part I.

Bibliography

1. "An Analysis of Plastics Consumption and Recovery in Western Europe 2000", Association of Plastics Manufacturers in Europe Report, 2002 Brussels.

2. Mark, J. E.; Allcock, H. R.; West, R. *Inorganic Polymers;* Prentice Hall: Englewood Cliffs, NJ., 1992.

3. Cowie, J. M. G. *Polymers: Chemistry & Physics of Modern Materials;* Blackie and Son Ltd.: Glasgow, 2 ed.; 1991.

4. Cameron, N. R. *Polymer* **2005,** *46,* 1439–1449.

5. Leber, N.; Fay, J. D. B.; Cameron, N. R.; Kranjc, P. *J. Polym. Sci. Part A: Polym. Chem.* **2007,** *45,* 4043–4053.

6. Dukhin, S. S.; Sjöblom, J.; Sæther, Ø. An Experimental and Theoretical Approach to the Dynamic Behaviour of Emulsions. In *Emulsions and Emulsion Stability*; Sjöblom, J., Ed.; CRC Press.: Florida, 2006; Chapter 1.

7. Rayleigh, J. S. *Phil. Mag.* **1871,** *41,* 107–120.

8. Forgiarini, A.; Esquena, J.; González, C.; Solans, C. *Progr. Colloid Polym. Sci.* **2000,** *115,* 36–39.

9. Solans, C.; Izquierdo, P.; Nolla, J.; Azemar, N.; Garcia-Celma, M. J. *Curr. Opin. Colloid Interf. Sci.* **2005,** *10,* 102–110.

10. Forgiarini, A.; Esquena, J.; González, C.; Solans, C. *Langmuir* **2001,** *17,* 2076–2083.

11. Sajjadi, S. *Langmuir* **2006,** *22,* 5597–5603.

12. Izquierdo, P.; Esquena, J.; Tadros, T. F.; Dederen, J. C.; Feng, J.; Garcia-Celma, M. J.; Azemar, N.; Solans, C. *Langmuir* **2004,** *20,* 6594–6598.

13. Tadros, T.; Izquierdo, P.; Esquena, J.; Solans, C. *Adv. Colloid Interf. Sci.* **2004,** *108-109,* 303–318.

14. Porras, M.; Solans, C.; González, C.; Martínez, A.; Guinart, A.; Gutiérrez, J. M. *Colloids Surf., A* **2004,** *249,* 115–118.

15. Luo, Y.; Schork, F. J. *J. Polymer Sci. Part A: Polymer Chem.* **2002,** *40,* 3200–3211.

16. Daniels, E. S.; Sudol, E. D.; El-Aasser, M. S. *Polymer Latexes: Preparation, Characterization and Applications;* American Chemical Society: Washington, DC., 1992.

17. Lovell, P.; El-Aasser, M. *Emulsion Polymerisation and Emulsion Polymers;* John Wiley & Sons: Chichester, 1999.

18. Antonietti, M.; Tauer, K. *Macromol. Chem. Phys.* **2003,** *204,* 207–219.

19. Smith, W. V.; Ewart, R. H. *J. Chem. Phys.* **1948,** *16,* 592–599.

20. Herrera-Ordóñez, J.; Olayo, R.; Carro, S. *J. Macromol. Sci., Polym. Rev.* **2004,** *C44,* 207–229.

21. Harkins, W. D. *J. Chem. Phys.* **1945,** *13,* 381–382.

22. Harkins, W. D. *J. Chem. Phys.* **1946,** *14,* 47–48.

23. Atik, S. S.; Thomas, J. K. *J. Am. Chem. Soc.* **1981,** *103,* 4279–4280.

24. Antonietti, M.; Basten, R.; Lohmann, S. *Macromol. Chem. Phys.* **1995,** *196,* 441–466.

25. Pavel, F. M. *J. Dispersion Sci. Technol.* **2004,** *25,* 1–16.

26. Antonietti, M.; Bremser, W.; Müschenborn, D.; Rosenauer, C.; Schupp, B.; Schmidt, M. *Macromolecules* **1991,** *4,* 6636–6643.

27. Ming, W.; Zhao, Y.; Cui, J.; Fu, S.; Jones, F. N. *Macromolecules* **1999,** *32,* 528–530.

28. Ming, W.; Jones, F. N.; Fu, S. *Macromol. Chem. Phys.* **1998,** *199,* 1075–1079.

29. Xu, X. J.; Chew, C. H.; Siow, K. S.; Wong, M. K.; Gan, L. M. *Langmuir* **1999,** *15,* 8067–8071.

30. Bléger, F.; Kamalakara-Murthy, A.; Pla, F.; Kaler, E. W. *Macromolecules* **1994,** *27,* 2559–2565.

31. Guo, J. S.; El-Aasser, M. S.; Vanderhoff, J. W. *J. Polymer Sci. Part A: Polymer Chem.* **1989,** *27,* 691–710.

32. Guo, J. S.; Sudol, E. D.; Vanderhoff, J. W.; El-Aasser, M. S. *J. Polymer Sci. Part A: Polymer Chem.* **1992,** *30,* 691–702.

33. Suzuki, K.; Goto, A.; Takayama, M.; Muramatsu, A.; Nomura, M. *Macromol. Symp.* **2000,** *155,* 199–212.

34. Puig, J. E.; Perez-Luna, V. H.; Perez-Gonzales, M.; Macias, E. R.; Rodriguez, B. E.; Kaler, E. W. *Colloid Polym. Sci.* **1993,** *271,* 114–123.

35. Chern, C.-S.; Wu, L.-J. *J. Polymer Sci. Pat A: Polymer Chem.* **2001,** *39,* 3199–3210.

36. Gan, L. M.; Chew, C. H.; Lye, I.; Ma, L.; Li, G. *Polymer* **1993,** *34,* 3860–3864.

37. Puig, J. E.; Mendizábal, E.; Delgado, S.; Arellano, J.; López-Serrano, F. *C. R. Chemie* **2003,** *6,* 1267–1273.

38. López, R. G.; no, M. E. T.; Peralta, R. D.; Cesteros, L. C.; Katime, I.; Flores, J.; Mendizábal, E.; Puig, J. E. *Macromolecules* **2000,** *33,* 2848–2854.

39. Hermanson, K. D.; Kaler, E. W. *J. Polymer Sci. Part A: Polymer Chem.* **2004,** *42,* 5253–5261.

40. Landfester, K.; Bechthold, N.; Tiarks, F.; Antonietti, M. *Macromolecules* **1999,** *32,* 2679–2683.

41. Blythe, P. J.; Morrison, B. R.; Mathauer, K. A.; Sudol, E. D.; El-Aasser, M. S. *Langmuir* **2000,** *16,* 898–904.

42. U.Yildiz,; Landfester, K.; Antonietti, M. *Macromol. Chem. Phys.* **2003,** *204,* 1966–1970.

43. Anderson, C. D.; Sudol, E. D.; El-Aasser, M. S. *Macromolecules* **2002,** *35,* 574–576.

44. Perrin, D.; Armarego, W. *Purification of Laboratory Chemicals;* Butterworth-Heinemann: Oxford, 1994.

45. Brookes, A.; Craston, D. *Internet J. Vib. Spectro.* **1999,** *3,* 3 Article 7.

46. Sears, W. M.; Hunt, J. L.; Stevens, J. R. *J. Chem. Phys.* **1981,** *75,* 1599–1602.

47. Speight, J. G. *The Chemistry and Technology of Petroleum (4th Edn.);* Marcel Dekker, Inc.: New York, 2006.

48. Brandrup, J.; Immergut, E.; Grulke, E. *Polymer Handbook (4^{th} Edn.);* Wiley Interscience: New York,.

49. Rouquerol, F.; Rouquerol, J.; Sing, K. *Adsorption by Powders and Porous Solids: Principles, Methodology and Applications;* Academic Press: London, 1999.

50. Brown, J. F.; Krajnc, P.; Cameron, N. R. *Ind. Eng. Chem. Res.* **2005,** *44,* 8565–8572.

51. Merrifield, R. B. *J. Am. Chem. Soc.* **1963,** *85,* 2149–2154.

52. Okay, O. *Prog. Polym. Sci.* **2000,** *25,* 711–779.

53. Antonietti, M. *Angew. Chem. Int. Ed. Engl.* **1988,** *27,* 1743–1747.

54. Antonietti, M.; Bremser, W. *Macromolecules* **1990,** *23,* 3796–3805.

55. Sherrington, D. C. *Chem. Commun.* **1998,** 2275–2286.

56. Mecerreyes, D.; Lee, V.; Hawker, C. J.; Hedrick, J. L.; Wursch, A.; Volksen, W.; Magbitang, T.; Huang, E.; Miller, R. D. *Adv. Mater.* **2001,** *13,* 204–208.

57. Gawdzik, B.; Maciejewska, M.; Pikus, S. *Adsorption Science and Technology* **2006,** *24,* 701–711.

58. McAllister, K.; Sazani, P.; Adam, M.; Cho, M. J.; Rubinstein, M.; Samulski, R. J.; DeSimone, J. M. *J. Am. Chem. Soc.* **2002,** *124,* 15198–15207.

59. Bai, F.; Huang, B.; Yang, X.; Huang, W. *Polymer* **2007,** *48,* 3641–3649.

60. Lee, J.-Y.; Kim, J.-H. *Chemistry Lett.* **2004,** *33,* 526–527.

61. Macintyre, F. S.; Sherrington, D. C. *Macromolecules* **2004,** *37,* 7628–7636.

62. Zhou, W.; Gu, T.-Y.; Su, Z.-G.; Ma, G.-H. *Polymer* **2007,** *48,* 1981–1988.

63. Erbay, E.; Okay, O. *J. Appl. Polym. Sci.* **1999,** *71,* 1055–1062.

64. Howdle, S. M.; Jerábek, K.; Leocorbo, V.; Marr, P. C.; Sherrington, D. C. *Polymer* **2000,** *41,* 7273–7277.

65. Okubo, M.; Ichikawa, K.; Fujimura, M. Production of Multihollow Polymer Particles by Stepwise Alkali-Acid Method. In *Polymer Latexes: Preparation, Characterization and Applications*; Daniels, E. S.; Sudol, E. D.; El-Aasser, M. S., Eds.; American Chemical Society: Washington, D.C., 1992; Chapter 18.

66. Chengyou, K.; Huihui, L.; Qing, Y.; Xiangzheng, K. *Korea Polymer Journal* **1997,** *5,* 221–227.

67. Kobayashi, H.; Miyanaga, E.; Okubo, M. *Langmuir* **2007,** *23,* 8703–8708.

68. Griffiths, P. C.; Wellappili, C.; Hemsley, A. R.; Stephens, R. *Colloid Polym. Sci.* **2004,** *282,* 1155–1159.

69. Zhao, G.; Ishizaka, T.; Kasai, H.; abd H. Nakanishi, H. O. *Chem. Mater.* **2007,** *19,* 1901–1905.

70. Davankov, V. A.; Tsyurupa, M. P. *React. Polym.* **1990,** *13,* 27–42.

71. Tsyurupa, M. P.; Davankov, V. A. *React. and Funct. Polym.* **2002,** *53,* 193–203.

72. Veverka, P.; Jeřábek, K. *React. and Funct. Polym.* **1999,** *41,* 21–25.

73. Veverka, P.; Jeřábek, K. *React. and Funct. Polym.* **2004,** *59,* 71–79.

74. Fontanals, N.; Cortés, J.; Galià, M.; Maria Marcé, R.; Cormack, P. A. G.; Borrull, F.; Sherrington, D. C. *J. Polym. Sci. Part A: Polym. Chem.* **2005,** *43,* 1718–1728.

75. Ahn, J.-H.; Jang, J.-E.; Oh, C.-G.; Ihm, S.-K.; Cortez, J.; Sherrington, D. C. *Macromolecules* **2006,** *39,* 627–632.

76. Macintyre, F. S.; Sherrington, D. C.; Tetley, L. *Macromolecules* **2006,** *39,* 5381–5384.

77. Subramonian, S. *React. and Funct. Polym.* **1996,** *29,* 129–133.

78. Kranjc, P.; Brown, J. F.; Cameron, N. R. *Org. Lett.* **2002,** *4,* 2497–2500.

79. Wall, J. "The Synthesis and Functionalisation of Hypercrosslinked Emulsion Templated Porous Polymers", Master's thesis, Department of Chemistry, Durham University, 2007.

80. Suen, C.-H.; Morawetz, H. *Macromolecules* **1984,** *17,* 1800–1803.

81. Dumistracel, I.; Ponchel, G.; Dănilă, G.; Duchêne, D.; Carov, A. *J. Microencapsulation* **2000,** *17,* 45–55.

82. Schärtl, W. *Adv. Mater.* **2000,** *12,* 1899–1908.

83. McDonald, C. J.; Devon, M. J. *Adv. Colloid Interface Sci.* **2002,** *99,* 181–213.

84. Sundberg, D. C.; Durant, Y. G. *Polym. React. Eng.* **2003,** *11,* 379–432.

85. Moinard-Checot, D.; Chevalier, Y.; Briançon, S.; Fessi, H.; Guinebretière, S. *J. Nanosci. Nanotechnol.* **2006,** *6,* 2664–2681.

86. Read, E. S.; Armes, S. P. *Chem. Commun.* **2007,** 3021–3035.

87. Bourgeat-Lami, E. Hollow Particles, Synthetic Pathways and Potential Applications. In *Colloidal Polymers Synthesis and Characterisation*; Elaissari, A., Ed.; Marcel Dekker, Inc.: New York, 2006; Chapter 8.

88. Geng, B. Y.; Ma, J. Z.; Du, Q. B.; Liu, X. W.; Zhang, L. D. *Mater. Sci. Eng. A.* **2007,** *466,* 96–100.

89. Kim, S.-W.; Kim, M.; Lee, W. Y.; Hyeon, T. *J. Am. Chem. Soc.* **2002,** *124,* 7642–7643.

90. Huang, W. X.; Skanth, G.; Baker, G. L.; Bruening, M. L. *Langmuir* **2001,** *17,* 1731–1736.

91. Sumerlin, B. S.; Lowe, A. B.; Stroud, P. A.; Zhang, P.; Urban, M. W.; McCormick, C. L. *Langmuir* **2003,** *19,* 5559–5562.

92. Fan, J. D.; Bozzola, J. J.; Gao, Y. *J. Colloid Interface Sci.* **2002,** *254,* 108–112.

93. Wu, M.; O'Neill, S. A.; Brousseau, L. C.; McConnell, W. P.; Schultz, D. A.; Linderman, R. J.; Feldheim, D. L. *Chem. Commun.* **2002,** 775–776.

94. Hotchkiss, J. W.; Lowe, A. B.; Boyes, S. G. *Chem. Mater.* **2007,** *19,* 6–13.

95. Watson, K. J.; Zhu, J.; Nguyen, S. T.; Mirkin, C. A. *J. Am. Chem. Soc.* **1999,** *121,* 462–463.

96. Spain, S. G.; Albertin, L.; Cameron, N. R. *Chem. Commun.* **2006,** 4198–4200.

97. Koenig, S.; Chechik, V. *Langmuir* **2006,** *22,* 5168–5173.

98. Marinakos, S. M.; Novak, J. P.; Brousseau, L. C.; House, A. B.; Edeki, E. M.; Feldhaus, J. C.; Feldheim, D. L. *J. Am. Chem. Soc.* **1999,** *121,* 8513–8522.

99. Zhu, C.; Chou, S.; He, S.; Liao, W.; Chen, C. *Nanotechnology* **2007,** *18,* 275604.

100. Kamata, K.; Lu, Y.; Xia, Y. *J. Am. Chem. Soc.* **2003,** *125,* 2384–2385.

101. Kim, M.; Sohn, K.; Na, H. B.; Hyeon, T. *Nano Lett.* **2002,** *2,* 1383–1387.

102. Yoon, S. B.; Sohn, K.; Kim, J. Y.; Shin, C. H.; Yu, J. S.; Hyeon, T. *Adv. Mater.* **2002,** *14,* 19–21.

103. Hah, H. J.; Um, J. I.; Han, S. H.; Koo, S. M. *Chem. Commun.* **2004,** 1012–1013.

104. Beck, J. S.; Chu, C. T.; Johnson, I. D.; Kresge, C. T.; Leonowicz, M. E.; Roth, W. J.; Vartuli, J. C. US Patent 5,108,725, Mobil Oil Corp., 1992.

105. Beck, J. S.; Vartuli, J. C.; Roth, W. J.; Leonowicz, M. E.; Kresge, C. T.; Chu, C. T.; Olson, D. H.; Sheppard, E. W.; McCullen, S. B.; Higgins, J. B.; Schlenker, J. L. *J. Am. Chem. Soc.* **1992,** *114,* 10834–10843.

106. Kresge, C. T.; Leonowicz, M. E.; Roth, W. J.; Vartuli, J. C.; Beck, J. S. *Nature* **1992,** *359,* 710–712.

107. Venkatathri, N. *Solid State Commun.* **2007,** *143,* 493–497.

108. Zhou, G.; Chen, Y.; Yang, J.; Yang, S. *J. Mater. Chem.* **2007,** *17,* 2839–2844.

109. Wang, Q.; Liu, Y.; Yan, H. *Chem. Commun.* **2007,** 2339–2341.

110. Caruso, F.; Caruso, R. A.; Möhwald, H. *Science* **1998,** *282,* 1111–1114.

111. Darbandi, M.; Thomann, R.; Nann, T. *Chem. Mater.* **2007,** *19,* 1700–1703.

112. Wu, Z.; Han, H.; Han, W.; Kim, B.; Ahn, K. H.; Lee, K. *Langmuir* **2007,** *23,* 7799–7803.

113. Fu, G. D.; Shang, Z.; Hong, L.; Kang, E. T.; Neoh, K. G. *Macromolecules* **2005,** *38,* 7867–7871.

114. Blomberg, S.; Ostberg, S.; Harth, E.; Bosman, A. W.; van Horn, B.; Hawker, C. J. *J. Polym. Sci. Part A: Polym. Chem.* **2002,** *40,* 1309–1320.

115. Lei, Z.; Bi, S. *Materials Lett.* **2007,** *61,* 3531–3534.

116. Sondi, I.; Fedynyshyn, T. H.; Sinta, R.; Matijević, E. *Langmuir* **2000,** *16,* 9031–9034.

117. Morinaga, T.; Onkura, M.; Ohno, K.; Tsujii, Y.; Fukuda, T. *Macromolecules* **2007,** *40,* 1159–1164.

118. Fleming, M. S.; Mandal, T. K.; Walt, D. R. *Chem. Mater.* **2001,** *13,* 2210–2216.

119. Zhang, Y. B.; Qian, X. F.; Xi, H. A.; Yin, J.; Zhu, Z. K. *Mater. Lett.* **2003,** *58,* 222–225.

120. Xu, P.; Wang, H.; Tong, R.; Du, Q.; Zhong, W. *Colloid Polym. Sci.* **2006,** *284,* 755–762.

121. Schmid, A.; Fujii, S.; Armes, S. P. *Langmuir* **2006,** *22,* 4923–4927.

122. Lee, J.; Hong, C. K.; Choe, S.; Shim, S. E. *J. Colloid Interface Sci.* **2007,** *310,* 112–120.

123. Schmid, A.; Fujii, S.; Armes, S. P.; Leite, C. A. P.; Galembeck, F.; Minami, H.; Saito, N.; Okubo, M. *Chem. Mater.* **2007,** *19,* 2435–2445.

124. Stöber, W.; Fink, A.; Bohn, E. *J. Colloid Interface Sci.* **1968,** *26,* 62–69.

125. Lu, Y.; McLellan, J.; Xia, Y. *Langmuir* **2004,** *20,* 3464–3470.

126. Deng, Z.; Chen, M.; Zhou, S.; You, B.; Wu, L. *Langmuir* **2006,** *22,* 6403–6407.

127. Antipov, A. A.; Sukhorukov, G. B.; Fedutik, Y. A.; Hartmann, J.; Giersig, M.; Möhwald, H. *Langmuir* **2002,** *18,* 6687–6693.

128. Ishizu, K.; Park, J.; Tanimura, K.; Uchida, S.; Tamura, T. *J. Mater. Sci.* **2004,** *39,* 4353–4357.

129. Okubo, M.; Ichikawa, K.; Tsujihiro, M.; He, Y. *Colloid Polym. Sci.* **1990,** *268,* 791–796.

130. Okubo, M.; Lu, Y. *Colloids Surf., A* **1996,** *109,* 49–53.

131. Park, M.-K.; Xia, C.; Advincula, R. C.; Schütz, P.; Caruso, F. *Langmuir* **2001,** *17,* 7670–7674.

132. Chainey, M.; Hearn, J.; Wilkinson, M. C. *Br. Polym. J.* **1981,** *13,* 132–136.

133. Kirsch, S.; Doerk, A.; Bartsch, E.; Sillascu, H.; Landfester, K.; Spiess, H. W.; Maechtle, W. *Macromolecules* **1999,** *32,* 4508–4518.

134. Dimonie, V.; El-Aasser, M. S.; Klein, A.; Vanderhoff, J. W. *J. Polymer Sci. Polymer Chem.* **1984,** *22,* 2197–2215.

135. Cairns, D. B.; Armes, S. P.; Bremer, L. G. B. *Langmuir* **1999,** *15,* 8052–8058.

136. Yassar, A.; Roncali, J.; Garnier, F. *Polymer Commun.* **1987,** *28,* 103–104.

137. Lee, S.; Rudin, A. *J. Polymer Sci. Part A: Polymer Chem.* **1991,** *30,* 865–871.

138. Landfester, K.; Rothe, R.; Antonietti, M. *Macromolecules* **2002,** *35,* 1658–1662.

139. Litchfield, W. J.; Craig, A. R.; Frey, W. A.; Leflar, C. C.; Looney, C. E.; Luddy, M. A. *Clin. Chem.* **1984,** *30,* 1489–1493.

140. Li, W.-H.; Stöver, H. D. H. *Macromolecules* **2000,** *33,* 4354–4360.

141. Jang, J.; Oh, J. H. *Adv. Funct. Mater.* **2005,** *15,* 494–502.

142. Cui, X.; Zhong, S.; Xu, J.; Wang, H. *Colloid Polym. Sci.* **2007,** *285,* 935–940.

143. Park, M.-K.; Onishi, K.; Locklin, J.; Caruso, F.; Advincula, R. C. *Langmuir* **2003,** *19,* 8550–8554.

144. Shi, X.; Briseno, A. L.; Sanedrin, R. J.; Zhou, F. *Macromolecules* **2003,** *36,* 4093–4098.

145. Jang, J.; Ha, H. *Langmuir* **2002,** *18,* 5613–5618.

146. Jang, J.; Oh, J. H.; Li, X. L. *J. Mater. Chem.* **2004,** *14,* 2872–2880.

147. Li, G.; Yang, X.; Bai, F. *Polymer* **2007,** *48,* 3074–3081.

148. Nakashima, K.; Bahadur, P. *Adv. Colloid Interface Sci.* **2006,** *123–126,* 75–96.

149. Saito, R.; Ishizu, K.; Fukutomi, T. *Polymer* **1991,** *32,* 531–536.

150. Guo, A.; Liu, G.; Tao, J. *Macromolecules* **1996,** *29,* 2487–2493.

151. Henselwood, F.; Liu, G. *Macromolecules* **1997,** *30,* 488–493.

152. Liu, Y.; Wang, L.; Pan, C. *Polymer* **2002,** *43,* 7063–7068.

153. Thurmond, II, K. B.; Kowalewski, T.; Wooley, K. L. *J. Am. Chem. Soc.* **1997,** *119,* 6656–6665.

154. Khoee, S.; Hassanzadeh, S.; Goliaie, B. *Nanotechnology* **2007,** *18,* 175602.

155. Rodríguez-Hernández, J.; Babin, J.; Zappone, B.; Lecommandoux, S. *Biomacromolecules* **2005,** *6,* 2213–2220.

156. Pan, D.; Turner, J. L.; Wooley, K. L. *Chem. Commun.* **2003,** 2400–2401.

157. Zhang, W.; Shi, L.; Miao, Z.-J.; Wu, K.; An, Y. *Macromol. Chem. Phys.* **2005,** *206,* 2354–2361.

158. Jiang, J.; Qi, B.; Lepage, M.; Zhao, Y. *Macromolecules* **2007,** *40,* 790–792.

159. Wooley, K. L. *J. Polymer Sci. Part A: Polymer Chem.* **2000,** *38,* 1397–1407.

160. Huang, H.; Remsen, E. E.; Kowalewski, T.; Wooley, K. L. *J. Am. Chem. Soc.* **1999,** *121,* 3805–3806.

161. Turner, J. L.; Wooley, K. L. *Nano Lett.* **2004,** *4,* 683–688.

162. Zhang, Q.; Remsen, E. E.; Wooley, K. L. *J. Am. Chem. Soc.* **2000,** *122,* 3642–3651.

163. Zang, Y.; Jiang, M.; Zhao, J.; Wang, Z.; Dou, H.; Chen, D. *Langmuir* **2005,** *21,* 1531–1538.

164. Antonietti, M.; Förster, S. *Adv. Mater.* **2003,** *15,* 1323–1333.

165. Hentze, H.-P.; Kaler, E. W. *Curr. Opin. Colloid Interf. Sci.* **2003,** *8,* 164–178.

166. Zhang, W.; Shi, L.; An, Y.; Gao, L.; Wu, K.; Ma, R.; He, B. *Phys. Chem. Chem. Phys.* **2004,** *6,* 109–115.

167. Ding, J.; Liu, G. *Chem. Mater.* **1998,** *10,* 537–542.

168. Ding, J.; Liu, G. *J. Phys. Chem. B* **1998,** *102,* 6107–6113.

169. Nardin, C.; Hirt, T.; Leukel, J.; Meier, W. *Langmuir* **2000,** *16,* 1035–1041.

170. Du, J.; Chen, Y.; Zhang, Y.; Han, C. C.; Fischer, K.; Schmidt, M. *J. Am. Chem. Soc.* **2003,** *125,* 14710–14711.

171. Du, J.; Chen, Y. *Macromolecules* **2004,** *37,* 5710–5716.

172. McDonald, C. J.; Bouck, K. J.; Chaput, A. B.; Stevens, C. J. *Macromolecules* **2000,** *33,* 1593–1605.

173. Tiarks, F.; Landfester, K.; Antonietti, M. *Langmuir* **2001,** *17,* 908–918.

174. Watnasirichaikul, S.; Davies, N. M.; Rades, T.; Tucker, I. G. *Pharma. Res.* **2000,** *17,* 684–689.

175. Jang, J.; Lee, K. *Chem. Commun.* **2002,** 1098–1099.

176. Ali, M. M.; Stöver, H. D. H. New Materials Using Atom Transfer Radical Polymerisation: Microcapsules Containing Polar Core Oil. In *Advances in Controlled/Living Radical Polymerization*; Matyjaszewski, K., Ed.; American Chemical Society: Washington, DC., 2003; Chapter 21.

177. van Zyl, A. J. P.; Sanderson, R. D.; de Wet-Roos, D.; Klumperman, B. *Macromolecules* **2003,** *36,* 8621–8629.

178. Cheng, D.; Ng, S.-C.; Chan, H. S. O. *Thin Solid Films* **2005,** *477,* 19–23.

179. van Zyl, A. J. P.; Bosch, R. F. P.; McLeary, J. B.; Sanderson, R. D.; Klumperman, B. *Polymer* **2005,** *46,* 3607–3615.

180. Luo, Y.; Gu, H. *Polymer* **2007,** *48,* 3262–3272.

181. Crespy, D.; Musyanovych, A.; Landfester, K. *Colloid Polym. Sci.* **2006,** *284,* 780–787.

182. Stoffelbach, F.; Belardi, B.; Santos, J. M. R. C. A.; Tessier, L.; Matyjaszewski, K.; Charleux, B. *Macromolecules* **2007,** *40,* 8813–8816.

183. Scott, C.; Wu, D.; Ho, C.-C.; Co, C. C. *J. Am. Chem. Soc.* **2005,** *127,* 4160–4161.

184. Wu, D.; Scott, C.; Ho, C.-C.; Co, C. C. *Macromolecules* **2006,** *39,* 5848–5853.

185. Crespy, D.; Stark, M.; Hoffman-Richter, C.; Ziener, U.; Landfester, K. *Macromolecules* **2007,** *40,* 3122–3135.

186. Hong, Z.; Guangsu, H.; Pin, G.; Chengqun, L. *Polym. Adv. Technol.* **2007,** *18,* 582–585.

187. Gaynor, S. G.; Qiu, J.; Matyjaszewski, K. *Macromolecules* **1998,** *31,* 5951–5954.

188. Matyjaszewski, K.; Qiu, J.; Tsarevsky, N. V.; Charleux, B. *J. Polymer Sci. Part A: Polymer Chem.* **2000,** *38,* 4724–4734.

189. Li, M.; Min, K.; Matyjaszewski, K. *Macromolecules* **2004,** *37,* 2106–2112.

190. Min, K.; Matyjaszewski, K. *Macromolecules* **2005,** *38,* 8131–8134.

191. Min, K.; Gao, H.; Matyjaszewski, K. *J. Am. Chem. Soc.* **2006,** *128,* 10521–10526.

192. Oh, J. K.; Perineau, F.; Matyjaszewski, K. *Macromolecules* **2006,** *39,* 8003–8010.

193. Kagawa, Y.; Zetterlund, P. B.; Minami, H.; Okubo, M. *Macromolecules* **2007,** *40,* 3062–3069.

194. Jankova, K.; Chen, X.; Kops, J.; Batsberg, W. *Macromolecules* **1998,** *31,* 538–541.

195. Reining, B.; Keul, H.; Höcker, H. *Polymer* **1999,** *40,* 3555–3563.

196. Angot, S.; Taton, D.; Gnanou, Y. *Macromolecules* **2000,** *33,* 5418–5426.

197. Matyjaszewski, K. *Controlled Radical Polymerization;* American Chemical Society: Washington, D.C., 1998.

198. Krishnan, R.; Sabdham, K.; Srinivasan, V. *Eur. Polym. J.* **2003,** *39,* 205–210.

199. Queffelee, J.; Raynor, S. G.; Matyjaszewski, K. *Macromolecules* **2000,** *33,* 8629–8639.

200. Graham, T. *Philos. Mag.* **1866,** *32,* 401–420.

201. Maier, G. *Angew. Chem. Int. Ed.* **1998,** *37,* 2960–2974.

202. Koros, W. J. Polymers, Laminations & Coatings Conference, TAPPI Proceedings, 1999 259–276.

203. Dodrill, D. *Medical Device Manufacturing & Technology* **2006,** 45–48.

204. Gao, Y.; Baca, A. M.; Wang, B.; Ogilby, P. R. *Macromolecules* **1994,** *27,* 7041–7048.

205. Schmidt, G.; Malwitz, M. M. *Curr. Opinion Coll. Interf. Sci.* **2003,** *8,* 103–108.

206. Moniruzzaman, M.; Winey, K. I. *Macromolecules* **2006,** *39,* 5194–5205.

207. Coleman, J. N.; Khan, U.; Blau, W. J.; Gun'ko, Y. K. *Carbon* **2006,** *44,* 1624–1652.

208. Yuan, Q.; Misra, R. D. K. *Materials Science and Technology* **2006,** *22,* 742–755.

209. Oberdisse, J. *Soft Matter* **2006,** *2,* 29–36.

210. Schaefer, D. W.; Justice, R. S. *Macromolecules* **2007,** *40,* 8501–8517.

211. Mizutani, Y.; Nagô, S.; Kawamura, H. *J. Applied Polym. Sci.* **1999,** *73,* 1089–1092.

212. Matteucci, S.; Kusuma, V. A.; Freeman, B. D. *Polymeric Materials: Science & Engineering - ACS Preprint* **2007,** *97,* 267–268.

213. Soloyov, S. E. *J. Phys. Chem. B* **2006,** *110,* 17977–17986.

214. Crank, J. *The Mathematics of Diffusion;* Oxford University Press: Oxford, 1975.

215. Ray, S.; Easteal, A. J. *Materials and Manufacturing Processes* **2007,** *22,* 741–749.

216. Ensley, S. "Data Report on Porous Nanoparticles to Increase OTR", Technical Report, Cryovac Inc., Sealed Air Corporation, 2005.

217. Chen, W.; Tao, X.; Xue, P.; Cheng, X. *Applied Surface Science* **2005,** *252,* 1404–1409.